Universität Hamburg
DER FORSCHUNG | DER LEHRE | DER BILDUNG

FAKULTÄT
FÜR MATHEMATIK, INFORMATIK
UND NATURWISSENSCHAFTEN

Doctoral Dissertation

Climate-related changes of coastal tidal ranges in the North Sea and their driving factors

Wenguo Li

dissertation submitted to the Faculty of Mathematics, Informatics and Natural Sciences, Department of Earth Sciences at University of Hamburg

Hamburg, 2021

Department of Earth Sciences

Date of Oral Defense:	27.09.2021
Reviewers:	Dr. Bernhard Mayer PD Dr. Thomas Pohlmann
Members of the examination commission:	PD Dr. Thomas Pohlmann Prof. Dr. Corinna Schrum Prof. Dr. Matthias Hort Dr. Alexa Griesel Dr. Uwe Mikolajewicz
Chair of the Subject Doctoral Committee Earth System Sciences:	Prof. Dr. Dirk Gajewski
Dean of Faculty MIN:	Prof. Dr. Heinrich Graener

Abstract

Tidal ranges are changing worldwide also by non-astronomic factors. Increasing tidal ranges coupled with sea-level rise induced by climate change widely threaten coastal environment and marine activities. Therefore, it is imperative to recognize the contributions of these non-astronomic factors on tidal ranges and to understand the underlying dynamics.

In the present study, the regional 3D baroclinic hydrodynamic Hamburg Shelf Ocean Model (HAMSOM) is applied to the North Sea for the period from 1948 to 2014 in order to investigate the influence of four different physical forcing mechanisms and their climate-induced changes on coastal tidal ranges: (1) open boundary sea surface height (SSH); (2) heat flux; (3) wind stress; (4) river input. Accordingly, five experiments are configured: a hindcast run with realistic forcing conditions serving as the reference run, and four scenario runs, where for each of the four forcing mechanisms the data of the first decade since 1950 are used repetitively over the entire simulation period. Besides, in order to better understand the underlying dynamics responsible for heat flux and river input, the influence of ocean stratification on tidal ranges was analyzed in detail, and in this context additional numerical simulations were carried out in the baroclinic and barotropic modes covering the same period.

Trends of annual and seasonal (winter and summer) mean tidal range (MTR) are analyzed over the period from 1950 to 2014 for 22 tide-gauge stations, where the simulated sea surface elevations agree well with observations. The open boundary SSH

rise is demonstrated to be the dominant contribution to the increasing annual MTR with 0.28 mm yr^{-1}. Increasing wind stress also has a significant impact but generally negatively correlates with changes in the coastal MTR. Particularly, it has a large impact in winter due to stronger wind in this season, with an average contribution of -0.10 mm yr^{-1}. Growing heat flux and river input add to the coastal MTR trends with a more significant contribution of about 0.06 mm yr^{-1} in summer despite the fact that compared to winter only minor changes of heat flux and river input occur in this season.

The governing dynamics responsible for observed changes in MTR caused by individual physical forcing are also discussed in the study. Boundary SSH rise directly alters the coastal MTR through increased coastal water depth. In contrast, increasing wind stress affects the MTR majorly via an enhanced bottom stress induced by an increased momentum input by the stronger winds.

Growing heat fluxes and river discharges modify the baroclinicity (majorly stratification) in the North Sea, subsequently resulting in a reduction of MTR trends along the British coast and an amplification in the German Bight. This was demonstrated by the contrast between baroclinic and barotropic simulations.

The baroclinicity has the potential to modulate surface tides through ocean stratification on seasonal and secular scales. The statistical analysis of the mean tidal range difference (TRD) between the baroclinic and the barotropic modes in winter and summer at 22 tide-gauge stations, shows that generally the TRD in summer is much larger than in winter, with a maximum magnitude of approximately 11 cm. The spatial distribution of the seasonal TRD, with negative values along the British coast and

positive ones in the German Bight indicates a westward shift in the amphidromic system of the North Sea due to baroclinity. This shift originates from altered vertically averaged tidal current velocities in stratified regions, as an effect of decoupling induced by stratification. As a secondary effect, this alteration also induces subsequent changes of tidal ranges in coastal well-mixed regions. It is also demonstrated that, on the secular scale, an altered stratification and ocean warming may lead to both, positive trends in the tidal range and the mean sea level, respectively.

Content

1. Introduction

1.1 Motivation

One of the major concerns linked to climate change is the sea-level rise, which leads to coastal inundations and a threatening of local inhabitants. The global average sea-level rise shows a linear trend of 1.7 ± 0.2 mm yr^{-1} from 1900 to 2009 as estimated from satellite and in-situ data (Church & White, 2006, 2011). A higher rate of 3.0 ± 0.7 mm yr^{-1} was observed between 1993 and 2010 (Hay et al., 2015). Projected future sea-level rise in 21st century is expected to be even faster, with a rise ranging from 0.5 to 1.4 m in 2100 compared to the 1990 sea level (Rahmstorf, 2007). At the same time, also tidal ranges have been increasing at many tide-gauge stations. Flick et al. (2003) observed that MTR increased at a significant rate of 5.42 mm yr^{-1} at Wilmington, N.C. These increasing tidal ranges in combination with a mean sea-level rise enhance the risks of coastal flooding hazards, in particular, when astronomic high tides coincide with storm surge induced by meteorological extreme events. Therefore, it is imperative to recognize and understand the changing of coastal tidal ranges.

1.2 Tides

Tides driven by gravitational and centrifugal forces in the rotating moon-earth-sun system have been changing worldwide at exceptional rates, which cannot be explained by changes in astronomic forcing (Devlin et al., 2017; Haigh et al., 2014; Müller et al., 2011; Woodworth, 2010).

Tide-gauge records have been studied locally, regionally, and globally (Hill, 2016).

Colosi & Munk (2006) recorded an increase of M2 amplitude from 16.1 to 16.9 cm during the period 1915 to 2000 at Honolulu, Hawaii. Woodworth et al. (1991) observed that secular trends in MTR varied between -1.8 and 1.3 mm yr^{-1} for 13 ports around the British Isles. Ray (2006) assessed an approximately linear increase of the M2 tidal amplitude during most of 20th century but a decrease for S2 tide (Ray, 2009) in the Gulf of Maine. Mawdsley et al. (2015) investigated sea level data from 220 globally distributed tide-gauge stations and found that more stations show a positive trend in tidal ranges than a negative trend.

Numerical models have been applied to simulate changing tidal characteristics. Most modelling studies for historic tides concentrated on paleotides and millennial timescales (Hill, 2016; Uehara et al., 2006; Hill et al., 2011; Hall et al., 2013; Thomas & Sündermann, 1999; Griffiths & Peltier, 2009). Studies regarding future tides mostly focused on the effect of the projected sea-level rise on the tidal characteristics (Greenberg et al., 2012; Pelling et al., 2013; Hall et al., 2013; Holleman & Stacey, 2014; Passeri et al., 2016). However, at present, modelling studies that investigate changes in historic tides on the decadal-to-century scale are still lacking and the contributions of other climate-related processes to the tidal characteristics are not fully understood.

Many physical processes in the ocean and at the ocean-air interface can modulate tides. Müller (2012) summarized six potential factors causing tidal variations: the generation of internal tides, sea ice coverage, sea level increase, mean current modification, currents driven by the meteorological forcing, and changes in ocean stratification. In this article, we will focus on those climate-related processes. As known, climate change not only leads to sea-level rise but also alters ocean stratification and ocean circulation due to climate-related changes of the atmospheric forcing conditions like heat flux and wind field. In addition, ocean warming also changes precipitation and evaporation and thus changes in river discharge may occur. All these climate-associated processes also have the potential to modify ocean tides.

1.3 The North Sea

The North Sea is a semi-closed marginal sea located on the northwestern European shelf. It covers approximately 570,000 km^2, with an extension of about 1000 km in north-south and 500 km in west-east direction (Steele et al., 2009). Most of the region in the North Sea is shallower than 100-meter depth, except the Norwegian Trench region, which has a maximum depth of more than 700 m (Winther & Johannessen, 2006).

The North Sea is connected to the Norwegian Sea in the north, the Baltic Sea in the east, and the North Atlantic Ocean in the northwest and southwest. It receives most of oceanic water masses from the North Atlantic Ocean through the Fair Isle Passage and an inflow east of the Shetland Islands, Smaller intrusions occur through the Pentland Firth and the Dover Strait. In addition, low salinity water enters into the North Sea from the Baltic Sea. All water masses leave the North Sea along the Norwegian coast.

The dominant partial tides in the North Sea are semi-diurnal tides. Currents away from offshore regions are mainly forced by M2, S2, N2, and K2 partial tides, while the influence of diurnal tides O1 and K1 is amplified near the edge of the shelf (Steele et al., 2009). The amplitude ratio of S2 vs. M2 is 0.34 over most parts of the North Sea, with the amplitude of the M2 tide is 1.61 m. The amplitude ratio is 0.08 for both K1 vs. M2 and O1 vs. M2 (British Admiralty, 2010).

Two tidal waves intrude into the North Sea, one from the north at the Scottish coast and one in the south through the English Channel. Both propagate as Kelvin waves cyclonically along the coastline of the North Sea. In the Southern Bight both waves merge, forming an amphidromic point in this region. The tidal wave gradually loses energy along the path of its propagation due to the dissipation by bottom friction, causing smallest tidal amplitudes at the Danish and Norwegian coast, where the wave leaves the North Sea. The wave speed depends on the water depth behaving as a shallow water wave.

The atmospheric conditions in the North Sea present pronounced seasonal variations, which mainly results from the seasonal changes of solar radiation. They are also affected by the warm subtropical water carried northward by the North Atlantic Current (Mathis et al., 2013).

The near-surface air temperature is mainly determined by sea surface temperature over the North Sea. Thus, the warm North Atlantic Current entering into the North Sea has a significant influence on the regional near-surface air temperature. According to the NCEP/NCAR Reanalysis 1 (NCEP R1) data (Kalnay et al., 1996), the monthly mean near-surface air temperature (1950 to 2014) varies from approximately -6 ℃ to 16 ℃ (Fig. 1). The near-surface air temperature over the North Sea is warmer than over the continent from autumn to winter and cooler from May to August as a result of different radiation absorption and heat capacity between sea water and land mass (Quante & Colijn, 2016).

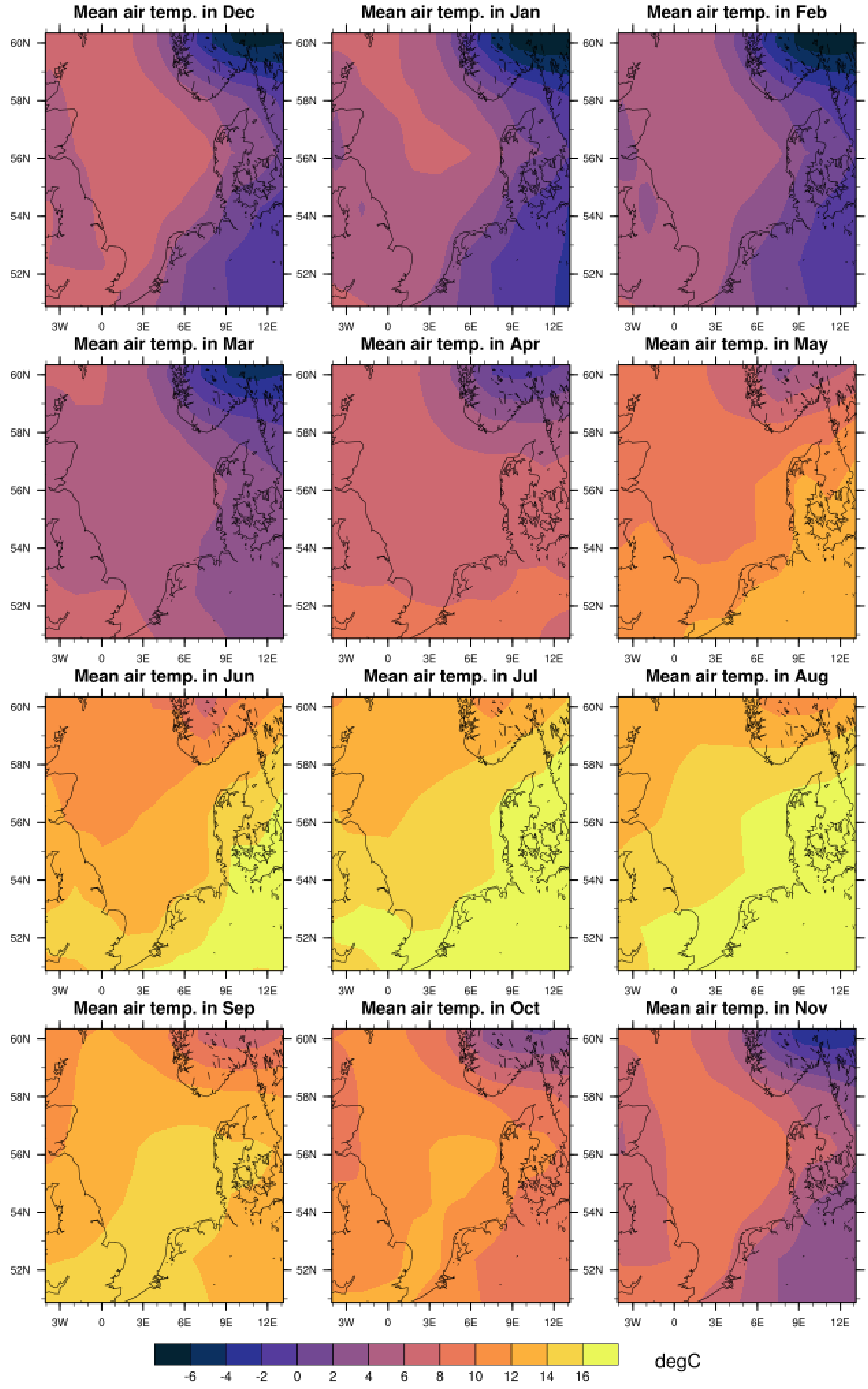

Fig. 1 Monthly mean air temperature at 2 m (1950-2014) in the North Sea. Data retrieved from NCEP R1 dataset and are interpolated into a fine resolution of 3 km.

Situated in the mid-latitudes between the subtropical high pressure belt and the polar low pressure belt, the prevailing wind direction over the North Sea is from west. The governing air pressure centers across the North Atlantic, i.e. the Icelandic Low and the Azores High, dominate the strength and persistence of westerly winds in winter. The strongest westerly winds are observed in autumn and winter as the low pressure system is strengthened by a larger temperature difference between the subtropical and polar regions in these two seasons (Quante & Colijn, 2016). The average wind direction over the North Sea varies when the air pressure centers are shifted and the pressure gradients are altered. The monthly wind direction in August and September is from west turning to southwesterly winds from October to March (Fig. 2). The wind speed declines markedly from March to April over the North Sea region. The high pressure center in Azores begins to extend towards the central Europe, and the gradient between Icelandic Low and the Azores High gets weakest in May. The high-pressure center expansion in June and July generally induces a weakening of the northwesterly winds (Quante & Colijn, 2016).

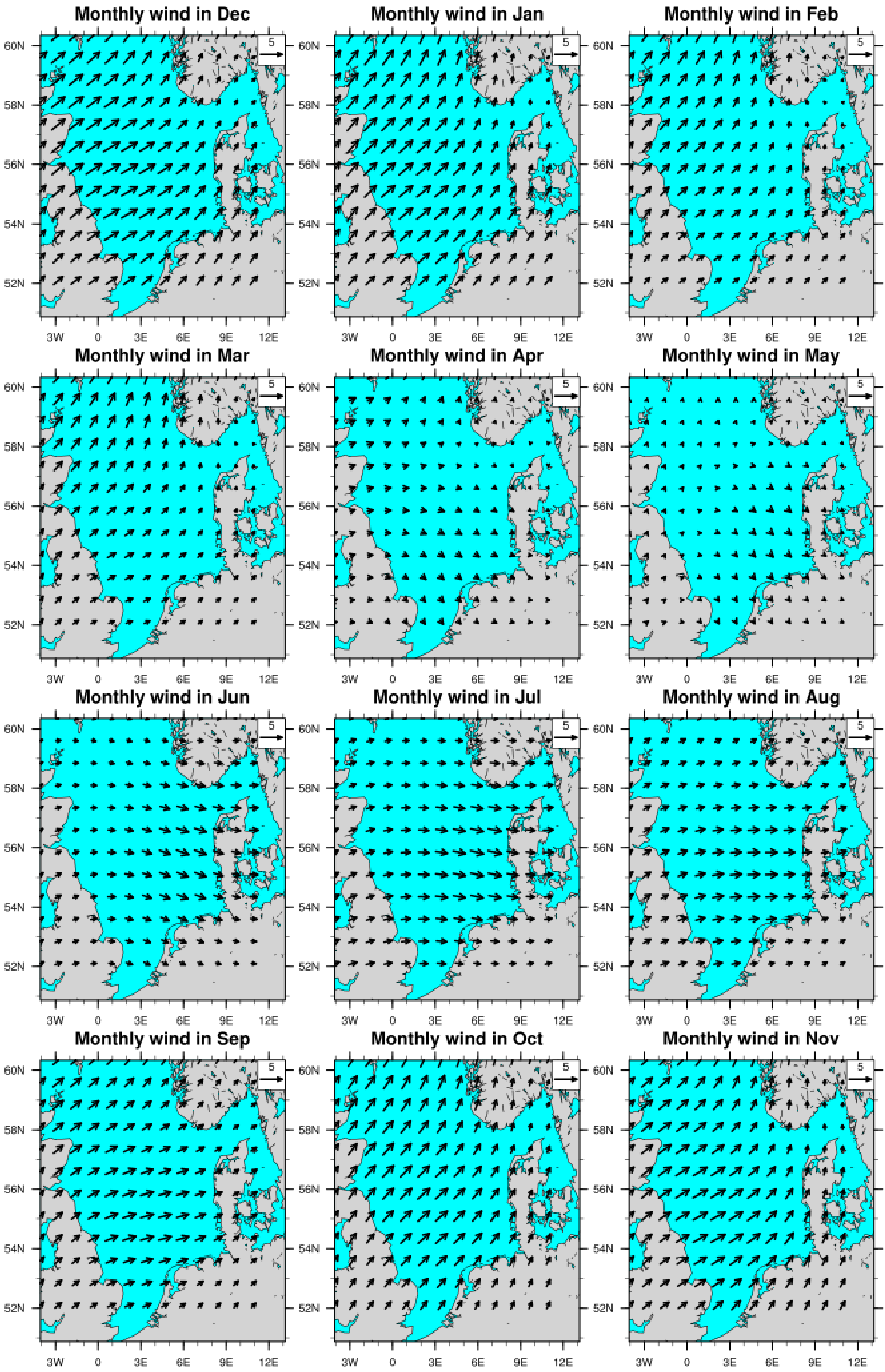

Fig. 2 Monthly mean near-surface wind (1950-2014) in the North Sea. Data retrieved from NCEP R1 dataset and are interpolated into a fine resolution of 3 km.

The atmospheric circulation over the North Sea is strongly impacted by the North Atlantic Oscillation (NAO) which is apparent throughout the year and most prominent in winter (Hurrell & Van Loon, 1997). Generally positive NAO phases, are characterized by enhanced gradients of air pressure over the North Atlantic. Positive NAO during winter usually indicates enhanced storm activities, relatively high air temperatures and precipitation in Norway and Scotland (Hurrell 1995; Hense & Glowienka-Hense, 2008). During negative NAO periods, the air pressure gradient gets weaker than the average, and relatively low air temperatures are observed in northern Europe (Trigo et al.2002).

The freshwater input into the North Sea originates from a number of European continental watersheds of which the Rhine River and the Elbe River are the largest and most important freshwater input sources (Ray & McCormick-Ray, 2009). The Baltic Sea also strongly contributes to the freshwater input into the North Sea with an average amount of 15000 $m^3 s^{-1}$ (Steele et al., 2009).

The circulation in the North Sea, like most other continental shelf seas, is forced by tides, winds, and density gradients. The dominant dynamic feature are the tidal motions, followed by wind driven currents forming the second largest contribution (Steele et al., 2009). In addition, the North Sea receives a high amount of freshwater from rivers and the Baltic Sea, which significantly contributes to the temperature driven density gradients. The long-term mean circulation is cyclonic following the general coastline of the North Sea. The Atlantic Ocean water flows mainly southward after entering into the North Sea through the entrance in the northwest, and in the southern

North Sea turns eastward and subsequently northward following the coasts of the Netherlands, Germany, and Denmark. At the Skagerrak region the North Sea water meets the brackish water from the Baltic Sea and finally it flows northward along the Norwegian coast becoming the Norwegian Coastal Current (Winther & Johannessen, 2006).

1.4 Stratification

With the exception of the Norwegian Trench, all parts of the North Sea are vertically well-mixed in winter season. Only the Norwegian Trench area is not well mixed due to haline stratification. In autumn, the surface water mass is cooled due a negative atmosphere-ocean heat balance in this season. Subsequently, the water, sinks down induced by the increased density. This process continues until the whole water column reaches a balanced state, forming a thick well-mixed layer (like at the Norwegian Trench) or even making the entire water column well-mixed. This mixing process is enhanced by predominantly strong winds in this season. In spring, the heat balance becomes positive leading to a warming of the surface waters, which keep staying at the surface due to its increasing buoyancy. The warm water mass at the surface continues receiving heat and forms a warm upper layer, which is separated from the cold bottom layer by a thermocline. In summer, the water column gets most stratified showing strongest vertical temperature gradient, as a maximum of heat has accumulated in this season and weak winds induce relatively small mixing of the water column. This thermocline majorly occurs in the central and northern North Sea, with a mean depth range from about 10 to 40 m. In general, the thermocline depth increases from early spring to late autumn (Mathis et al., 2013).

In contrast, fresh water discharge from rivers generate a thin light surface layer around the river mouth, establishing a halocline nearby. This halocline can occur at any time of the year; it is strongly affected by the high variability of river discharge into the North Sea (Mathis et al., 2013). In addition, the Baltic Sea transports low salinity water into the North Sea. These low saline waters stay at the surface in the Kattegat, the Skagerrak and off the Norwegian coast, resulting in a stable halocline lasting for all seasons (Mathis et al., 2013). Noteworthy, the density, which forms the ocean stratification is influenced by both, temperature and salinity. This also means, that the pycnocline cannot only be determined by the thermocline but as in Norwegian Trench area also by the halocline.

Stratification decouples the surface and deep layers, potentially altering tidal current profiles. Observations of tidal current profiles in the central North Sea showed seasonal variations in the vertical structures, and Howarth (1998) ascribed these variation to different turbulence levels resulting from seasonal stratification. Van Haren (2000) observed that the largest velocity shear in the current profile occurs at the depth of strongest stratification. Further, Müller (2012) investigated the relationship between changing stratification and barotropic tidal transport and in this context discussed the role of vertical eddy viscosity and bottom friction by applying an analytical model.

However, the influence of stratification on tidal amplitudes or tidal ranges is relatively unexplored. Most studies of tidal ranges concentrated on century or millennial timescales under sea level rising scenarios (Hill, 2016; Pelling et al., 2013;

Hall et al., 2013; Holleman and Stacey, 2014). Müller et al. (2014) studied the seasonal variation of the M2 tide in a continental shelf sea due to seasonal stratification by applying a global model. Nevertheless, the knowledge of stratification effects on overall tidal ranges is still lacking, although it is actually more directly related to the coastal environment and maritime activities.

1.5 Objectives

The current study aims to improve the knowledge about tides of the recent past under special consideration of the aspects mentioned above. In details, it investigates changing tides from 1950 to 2014 in the North Sea by means of a regional ocean model. It quantifies the contributions to changes of tidal ranges at 22 tide-gauge stations by looking at the individual climate-related factors, such as sea-level rise from the open ocean, changing heat flux, wind stress variations and changes of the river runoff. The underlying dynamics explaining those individual contributions to the MTR changes are also discussed in this thesis, with a major focus on the effect of stratification in order to particularly explain the influence of heat flux and river input. Noteworthy, this study only concentrates on changes induced by mechanisms generated on the Northwestern European shelf. Whereas, the influence of the entire North Atlantic Ocean or even the global ocean is not considered.

2. Methods

In this section, the model configurations of the simulations are described. A three-dimensional prognostic model, Hamburg Shelf Ocean Model (HAMSOM) (Backhaus, 1985), was applied for the simulation of the circulation in the North Sea. Two contrast numerical experiment groups are set up in order to investigate the contributions of climate-related processes on the trends of coastal tidal ranges and their underlying dynamics.

2.1 HAMSOM model

The HAMSOM model is a three-dimensional regional, free surface, baroclinic, hydrodynamic model. The primitive equations in HAMSOM are defined in Cartesian x, y, z coordinate on the Arakawa C-grid (Arakawa & Lamb, 1977). The partial differential equations of momentum and continuity are integrated over each layer. A semi-implicit scheme is applied to solve for free surface problem and vertical momentum transfer (Backhaus, 1983). Incompressibility and hydrostatic equilibrium are assumed and Boussinesq approximation is implemented in the model. The Coriolis terms utilize a stable second-order approximation. The Lax-Wendroff scheme is applied for temperature and salinity advection in the transport equations for heat and salinity. The equation of state utilizes UNESCO formula.

The quadratic stress terms are applied for the bottom friction. The bottom layer is defined as 30 m upward from seabed in the model. The non-dimensional friction parameter is set to 0.0020 and was applied uniformly to the entire North Sea as suggested by the master thesis (Li et al., 2018).

Horizontal eddy viscosity is calculated according to Smagorinsky scheme (Smagorinsky, 1993). CFL condition and Reynolds number constrains on horizontal eddy viscosity are included for model stability recommended by Griffies & Hallberg (2000). The vertical turbulence closure scheme is associated with the Mellor-Yamada level-2 type formulation (Mellor & Yamada, 1974). The nondimensional parameters used in the calculation of horizontal and vertical eddy viscosity coefficients for the North Sea are discussed in the master work by Li et al. (2018).

Total surface heat flux is calculated by bulk formulas using sea surface temperature and atmospheric variables (Pohlmann, 2006). It is the sum of solar incoming short wave radiation, net long wave radiation, sensible heat flux, and latent heat flux. The original model does not output this variable. For further analysis of surface heat flux variations, we implemented a module inside the model for its daily storage.

2.2 Model configurations

In this study, two model grids were set up: the coarser outer model grid “NWCS20D” (47.68° N - 63.88° N, 15.08° W – 13.92° E) with a horizontal resolution of 1/3° longitude and 1/5° latitude (c.a. 20 km) and vertically 31 layers (thickness range from 5 to 1000 m) covering the whole northwest European shelf ocean, and - within this domain - the fine resolved model grid “NS” (50.87° N - 60.35° N, 4.06° W - 13.15° E) with a horizontal resolution of 1/24° longitude and 1/40° latitude (c.a. 3 km) and vertically 30 layers (thickness range from 5 to 50 m) covering the whole North Sea

(Fig. 3a). The NWCS20D model was applied to produce open boundary conditions for the fine NS model. The fine resolution in the North Sea is used to get a more accurate representation of the SSH values at tidal stations. We cannot apply an even finer resolution due to limited computing resources, and also due to the fact that the model does not account for drying and flooding, which should be considered if the current resolution is increased, in particular for the Wadden Sea area.

The entire simulation period of both models is from 1948 to 2014, with a time step of 3 min. The initial two-year period is used for model spin-up and the rest is our period of interest during which the observational data are also available. The results of the NWCS20D model was saved every 12 min for the boundary forcing of the inner model, in order to allow a smooth propagation of tidal waves into the North Sea. In addition, hourly results of the NS model were saved in order to compare them with the observational data and for a further analysis of the tidal characteristics.

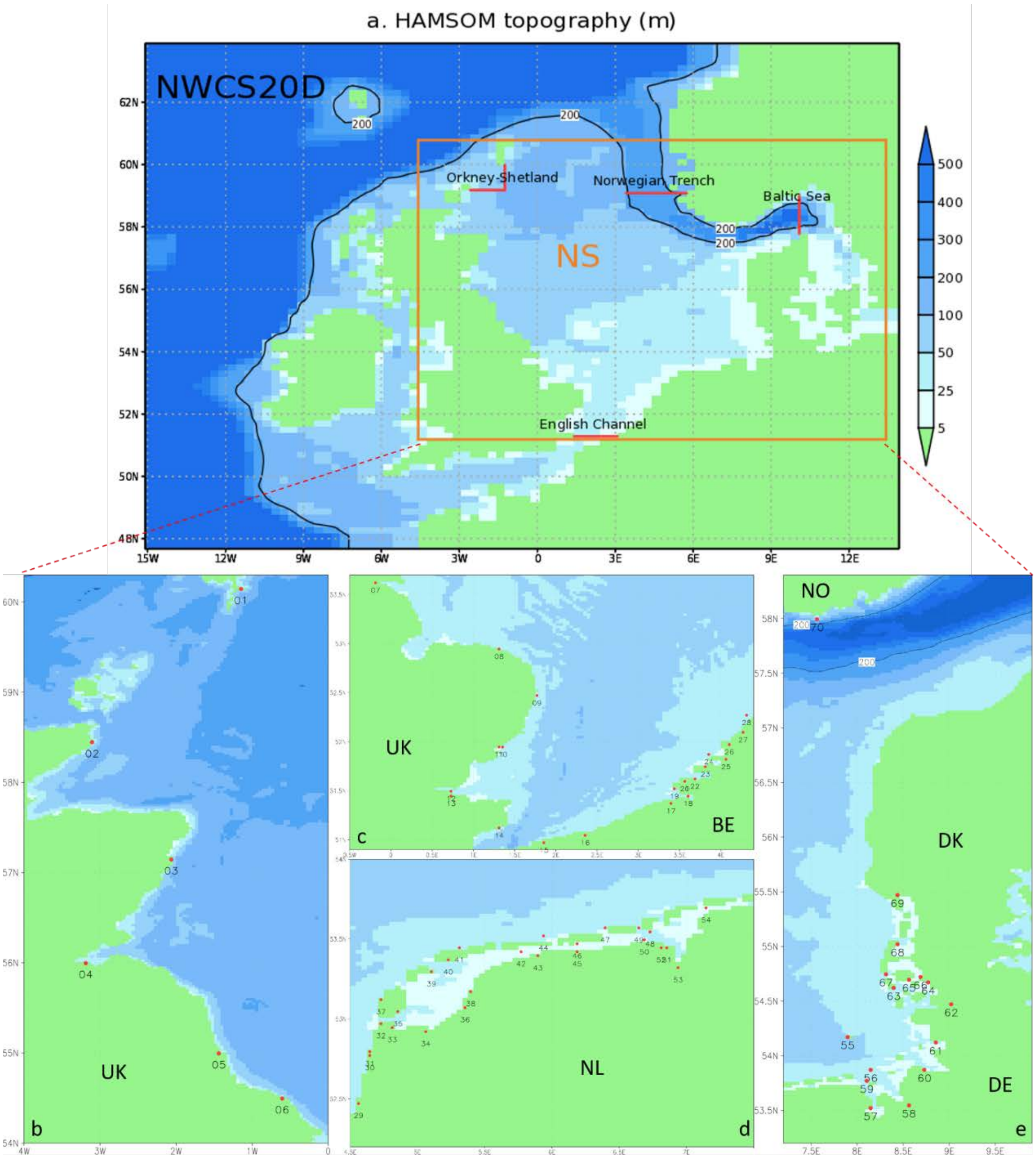

Fig. 3 a HAMSOM topography in NWCS20D model domain with 20 km resolution. The NS model domain is inside the orange rectangle. The red lines display the sections for transport validation. b-e The location of 70 tidal stations with numbering. UK: United Kingdom: BE: Belgium; NL: Netherlands; DE: Germany; DK: Denmark; NO: Norway.

2.3 Forcing data

The bathymetry data was derived from the SRTM30_PLUS database with a spatial resolution of 30″ (https://topex.ucsd.edu/WWW_html/srtm30_plus.html). It is an estimated topography product based on a satellite-gravity model (Becker et al., 2009). The original data was interpolated to both the outer and inner model grids (Fig. 4).

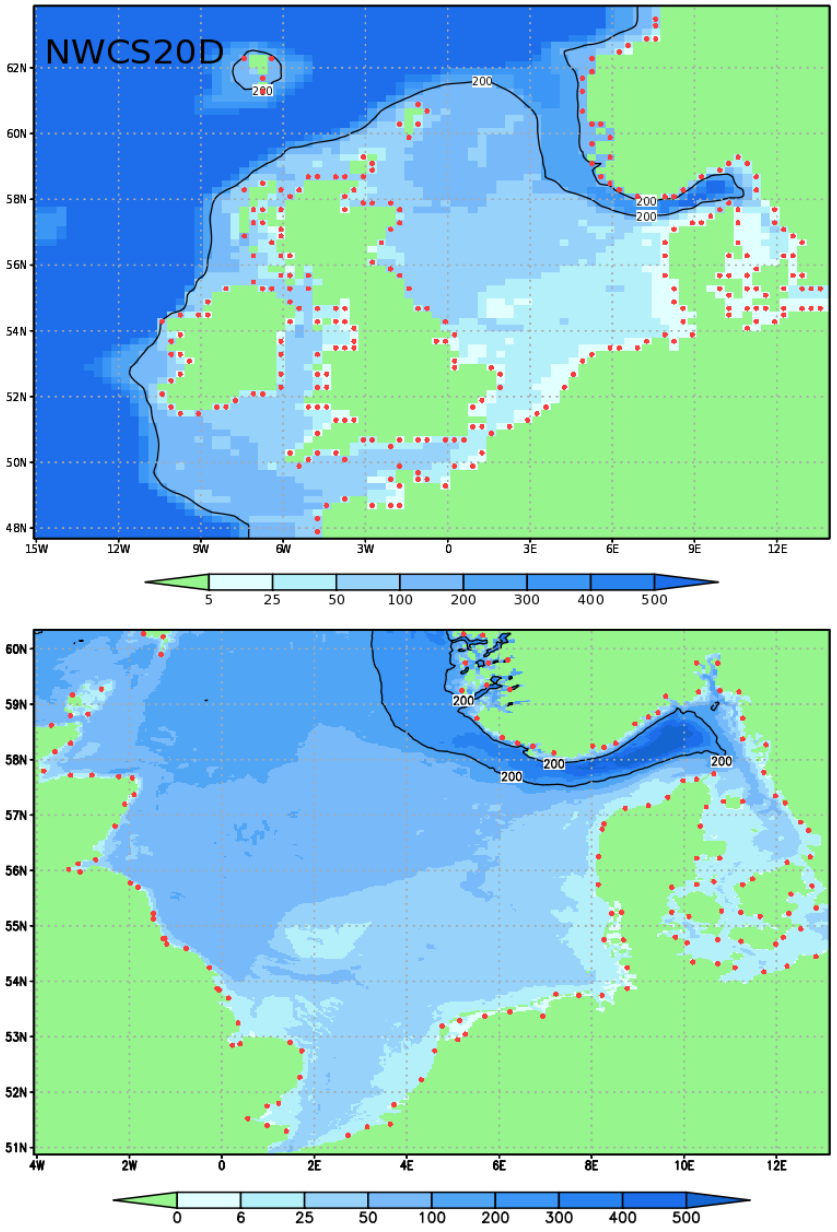

Fig. 4 Interpolated topography for NWCS20D (upper panel) and NS (lower panel) model domains. Red dots marks the locations of river input points for both model domains.

Both models were driven by tides, atmospheric forcing (including heat flux, wind stress, and sea level pressure), and river input. The atmospheric forcing was derived from the NCEP R1 dataset (Kalnay et al., 1996). Parameters, i.e., air temperature at 2 m, special humidity at 2 m, sea level pressure, total cloud cover, surface precipitation rate, and wind u/v components at 10 m, were used to calculate surface heat flux, precipitation and wind stress. The spatial resolution of the original dataset is 2.5° longitude and 2.5° latitude with a temporal resolution of 6 hours. Even though reanalysis dataset with a finer spatial and temporal resolutions, like CFSR, ERA-Interim and ERA5 are available for recent years, only very few dataset cover the entire period from 1948 until present.

The river discharge was also included using daily WaterGap model data (Müller Schmied et al., 2014), a global hydrological model with a horizontal resolution of 0.5 degrees. The WaterGap model data were integrated to the closest coastline points in the HAMSOM grid (Fig. 4) to assure a consistent volume input of freshwater into the ocean.

Regarding the open boundary conditions of the NWCS20D model, the tidal signal and the dynamic heights were prescribed at the open lateral boundaries. We applied 13 tidal components (eight primary: M2, S2, N2, K2, K1, O1, P1, Q1; two long period: Mf, Mm; and three non-linear: M4, MS4, MN4) derived from the TPXO8-atlas model data (https://www.tpxo.net/global/tpxo8-atlas) with OSU Tidal Prediction Software (Egbert et al. 2002). The open boundary temperature and salinity (T and S) profiles were extracted from the WOA13 V2 monthly climatology dataset (Locarnini, et al., 2013; Zweng, et al., 2013), and the same was true for initial T and S field. The original T and S variables have a horizontal resolution of 0.25 degrees. Using the open boundary T and S distribution, the dynamic height was calculated. In addition, the eastern boundary SSH of the outer model was set to by 0.13 m to match the observed inflow from the Baltic Sea presented in Fig. 15 of Pätsch et al. (2017). More details will be provided in the Section 3 Validation.

Hourly dynamic height anomalies are also considered but only for the experiment group aiming to quantify the contributions of climate-related processes. The dynamic height anomalies, i.e., deviations from the mean dynamic height averaged over the entire period, were derived from satellite data, and provided by the Siegen University (Dangendorf et al., 2019). This anomaly signal contains significant inter-annual variations of the local MSL along the open boundary.

As the calculation time step of both models is 3 min, these forcing data, i.e. 6-hourly atmospheric forcing parameters, daily river discharge, monthly T and S, and hourly dynamic height anomalies, are linearly interpolated to the calculation time step inside the model. They are also spatially interpolated into wet grid points of both outer and inner model in the model preprocess procedure.

2.4 Numerical experiments

2.4.1 Contrast group A

Four potential influencing factors, i.e. MSL rise along the open boundary, changes in surface heat flux, changes of wind stress, and changes in riverine freshwater input, were investigated in Group A in order to quantify the contribution of each process responsible for the observed positive trends of tidal ranges at coastal tide-gauge stations. Subsequently, the following five experiments were set up:

1) reference run (control run, CR): the realistic run from 1948 to 2014;

2) scenario 1 (BS): changing boundary SSH conditions for the outer model: repeated application of the dynamic height anomalies of the first decade (1950-1959) for the later decades (1960-2014);
3) scenario 2 (HF): changing surface heat flux for both the outer and the inner models: repeated application of heat flux variables (air temperature at 2 m, total cloudiness, specific humidity, precipitation, and wind speed) of the first decade for the later decades;
4) scenario 3 (WS): changing wind stress for both the outer and the inner models: repeated use of the first-decade wind stress forcing for the later decades;
5) scenario 4 (RI): changing river input for both the outer and the inner models: repeat use of the first-decade river discharge for the later decades.

Noteworthy, dynamic height anomalies are included for all experiments in Group A. Each experiment contains two simulations: the outer and the inner model simulations. All scenario runs share the same initial conditions as for the reference run. Necessary corrections like interpolation (non-leap to leap year) and omission (leap to non-leap year) were carried out for repeatedly applied forcing data in leap years and non-leap years. Besides, wind not only inputs momentum into the ocean but also influences ocean thermodynamics through surface heat flux. In HF scenario, the wind effect on surface heat flux are considered, whereas the momentum input effect is ignored. However, in WS scenario, the momentum input into the ocean is taken into account, while the thermodynamic influence is neglected.

2.4.2 Contrast group B

The numerical experiments in Group B investigate the influence of baroclinicity on coastal tidal ranges, which should help to understand the underlying dynamics responsible for the phenomena observed in the Group A scenarios. For this purpose, two contrasting experiments were carried out, namely a baroclinic (BC) and a barotropic (BT) one. The dynamic height anomalies were not considered for experiments in Group B. For the barotropic runs, the outer and the inner model were both set into the barotropic mode. The open boundary SSH for the outer model does not consider the dynamic height, since the dynamic height compensates the lateral density gradients which are ignored in the barotropic case. In order to allow a proper comparison of the two contrasting experiments an identical average MSL along the open boundaries is prescribed. For this reason, the averaged dynamic height along the open boundaries of the outer model was set to zero in the baroclinic simulations. Noteworthy, the river discharge was also applied in barotropic mode, however, it only causes a volume input and a subsequent increase of the local SSH without any influence on the density.

2.5 Interpolation for tidal stations

The inverse distance weight (IDW) method was applied to the model data in order to interpolate the simulated SSH values exactly to the positions of the tidal stations by using the neighboring 16 model grid points. For this interpolation, several tidal gauge stations had to be omitted, since their locations were too far away from the wet grid points of the model, e.g. Station No. 58 and 62 (Fig. 5). 16 neighboring points were chosen for the IDW method, in order to have more stations available for analysis, e.g., along the British coast.

A sensitive test for selecting the optimal number of neighboring points used in the IDW method was implemented. For this purpose, we compare the SSH time series interpolated by surrounding 4, 16 and 36 points. The derived error metrics, like bias and root mean square error (RMSE), were used to evaluate the specific differences. As seen for the station Helgoland Binnenhafen (No. 55), the interpolated SSH time series derived from different numbers of surrounding grid points are relatively similar (Fig. 6). Obviously, the biases and RMSEs among those differently interpolated SSH time series are also quite small. Hence, it can be concluded that the interpolated SSH values are not sensitive to the number of neighboring points used for the IDW method.

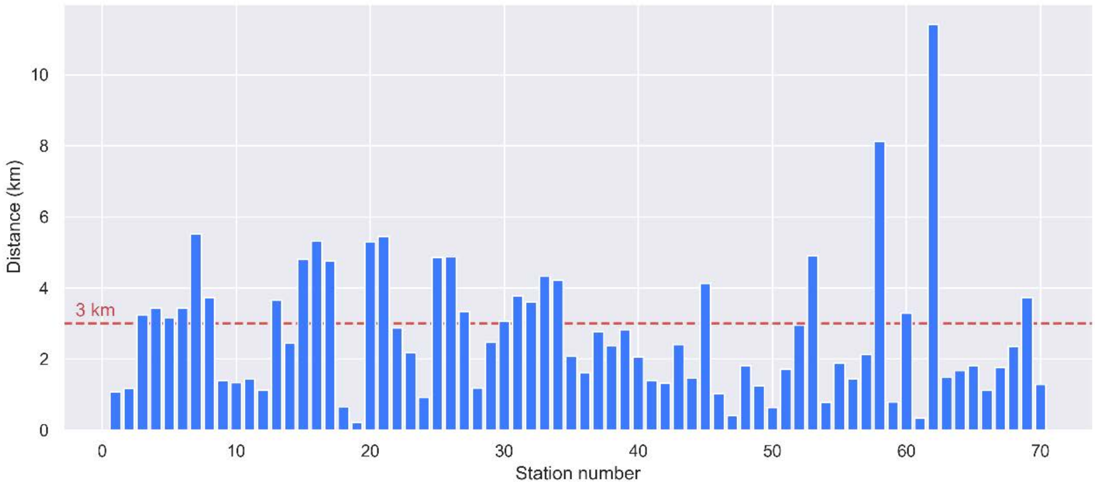

Fig. 5 The distance between tidal stations and the closest model wet point.

After interpolation, the mean SSH was subtracted from both, the simulated and the observed SSH, since their reference levels are different and our study is focused on the variation of the sea surface elevation. Hence, in the following, the term SSH refers always to values with a subtracted mean value.

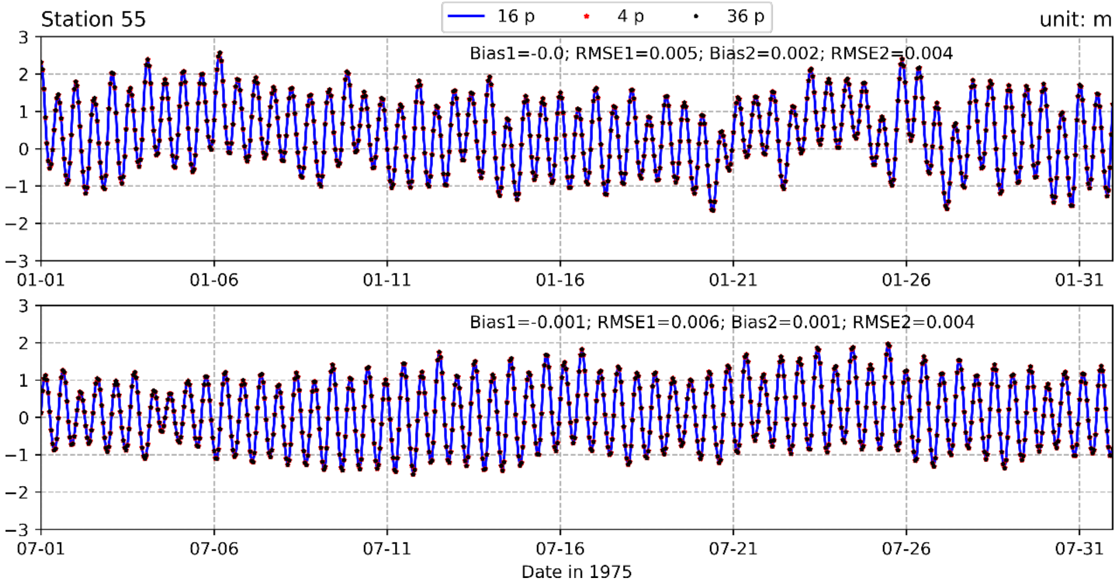

Fig. 6 Time series of modelled SSH at the station 55 (Helgoland Binnenhafen) for January (upper panel) and July (lower panel) 1975. Blue lines, red stars, and black dots represent SSH values interpolated from 16, 4, and 36 neighboring model grid points, respectively. Bias1 and RMSE1 are error metrics for blue lines and red stars; Bias2 and RMSE2 are error metrics for blue lines and black dots.

3. Model validation

Before the analysis of the model results, the quality of the model behavior should be verified. The water volume transports into and out of the North Sea are a good first indication for the quality of the simulated North Sea circulation. Reasonable inflow and outflow rates through sections near the boundaries of the North Sea are a prerequisite. A further comparison of sea surface elevations between model results and tidal gauges obviously is another significant indication for the model quality with respect to an accurate reproduction of the tidal characteristics in the North Sea. Besides, a brief comparison of T and S fields is also conducted in this section.

3.1 Section transport

In this subsection, the 12-year average transports (1998-2009) through selected sections (see Fig. 3) are compared to estimations from observations in Fig. 15 of Pätsch et al. (2017). The positions of selected sections are similar to the definition in the paper. These section transports determine the basic water mass fluxes into and out of the North Sea.

The outflow from the Baltic Sea significantly influences the circulation in the North Sea and in turn also in the German Bight. Thus, the SSH along the eastern open boundary of the outer model must be chosen adequately, in order to prescribe the correct outflow of Baltic Sea water into the North Sea. A sensitive test regarding the eastern boundary SSH was performed to determine the most suitable SSH value. We conducted these numerical experiments with an eastern open boundary SSH value of 0.12, 0.13, 0.14, and 0.16 m, respectively, and calculated the corresponding water transport through selected sections for each of the chosen eastern boundary conditions.

Table 1 Simulated and observed (reference) 12-year (1998-2009) average transports through selected sections. Positive (negative) values represent transports into (out of) the North Sea. Unit in Sv.

East boundary SSH rise	English Channel	Baltic Sea	Norwegian Trench	Orkney-Shetland
reference	0.100-0.170	0.015	-0.90	0.30
0.12 m	0.102	0.012	-1.34	0.31
0.13 m	0.102	0.016	-1.34	0.31
0.14 m	0.101	0.017	-1.34	0.32
0.16 m	0.099	0.025	-1.31	0.33

Table 1 lists the simulated section transports for different boundary SSH values as well as observed reference values. An increasing eastern boundary SSH value leads to an increased outflow from the Baltic Sea as expected, whereas the inflow through English Channel slightly declines. In the same way, also the Norwegian Trench outflow decreases, whereas the inflow through the Orkney-Shetland section intensifies. Comparing the section transports with observed reference values given in Pätsch et al. (2017), it turned out that an eastern boundary SSH value of 0.13 m gives the best agreement with observations. Therefore, in the following study this value was chosen for the SSH along the eastern open boundary.

The comparison with the reference section transports reflects that our model well reproduces the English Channel inflow, and the Orkney-Shetland current, whereas the Norwegian Trench outflow is not captured exactly (simulation is about 50% larger). However, it is not clear, whether the observed values for the Norwegian Trench outflow are really correct. Also in Pätsch et al. (2017) most models show significantly larger outflow values than the observations for this section.

3.2 Tide gauges

In this subsection, the simulated sea surface elevation was compared for 70 tide gauges from 1950 to 2014 kindly provided by Siegen University (Jänicke et al, 2021). Fig. 3b-e displays the locations of these 70 tidal stations. To compare the model results with tidal gauge data, first the IDW method was applied to the model data to interpolate the simulated SSH values exactly to the positions of the tidal stations by using the neighboring 16 model grid points, suggested in the Section 2.5.

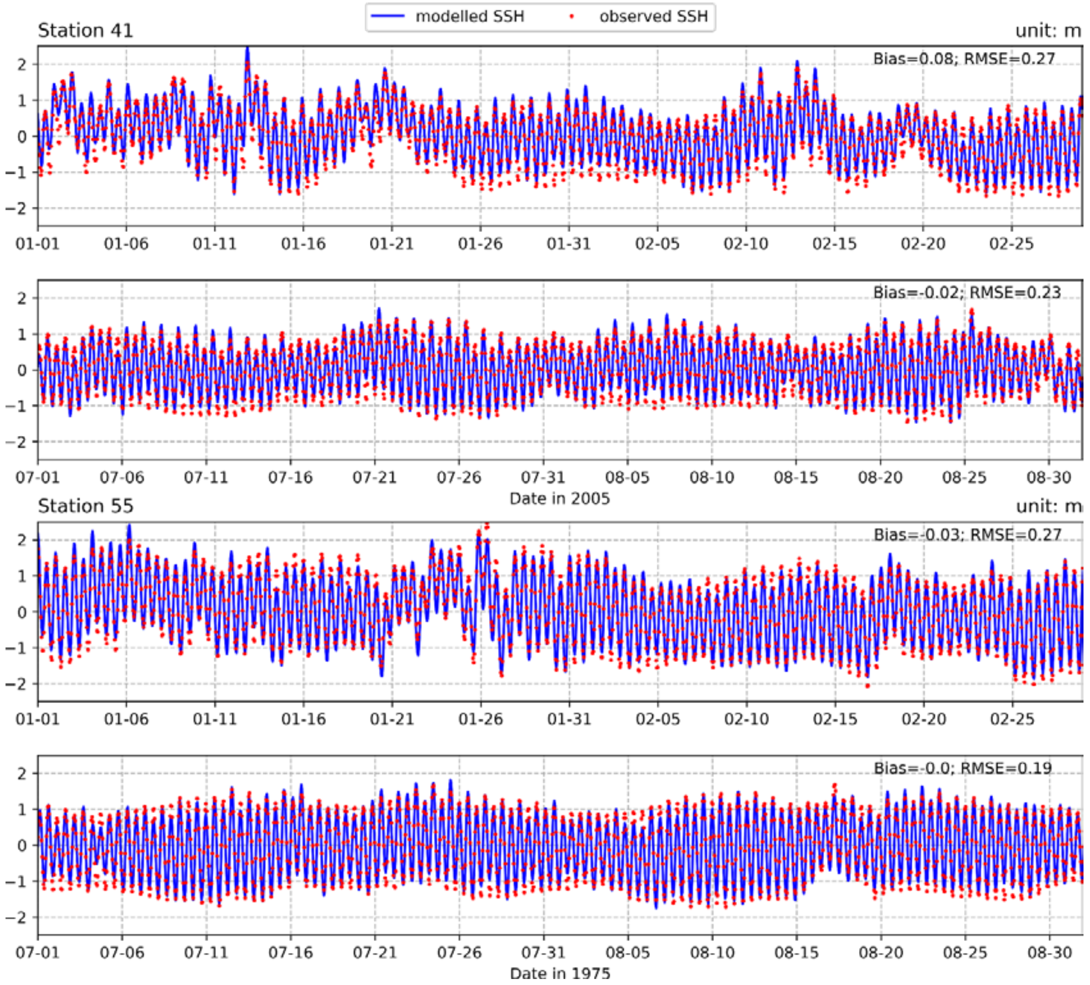

Fig. 7 Time series of modelled and observed SSH at the station Terschelling Noordzee (No. 41) in Jan-Feb and Jul-Aug 2005 (upper two panels) and at the station Helgoland Binnenhafen (No. 55) in the same months in 1975 (lower two panels), respectively. Blue lines are modelled SSH data; red dots are observed SSH data.

The time series of SSH at the stations Terschelling Noordzee (No. 41) and Helgoland Binnenhafen show that the model well reproduced sea surface elevation. The blue lines showing the model SSH and red dots representing the observational data (Fig. 7) agree well in phase and magnitude (small bias and RMSE of about 0.1 and about 0.2, respectively). Furthermore, the accuracy of model results is reflected by the correlation in the scatter plots for different stations in Fig. 8a as well as by the slope of model values vs. observation values. The slope here was calculated by the least-squares fitting method. For 22 stations, correlation coefficients were calculated to be above 0.90 and the slopes were within 0.90 and 1.10. Our further analyses will focus on these 22 stations.

a. baroclinic

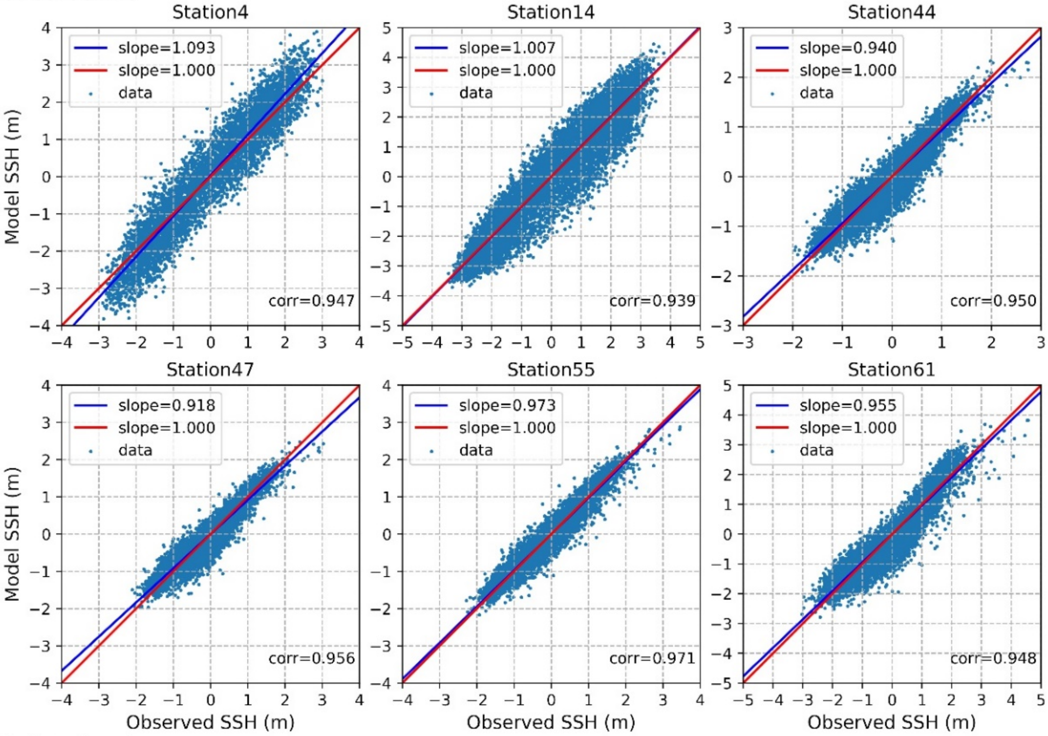

b. barotropic

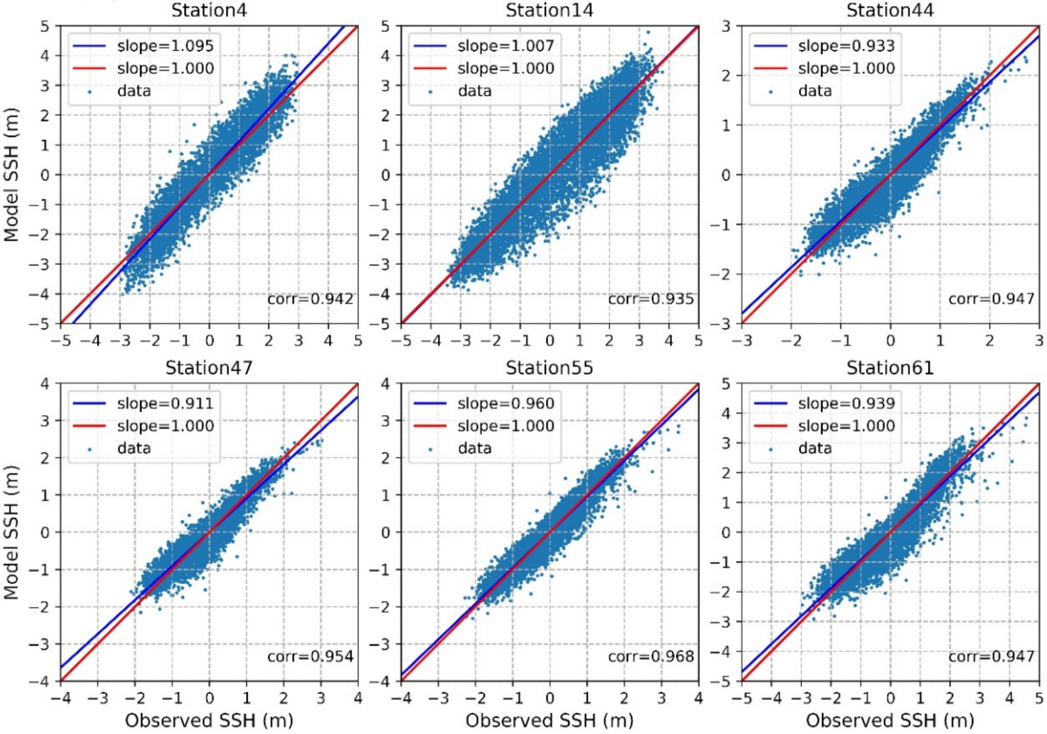

Fig. 8 Modelled versus observed SSH for the baroclinic simulation (a) and the barotropic simulation (b) with slopes and correlation coefficients. The blue lines are the regression lines of scatter dots calculated with least squares method. The red lines display reference lines with slope 1.

The limitations related to a validation by means of tidal gauges should also be noticed. The tidal stations are not exactly located on the model grid points, so normally an interpolation has to be applied using model values of surrounding wet grid points. The IDW method was used in this study, which produces reasonable sea surface elevations at the tidal stations, but still the distance between wet model grid points and tidal stations limits the quality of validation, since the sea surface elevation in general is strongly influenced by local processes. It is more reasonable to do the validations for stations with a distance of 3 km (model resolution) or less between model grid points and tidal gauge location (see Fig. 5). Topography also strongly dominates sea surface elevations especially for coastal regions. Most stations shown in Fig. 3d are located in the Wadden Sea, where the model bathymetry is modified artificially, since the HAMSOM model is not able to reproduce drying and flooding. Therefore grid cells are only allowed to be land cell or grid cells with minimum depth of 6 m. This specific modification of the topography strongly limits the adequate simulation of the SSH at the stations in Wadden Sea.

3.3 T and S

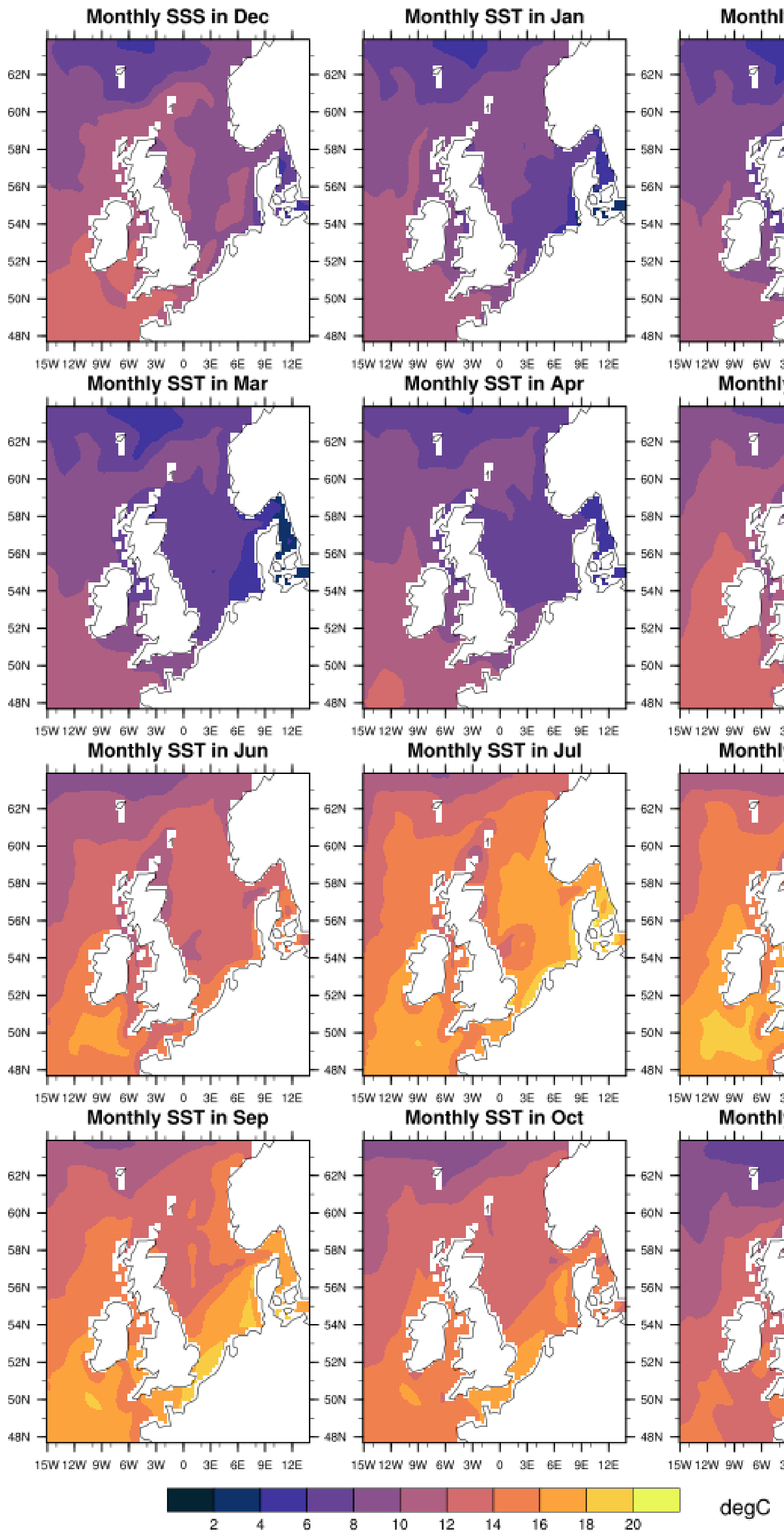

Monthly SSS in Dec

Monthly SST in Jan

Monthly SST in Feb

Monthly SST in Mar

Monthly SST in Apr

Monthly SST in May

Monthly SST in Jun

Monthly SST in Jul

Monthly SST in Aug

Monthly SST in Sep

Monthly SST in Oct

Monthly SST in Nov

Fig. 9 Monthly mean temperature at the surface layer in 2001 in the North Sea. Data retrieved from HAMSOM simulation results.

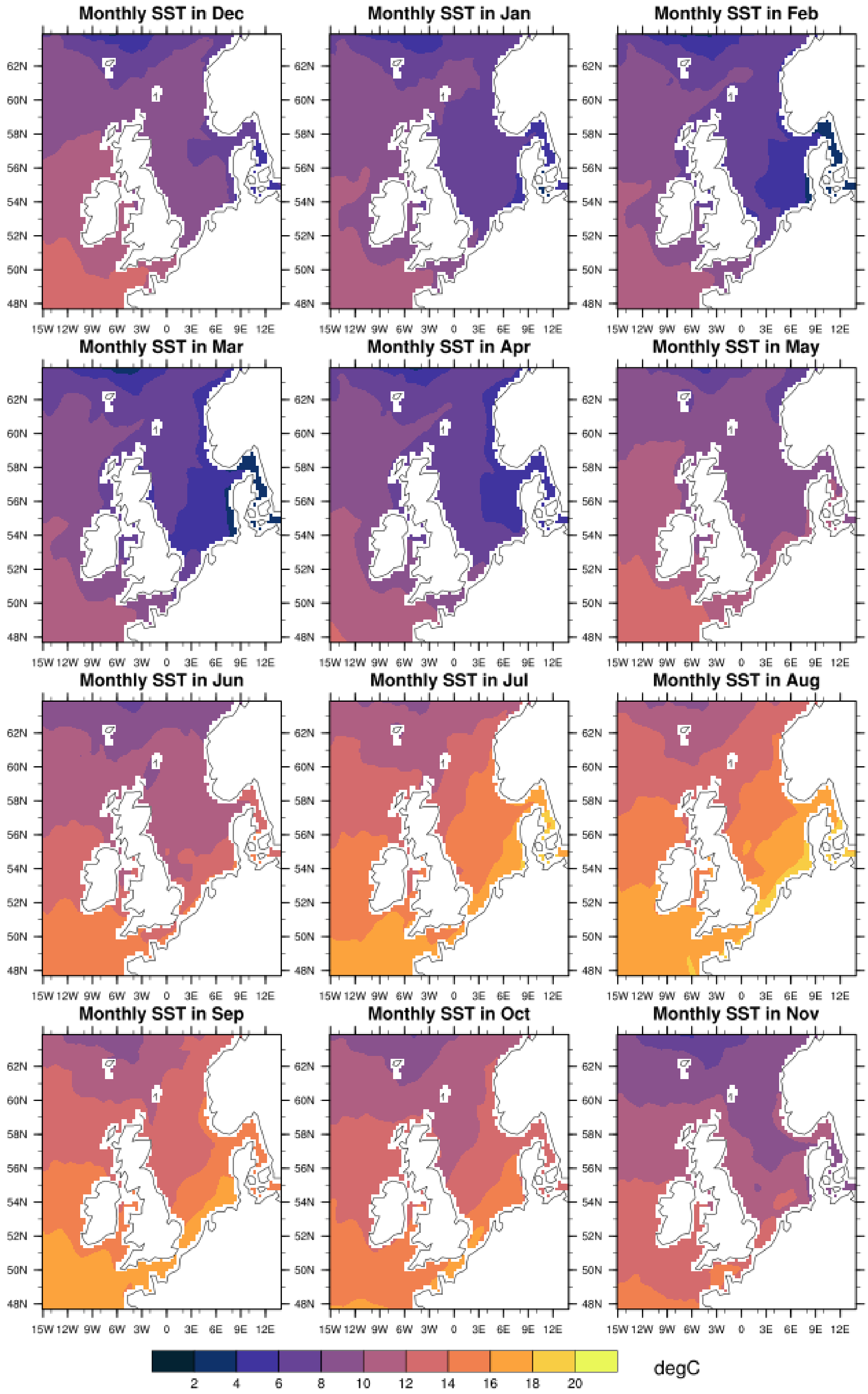

Fig. 10 Monthly mean temperature at the surface layer in 2001 in the North Sea. Data retrieved from ORAS5 reanalysis data.

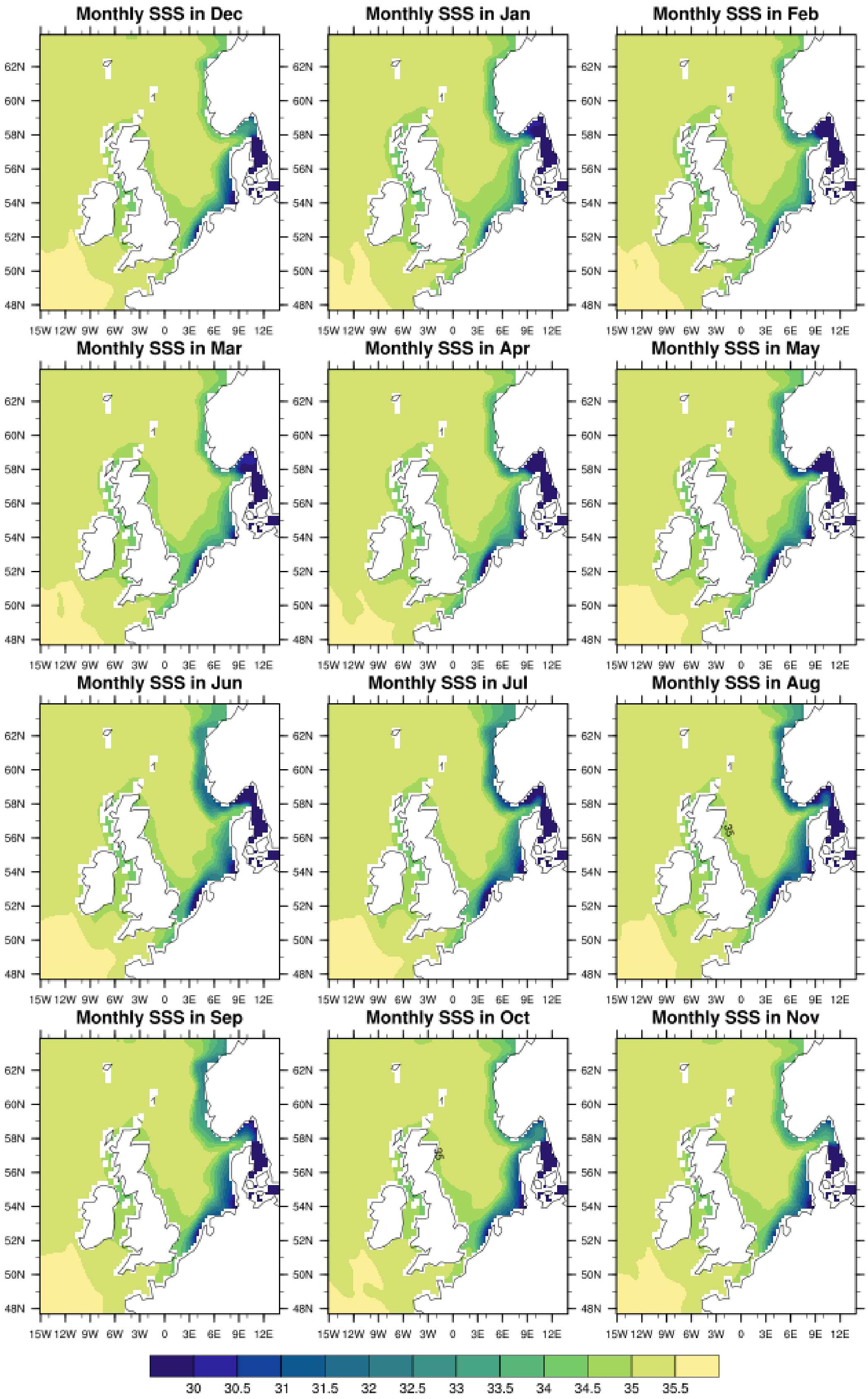

Fig. 11 Monthly mean salinity at the surface layer in 2001 in the North Sea. Data retrieved from HAMSOM simulation results.

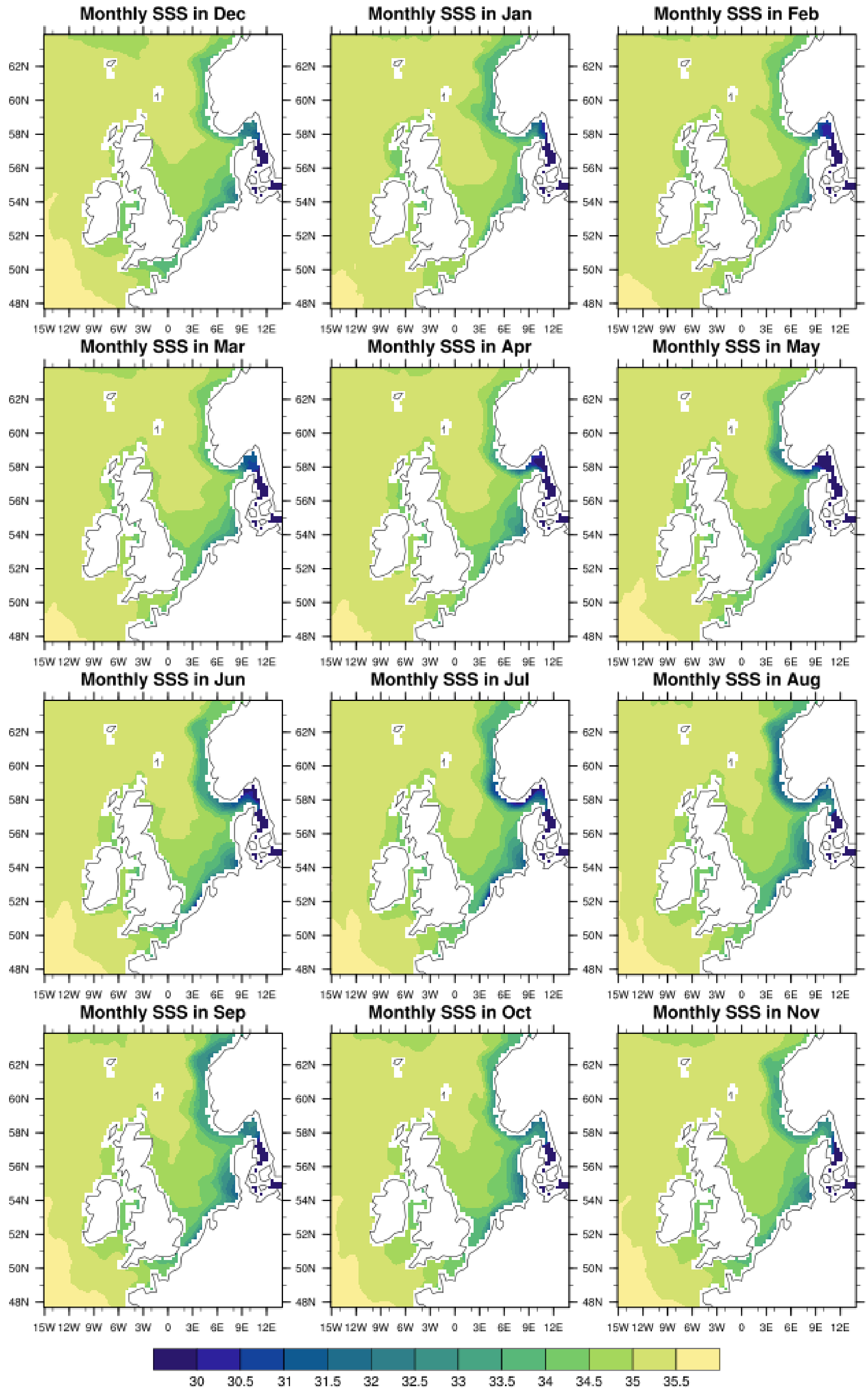

Fig. 12 Monthly mean salinity at the surface layer in 2001 in the North Sea. Data retrieved from ORAS5 reanalysis data.

A rough comparison of T and S fields at the surface layer between simulation and reanalysis data is conducted in 2001. The reanalysis data is ORAS5 reanalysis data (Zuo et al., 2019) with a horizontal resolution of 0.25°. They are interpolated into the outer model girds and vertically averaged for the upper 10 m depth in order to compare with the model results. As shown in Fig. 9, Fig. 10, Fig. 11, and Fig. 12, the HAMSOM model generally captures reasonable seasonal variations of T and S field. The magnitude ranges of T and S show good agreement with reanalysis data, as well as horizontal distribution patterns. More details about HAMSOM model behavior on temperature and salinity distribution and development, can be seen from Pohlmann (1996) and Pätsch et al. (2017).

4. Results

In the last section, our model has been proven capable to well reproduce the sea surface elevation in the North Sea. Based on these convincing results, we analyze MTR and MSL at those 22 tide-gauge stations where the simulated SSH show good agreement with observed ones. The MTR used in this study is defined as the mean high water minus the mean low water with the mean calculated over the corresponding investigation period, i.e. annual and seasonal (majorly winter and summer) period in this paper. Similarly, the MSL is defined as the mean sea surface elevation with the mean calculated over the same corresponding investigation period.

4.1 Sensitivity with respect to different forcing mechanisms

In this subsection, the MSL trends and MTR trends over the period from 1950 to 2014 at 22 tide-gauge stations for the reference run (CR) and different scenario runs (BS, HF, WS, RI) are presented and they are associated with the variation of the corresponding driving mechanisms. The trend analysis in this study generally applies mann-kendall test (Mann, 1945; Kendall, 1975; Gilbert, 1987), which is a distribution-free trend test. For time series with autocorrelation over time, we applied a modified mann-kendall test by Yue & Wang (2004), which takes the effect of autocorrelation into account. The significance of calculated trends are presented in the Supplementary (Fig. S3-S8).

4.1.1 MSL trends

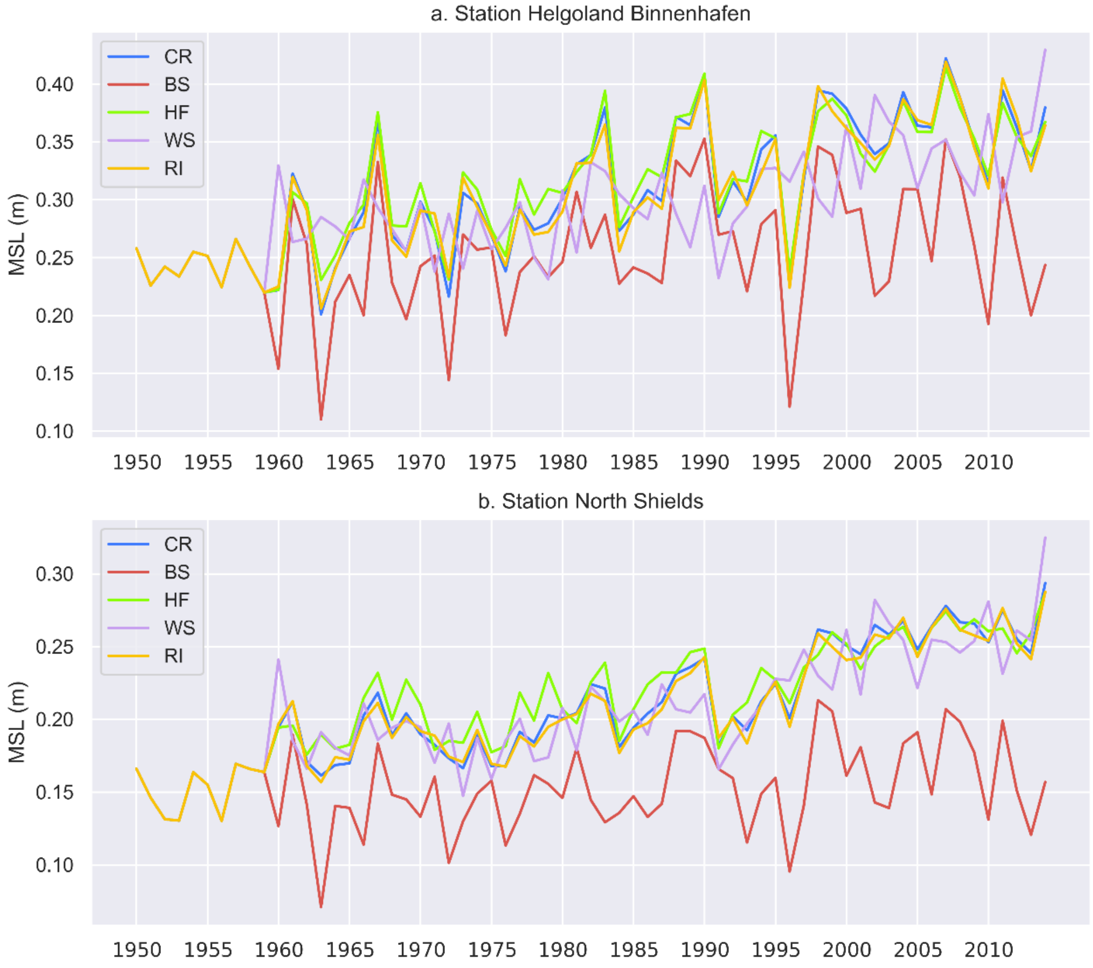

Fig. 13 Annual MSL time series at Helgoland Binnenhafen (a) and North Shields (b) for five experiments (CR, BS, HF, WS, RI).

Fig. 13a and b present the time evolution of the simulated annual MSL at station Helgoland Binnenhafen, Germany, and North Shields (No. 5), UK. These two stations are selected as being representative to exhibit coastal tidal behavior close to the northern entrance of the North Sea and in the inner part of the North Sea, respectively. The MSL for CR (blue) at both stations show clear positive trends over the period from 1950 to 2014, which commonly exists for other stations in the North Sea as well. This reflects that the open boundary SSH rise signal spreads to coastal regions of the North Sea. The

MSL for HF (green), WS (purple) and RI (orange) also exhibit positive trends except the MSL in the BS (red) scenario. Moreover, the MSL for HF, WS and RI differ from the MSL in the reference run, especially the MSL for WS.

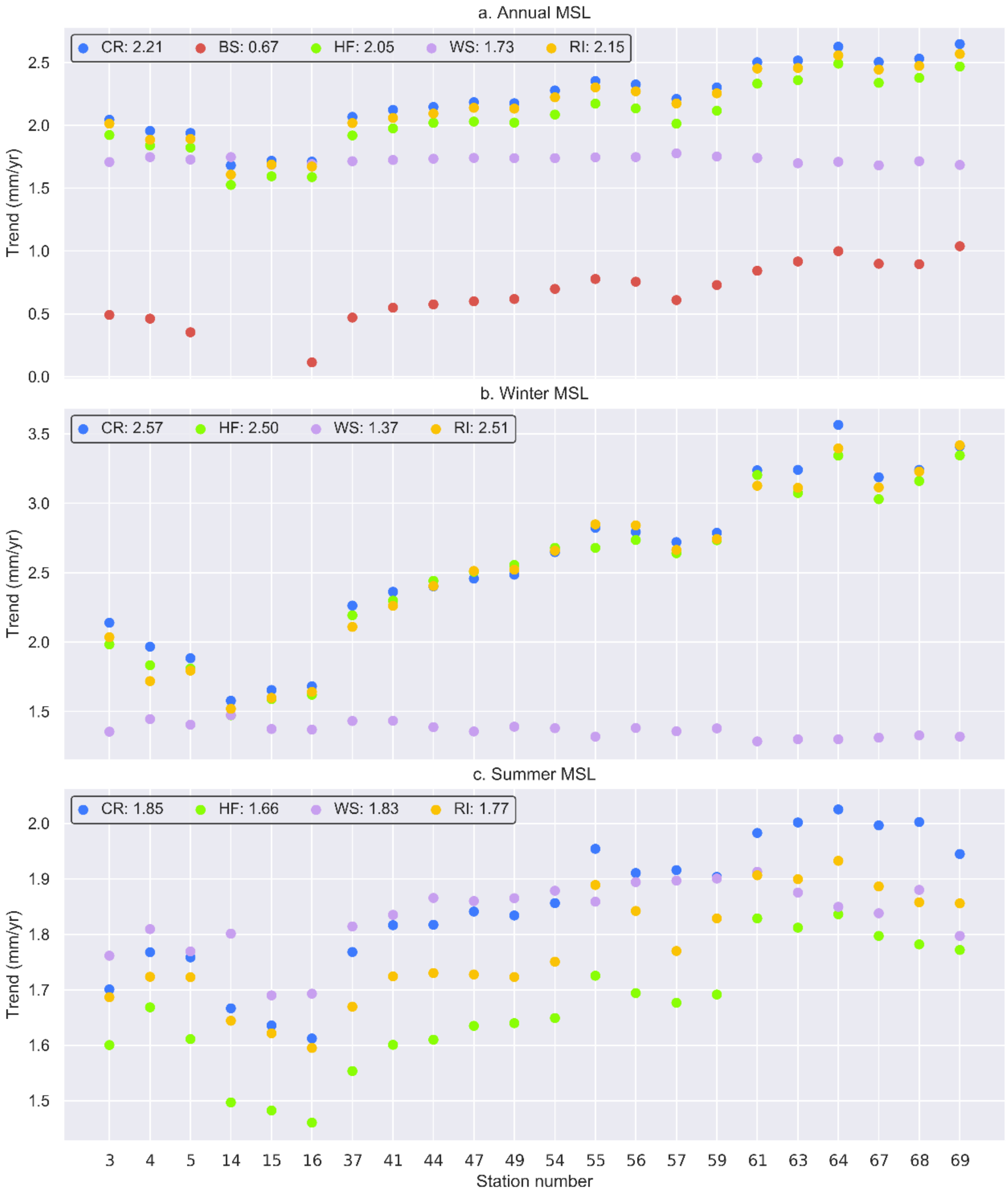

Fig. 14 a. Trends of annual MSL at 22 stations for five experiments (CR, BS, HF, WS, RI); b. Trends of winter MSL at 22 stations for four experiments (CR, HF, WS, RI); c. Trends of summer MSL at 22 stations for the same experiments as in 3b.

The annual MSL trends were analyzed at the 22 tide-gauge stations for all of these five experiments, shown in Fig. 14a. Regarding CR, all stations exhibit positive trends, the largest one is about 2.60 mm yr^{-1}. The trend averaged over all of these 22 stations is 2.21 mm yr^{-1}. Among the four scenario runs, trends of annual MSL are lowest for BS, with an average value around 0.67 mm yr^{-1}. Trends for HF are smaller than for CR, reaching an average of 2.05 mm yr^{-1}. Trends for WS exhibit the lowest spatial variance over the investigated stations, with an average value of 1.73 mm yr^{-1}. Besides, trends for RI are smaller than for CR but larger than for HF, with an average value of 2.15 mm yr^{-1}. The comparison of annual MSL trends for the different experiments indicates that the coastal MSL rise mainly originates from the open boundary SSH signal. Besides, the wind stress, the heat flux and river input also present significant influence on coastal MSL.

4.1.2 MTR trends

The tidal ranges at costal tide-gauge stations generally exhibit positive trends over the period from 1950 to 2014. Fig. 15a and c present the time evolution of the simulated annual MTR (CR) at station Helgoland Binnenhafen and station North Shields, respectively. The blue line shows the original time series. After removing higher frequencies (>1/18.61 yr^{-1}), depicted by the red line, clear positive trends can be seen at both stations, even though the trend for station North Shields is quite small. This positive trend commonly exists also for other stations in the North Sea. It reflects that, besides astronomical tidal oscillations (e.g. nodal tide), tidal ranges in coastal regions of the North Sea have been increasing since 1950.

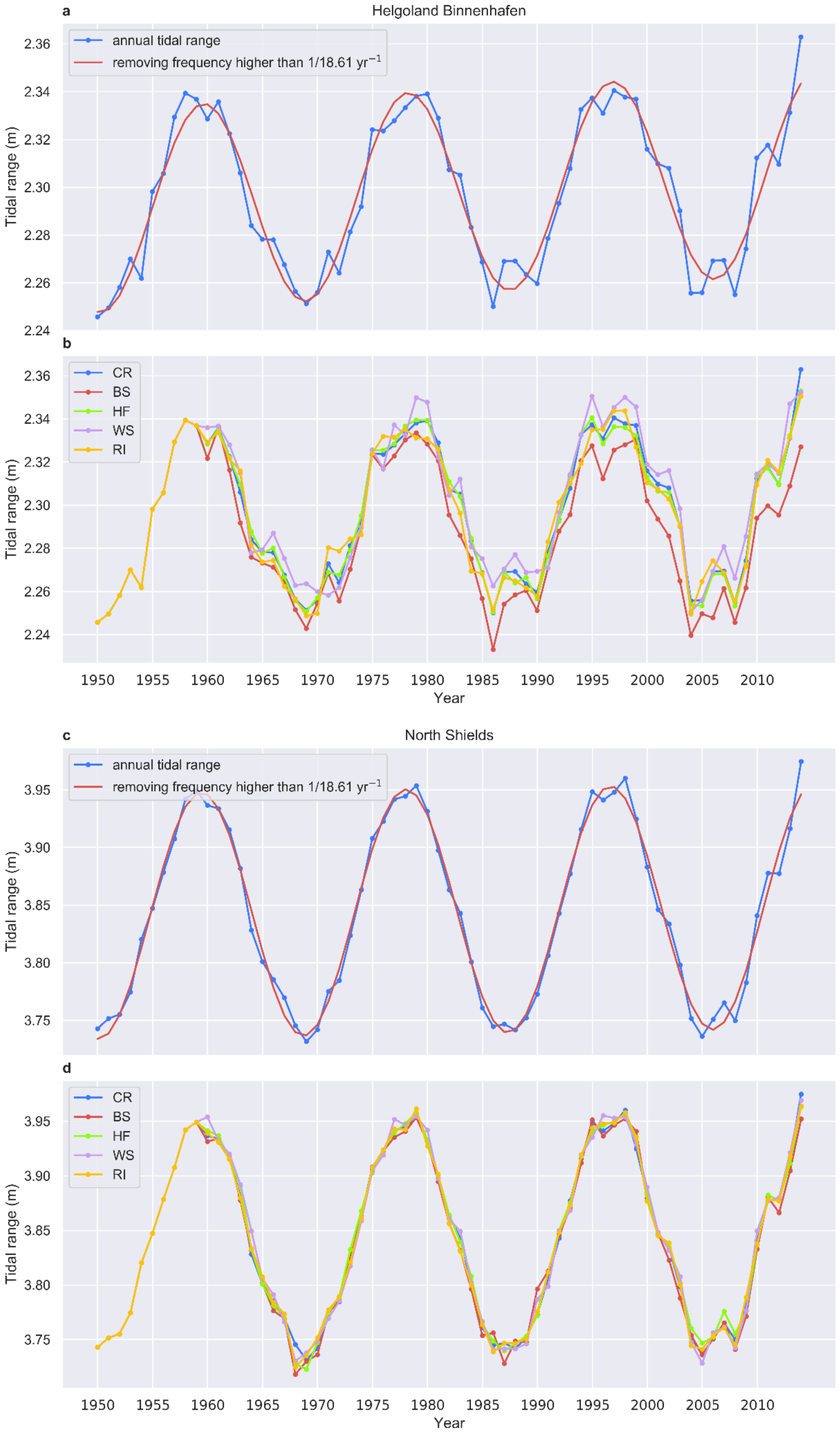
a
Helgoland Binnenhafen
annual tidal range
removing frequency higher than 1/18.61 yr^{-1}
Tidal range (m)
2.24
2.26
2.28
2.30
2.32
2.34
2.36
b
CR
BS
HF
WS
RI
Tidal range (m)
2.24
2.26
2.28
2.30
2.32
2.34
2.36
1950
1955
1960
1965
1970
1975
1980
1985
1990
1995
2000
2005
2010
Year
c
North Shields
annual tidal range
removing frequency higher than 1/18.61 yr^{-1}
Tidal range (m)
3.75
3.80
3.85
3.90
3.95
d
CR
BS
HF
WS
RI
Tidal range (m)
3.75
3.80
3.85
3.90
3.95
1950
1955
1960
1965
1970
1975
1980
1985
1990
1995
2000
2005
2010
Year

Fig. 15 Time series at Helgoland Binnenhafen: a. Simulated annual MTR for CR (filtered, unfiltered); b. Annual MTR for five experiments (CR, BS, HF, WS, RI). Time series at North Shields: c. Simulated annual MTR for CR (filtered, unfiltered); d. Annual MTR for five experiments (CR, BS, HF, WS, RI).

The evolution of annual MTR under different scenarios differs significantly from the one in CR (Fig. 15b). To clearly identify the differences of tidal ranges obtained from the different experiments, trends of annual MTR from 1950 to 2014 were calculated at 22 tide-gauge stations (shown in Fig. 16a) for all of these five experiments after removing the major nodal cycle by S_TIDE toolbox (Pan et al., 2018). The idea of the fitting is applying a linear regression model with a major nodal-cycle term for MTR (Mawdsley et al, 2015):

$$\mathrm{MTR(t)} = \mathrm{a} + \mathrm{bt} + \mathrm{c}\cos(\omega t + d)$$

where, $\mathrm{MTR(t)}$ is a function of time t in years. a, c, and d are constants. b is the linear trend for MTR that we aim to obtain. ω is the frequency for 18.61-year lunar nodal cycle with the value of $2\pi/18.61$ radians yr^{-1}.

Regarding CR, most stations exhibit positive trends in MTR, the largest one reaches around 0.5 mm yr^{-1}. The trend averaged over all of these 22 stations is 0.29 mm yr^{-1}. Among the four scenario runs, trends of annual MTR are lowest for BS, with an average value around zero. Trends for HF are generally smaller than for CR, reaching an average of 0.25 mm yr^{-1}. However, trends for WS are generally higher than for CR, reaching an average value of 0.34 mm yr^{-1}. Nevertheless, trends for RI are mostly smaller than for CR but larger than for HF, with an average value of 0.27 mm yr^{-1}. The comparison of annual MTR trends for the different experiments indicates that the tidal range increase mainly originates from the open boundary SSH signal. Besides, the wind stress, the heat flux and river input also significantly influence the tidal ranges.

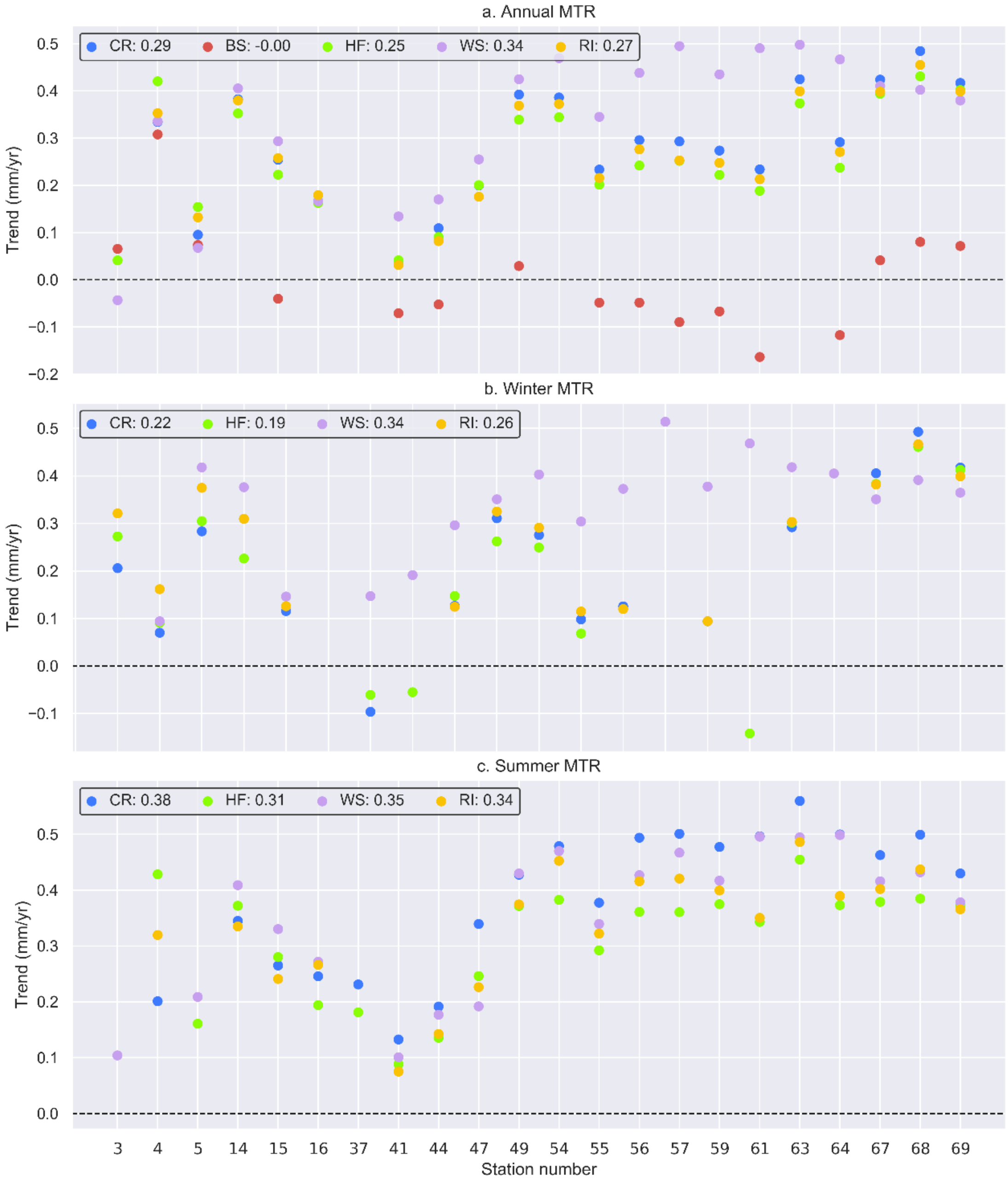

Fig. 16 a. Trends of annual MTR at 22 stations for five experiments (CR, BS, HF, WS, RI); b. Trends of winter MTR at 22 stations for four experiments (CR, HF, WS, RI); c. Trends of summer MTR at 22 stations for the same experiments as in 3b.

4.1.2 Effect of changing boundary SSH

The SSH signal at the open boundary of the outer model is composed of tides, dynamic height and dynamic height anomaly. No trends exist for the former two, while the dynamic height anomaly extracted from satellite data contains a clear positive trend. Fig. 17 displays the evolution of the annual SSH averaged along the open boundary of the outer model for the CR and the BS experiments. The SSH values for CR exhibit a positive trend of 1.73 mm yr^{-1}. This matches the trends observed by Church & White (2011) and Hay et al., (2015). In the BS experiment, the open boundary conditions show a constant periodic oscillation of the SSH, which corresponds to the copy of the 1950s time series. Since, compared to CR, much smaller trends of MSL (mostly within 0 to 1 mm yr^{-1}) and of MTR (mostly within -0.1 to 0.1 mm yr^{-1}) were only observed for BS (Fig. 14a and Fig. 16a, respectively), it can be concluded that the contribution of the increasing boundary SSH is the major factor for the coastal MSL rise and for the positive trend of costal tidal ranges. The seasonal trends are not investigated for the BS scenario, since the seasonal variation of the open boundary SSH is not as for important as the other physical processes.

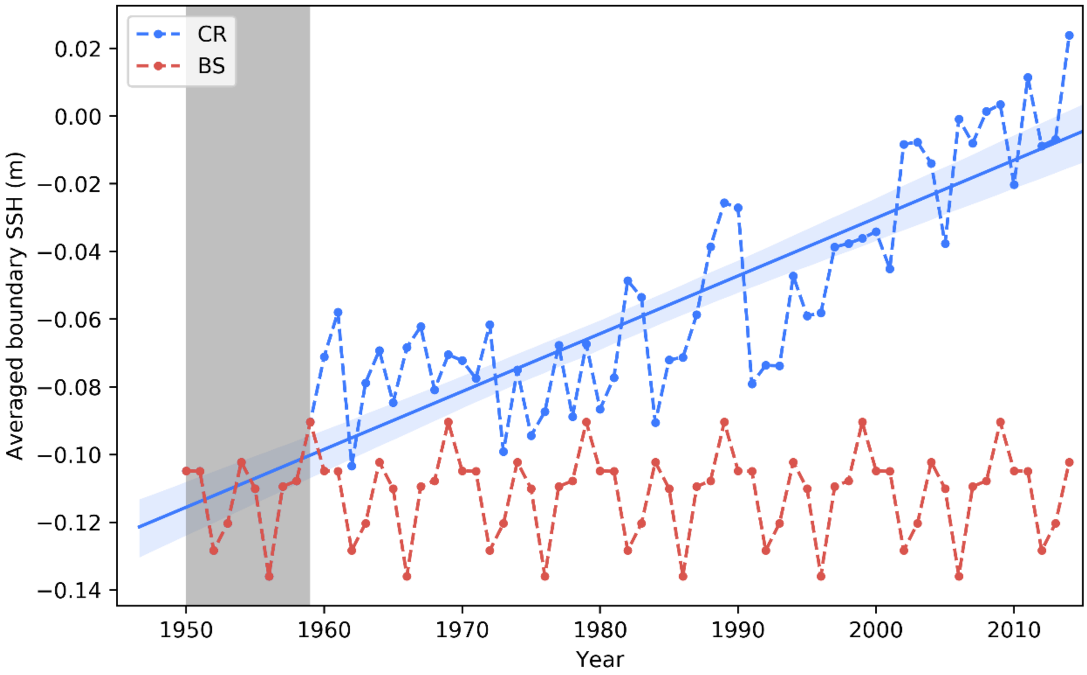

Fig. 17 Annual SSH averaged along the open boundary of the outer model for CR and BS.

4.1.3 Effect of changing heat flux

The ocean surface heat flux is determined by the atmospheric state variables and sea surface temperature. Regarding the atmospheric state variables, obvious seasonal variations are observed from near-surface air temperature (Fig. 1), precipitation (Fig. S1), total cloud cover (Fig. S2), and wind filed (Fig. 2). Therefore, heat flux also exhibits significant seasonal variability, shown in Fig. 18.

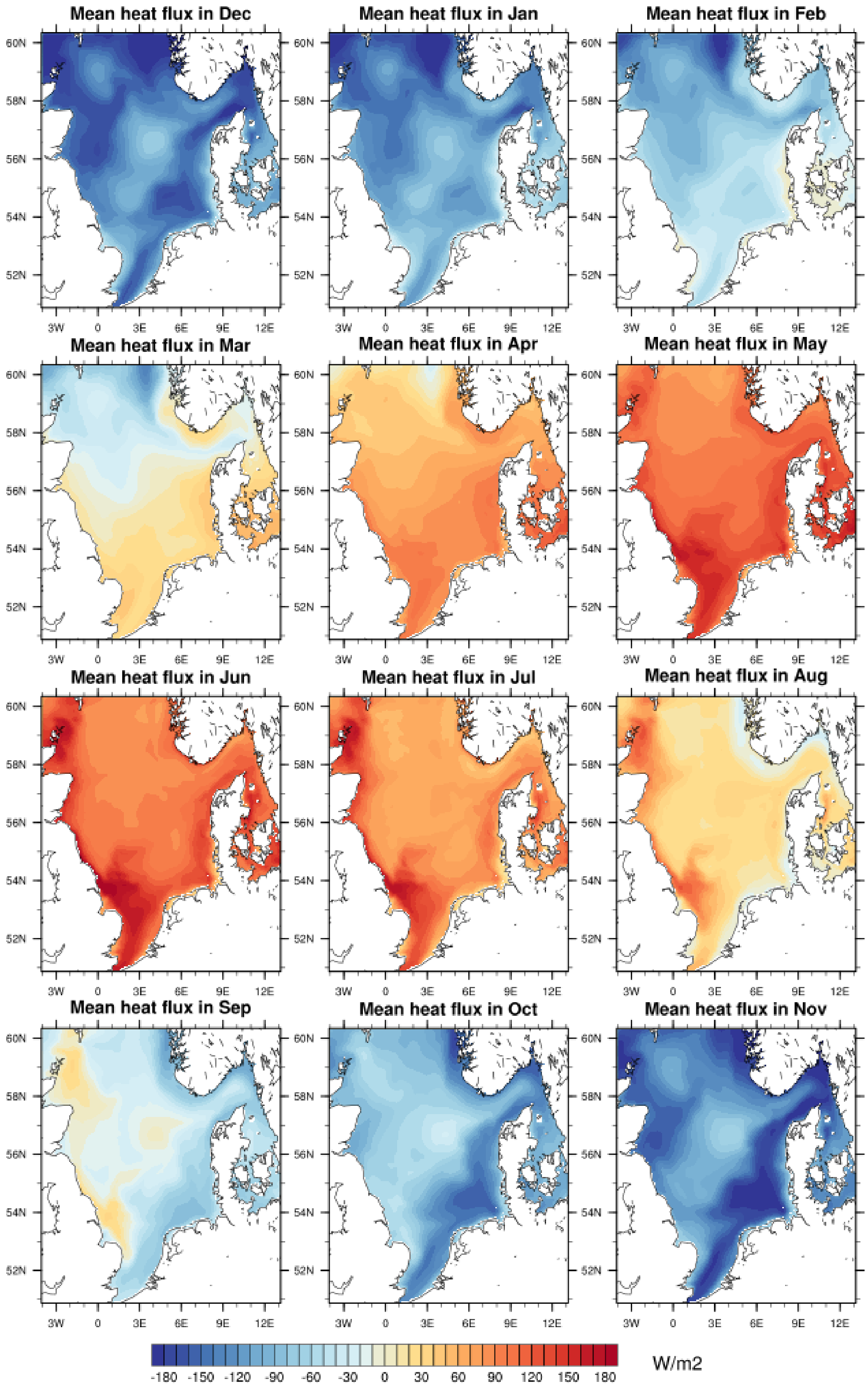

Fig. 18 Monthly mean surface heat flux (1950-2014) in the North Sea. Positive (negative) means ocean receives (releases) heat form (into) the atmosphere.

The heat flux shows significant seasonal variations. Thus, it is also interesting to have a look at the trends of seasonal MSL and MTR for HF. Fig. 19 shows the temporal evolution of the annual, winter (December to February) and summer (June to August) mean surface heat flux averaged over the whole NS domain for both, CR and HF. For CR the summer heat flux exhibits the largest trend of 0.08 W m^{-2} yr^{-1}, whereas no significant trends for the annual and winter means. In contrast, the model calculated surface heat fluxes for HF do not show a consistent positive trend. The annual and the winter mean heat fluxes display negative trends of -0.04 W m^{-2} yr^{-1} and -0.10 W m^{-2} yr^{-1}, respectively, while the summer means a small positive trend of 0.02 W m^{-2} yr^{-1}. In winter (0.10 W m^{-2} yr^{-1}) a larger difference of heat flux trends between CR and HF is simulated than in summer (0.06 W m^{-2} yr^{-1}).

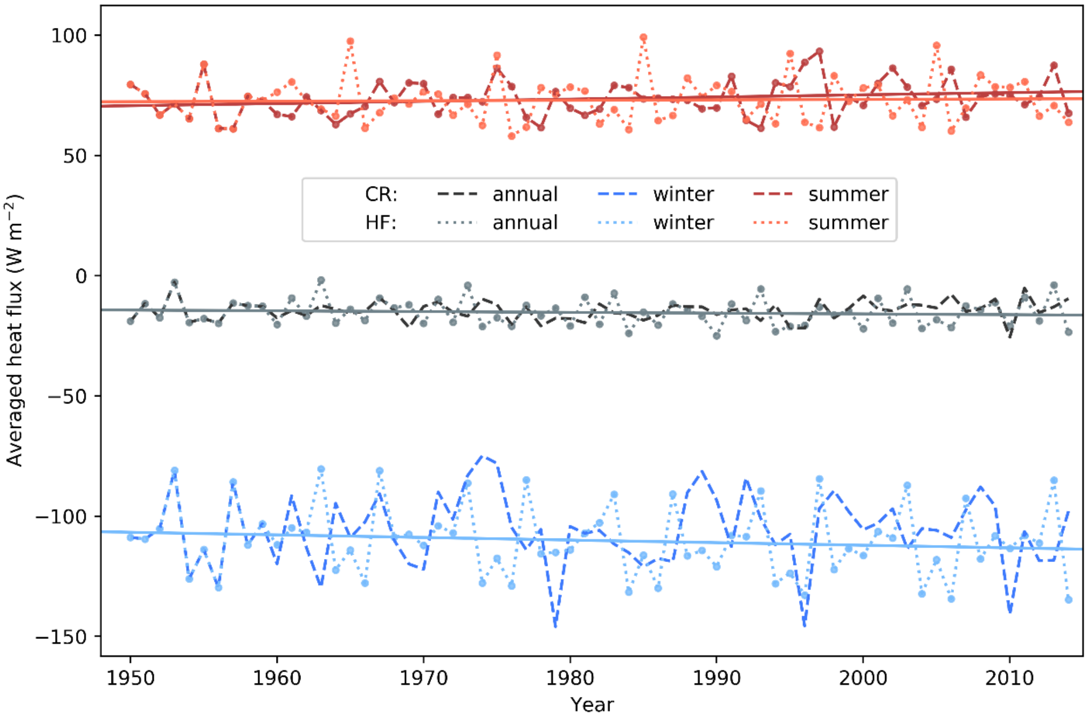

Fig. 19 Annual, winter and summer mean surface heat fluxes of the North Sea for CR and HF. Solid lines suggests positive or negative trends.

In scenario HF, these trends of the heat flux are overlaid by a 10-years' periodic cycle due to the repeated use of the 1950s atmospheric heat flux variables. Noteworthy, the derived heat fluxes in scenario HF do not exhibit a pure periodic behaviour. Since the net surface heat flux results from the interaction between atmosphere and ocean, it does not only depend on atmospheric forcing but also on the state of ocean.

The comparison of MSL trends between scenario CR and HF reflects the influence of surface heat flux on coastal MSL. Trends of the annual MSL are larger for CR than for HF (Fig. 14a). This also holds true for winter and summer MSL (Fig. 14b and c).

The comparison of MTR trends between scenario CR and HF presents the spatial variability of the influence of surface heat flux on tidal ranges. Stations No. 3-14 in Fig. 16 are located along the British coastline, while the rest are mostly inside the German Bight. Trends of the annual MTR along the British coast are smaller for CR than for HF, whereas trends at the stations in the German Bight are higher for CR than for HF (Fig. 16a). This phenomenon is most significant for trends of MTR in summer, and it also holds true for the winter trends, although the differences between CR and HF are rather small (Fig. 16b and c).

4.1.4 Effect of changing wind stress

As shown, the wind stress also has a significant influence on tidal ranges. Repeating wind stress data of the first decade (WS) results in a larger MTR increase compared to the reference run (CR) (Fig. 16a). The magnitude of wind stress is proportional to the square of wind speed, and thus our following analysis focuses on wind speed.

Looking at the original wind data employed in CR, the annual mean wind has a positive trend of 0.011 m s^{-1} yr^{-1} (p value: 0.02) in wind speed. Considering winds at prevalent wind directions, the most frequent basin-wide wind direction in the North Sea for the entire investigation period is southwest (SW, accounting for 19%), followed by west (W, 17%) northwest (NW, 14%), and south (S, 13%), as shown in Fig. 1. For these top four frequent wind directions, positive trends of the annually averaged wind speed were observed (Fig. 21a-d). SW, W, NW and S winds show clear trends of approximately 0.014 m s^{-1} yr^{-1}, 0.009 m s^{-1} yr^{-1}, 0.007 m s^{-1} yr^{-1}, and 0.012 m s^{-1} yr^{-1}, respectively.

Considering these results, one can conclude that the increasing wind stress due to increasing wind speed in CR generally leads to (a) an increase of coastal MSL trends; (b) a reduction of the MTR trends, compared to the periodic wind stress forcing in WS. This in turn indicates that wind stress generally positively correlates to coastal MSL but negatively to coastal tidal ranges.

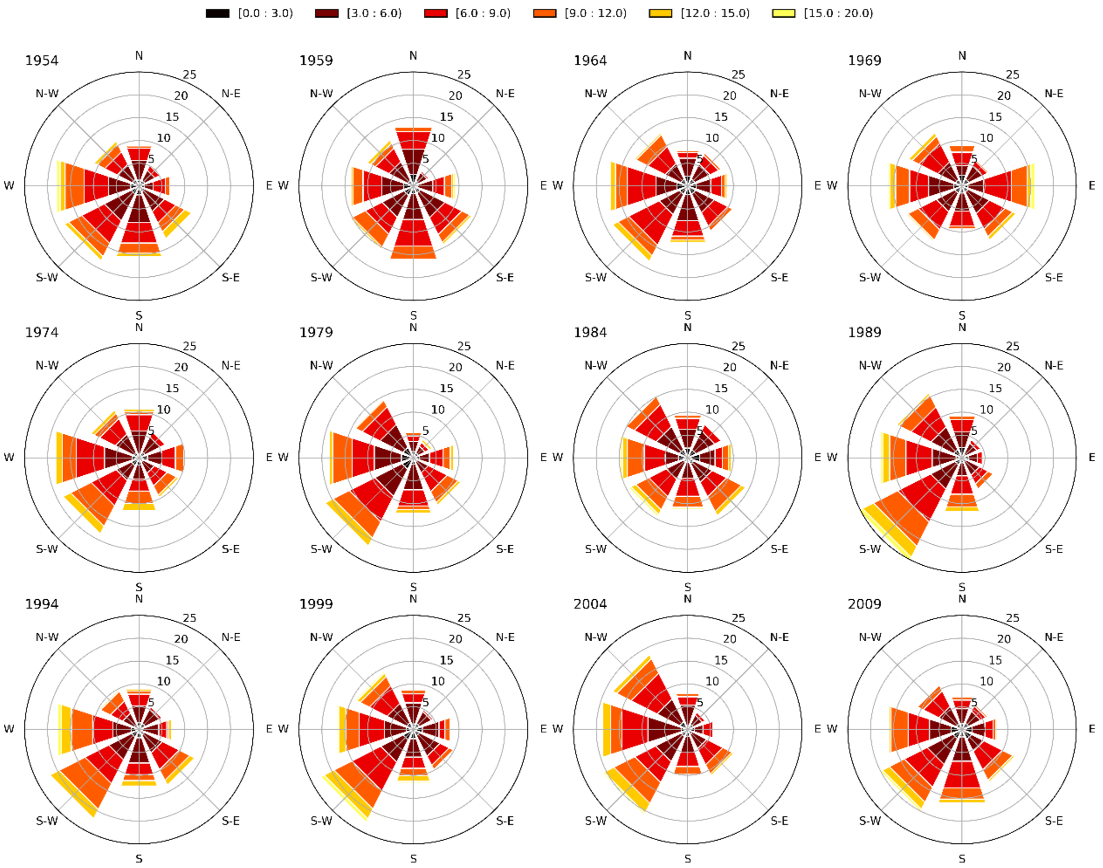

Fig. 20 North Sea wind rose patterns for a yearly period displayed every 5th year starting from 1954. Colour shading depicts wind speed range (m s^{-1}). Bar length reflects the frequency (%) of occurrence.

Wind stress shows a seasonally different behaviour, and hence, its impact on tidal ranges also shows a seasonality. As stated before, for winter MTR trends in the WS experiment are generally higher than the ones in CR (Fig. 16b). However, trends for WS in summer are higher than for CR along the British coast but smaller in the German Bight. Furthermore, the trend differences between WS and CR in winter are generally larger than in summer.

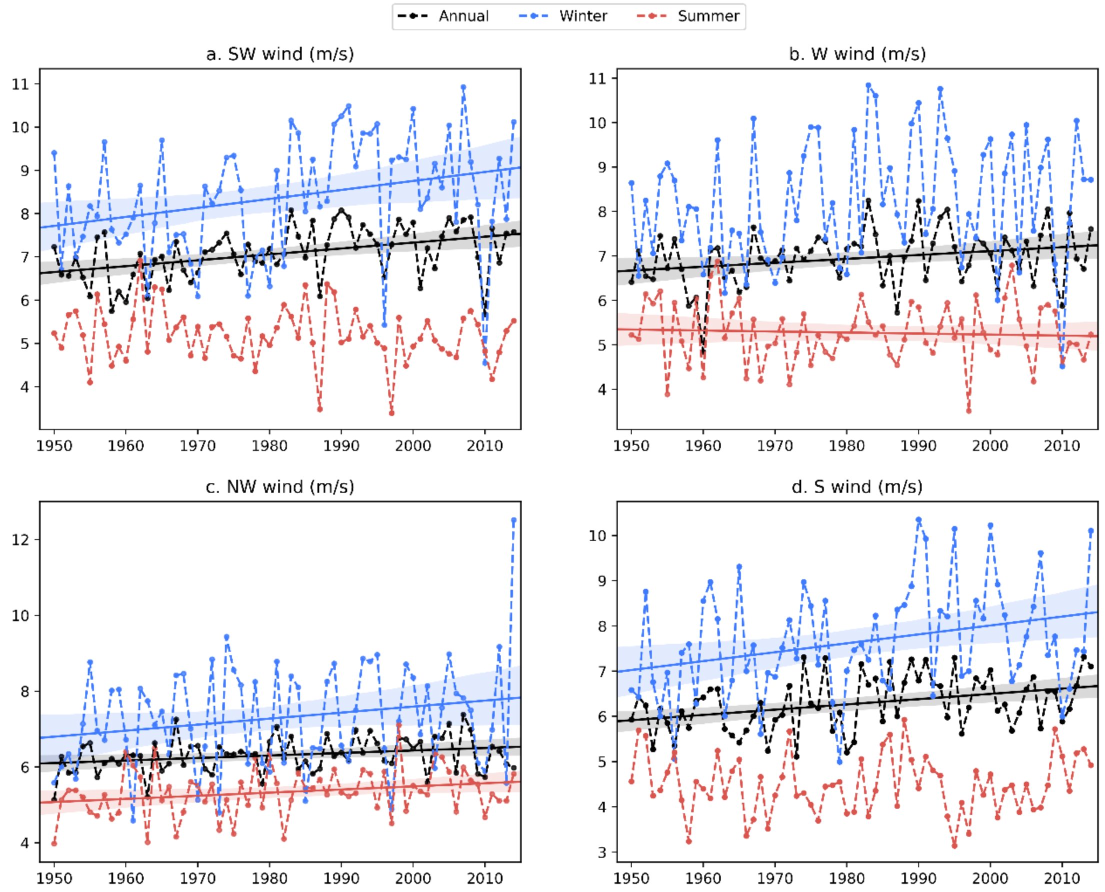

Fig. 21 Time series of annual mean, winter and summer winds from directions SW, W, S and NW.

Looking at the winter and summer wind data, the averaged wind speed in winter exhibits a trend of 0.027 m s^{-1} yr^{-1} (p value: 0.01), while the summer values show no significant trends (p value: 0.39). For the top four frequent wind directions, SW (21%), W(18%), S (14%), and NW(12%) wind speeds in winter show larger trends than in the annual case (Fig. 21) with values of 0.021 m s^{-1} yr^{-1} for SW, 0.020 m s^{-1} yr^{-1} for S and 0.016 m s^{-1} yr^{-1} for NW, and no significant trend for W. In contrast, W (20%), NW (19%), SW (18%), and S (11%) wind speeds in summer show minor trends of 0.008 m s^{-1} yr^{-1} for NW, and no significant trends for the others. Considering these seasonal differences, it can be explained that both (a) the difference of the MSL trend between

WS and CR, and (b) the difference of the MTR trend between WS and CR, are larger in winter than in summer.

4.1.5 Effect of changing river input

River input of fresh water can influence the coastal tidal ranges due to its potential vertical and horizontal baroclinic effects. Time series of annual river discharge into the North Sea averaged over all 145 river input points (shown in Fig. 4b) exhibits a positive trend starting from 1950, amounting to 0.10 $m^3\ s^{-1}\ yr^{-1}$ (Fig. 22). A much larger trend can be observed for the winter river input (0.28 $m^3\ s^{-1}\ yr^{-1}$), while the summer one only shows no significant trends.

As shown in Fig. 14a, smaller trends of annual MSL were found for RI compared to CR, which suggests that the increasing river input has a positive influence on the annual MSL. On the seasonal scale, the influence of river input on MSL in summer is slightly smaller than in winter (Fig. 14b and c), which can be seen from the difference of averaged trends between CR and RI. However, in summer much smaller trends of river input were detected than in winter (Fig. 22).

Similarly, as shown in Fig. 16a, smaller trends of annual MTR were simulated for RI compared to CR. This suggests that the increasing river input has a positive influence on the annual MTR. On the seasonal scale, the influence of river input on MTR in summer is higher than in winter (Fig. 16b and c), which can be seen from the difference of averaged trends between CR and RI. This is in contradiction to the larger trend of river input in winter than in summer.

Noteworthy, trends of MTR in summer for scenario RI exhibit a similar behaviour as for scenario HF with higher trends compared to scenario CR along the British coast but smaller ones in the German Bight (Fig. 16c). However, trends in winter for scenario RI are mostly close to CR and HF.

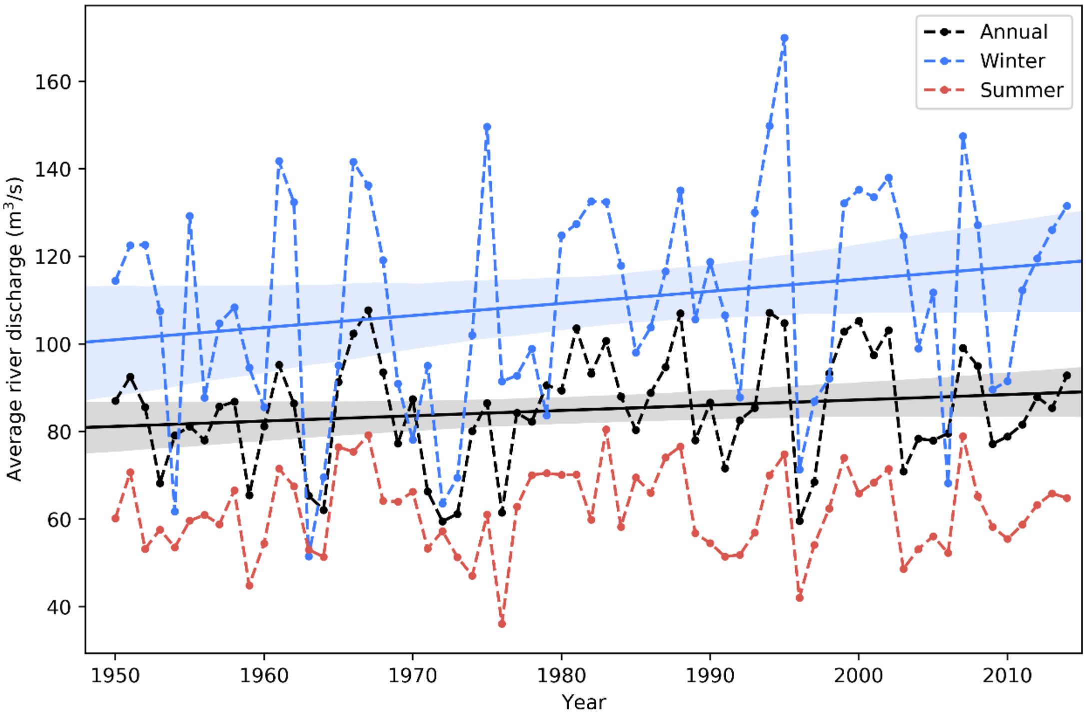

Fig. 22 Annual, winter and summer mean river discharges into the North Sea averaged over 145 river input points.

4.2 Sensitivity test with respect to baroclinicity

As the surface heat flux and river discharge, described in the last subsection, both are capable to alter ocean stratification, the influence of baroclinity on MSL and tidal ranges is investigated in this subsection by comparing the model results of the BC and BT experiments.

4.2.1. Improvement of SSH accuracy

Similarly, to the scatter plots showing simulated versus observed SSH data at different tide-gauge stations presented within the verification section, we construct the same plots with simulated SSH data from our barotropic simulations, see Fig. 8b. We detect higher correlation coefficients and slopes being closer to 1 in Fig 8a for the full baroclinic run, compared to the barotropic one displayed in Fig. 8b. This indicates that coherent improvements in modelled SSH obviously occur when baroclinicity is included, even though these improvements are rather small. This agrees well with findings by Arbic et al. (2004) that the surface elevation accuracy improves in the two-layer baroclinic model compared to a one-layer simulation. For a multi-layer model like the one we applied here, improvement due to baroclinity should even be clearer.

4.2.2 MSL difference

Since most tide-gauge stations are located in well-mixed areas, it must be expected that the local sea level can affect local tidal ranges. Consequently, at the beginning the MSL at those tide-gauge stations resulting from the baroclinic and the barotropic simulations is compared. The MSL difference is defined as the baroclinic MSL minus the barotropic one.

4.2.2.1 Seasonal scale

Fig. 23a and b show that the winter and summer MSL differences are both positive at the stations Helgoland Binnenhafen and North Shields over the entire period from 1950 to 2014, which could be observed for all other stations as well (not shown). This reflects that the baroclinic MSL is generally higher than the barotropic one for both winter and summer seasons, which could be the result of the steric effect discussed in Section 5 “Discussion”. In addition, the MSL difference in winter is smaller than the one in summer at the station Helgoland Binnenhafen while the winter MSL difference is slightly higher at the station North Shields.

a. Station Helgoland Binnenhafen

b. Station North Shields

Fig. 23 Seasonal MSL difference (BC minus BT) in winter and summer at the station Helgoland Binnenhafen (a) and North Shields (b).

4.2.2.2 Secular scale

Another interesting aspect concerns the question whether baroclinicity also has an effect on long-term changes of tidal ranges and MSL. Regarding the secular change of MSL difference, as shown in the lower panel of Fig. 24, the annual MSL difference shows a positive trend over our investigation period at station Helgoland Binnenhafen. The summer MSL difference exhibits a larger trend than the annual one while slightly smaller trend is found for the winter MSL difference. These positive trends exist for most stations with higher trends for the tide-gauge stations in the German Bight.

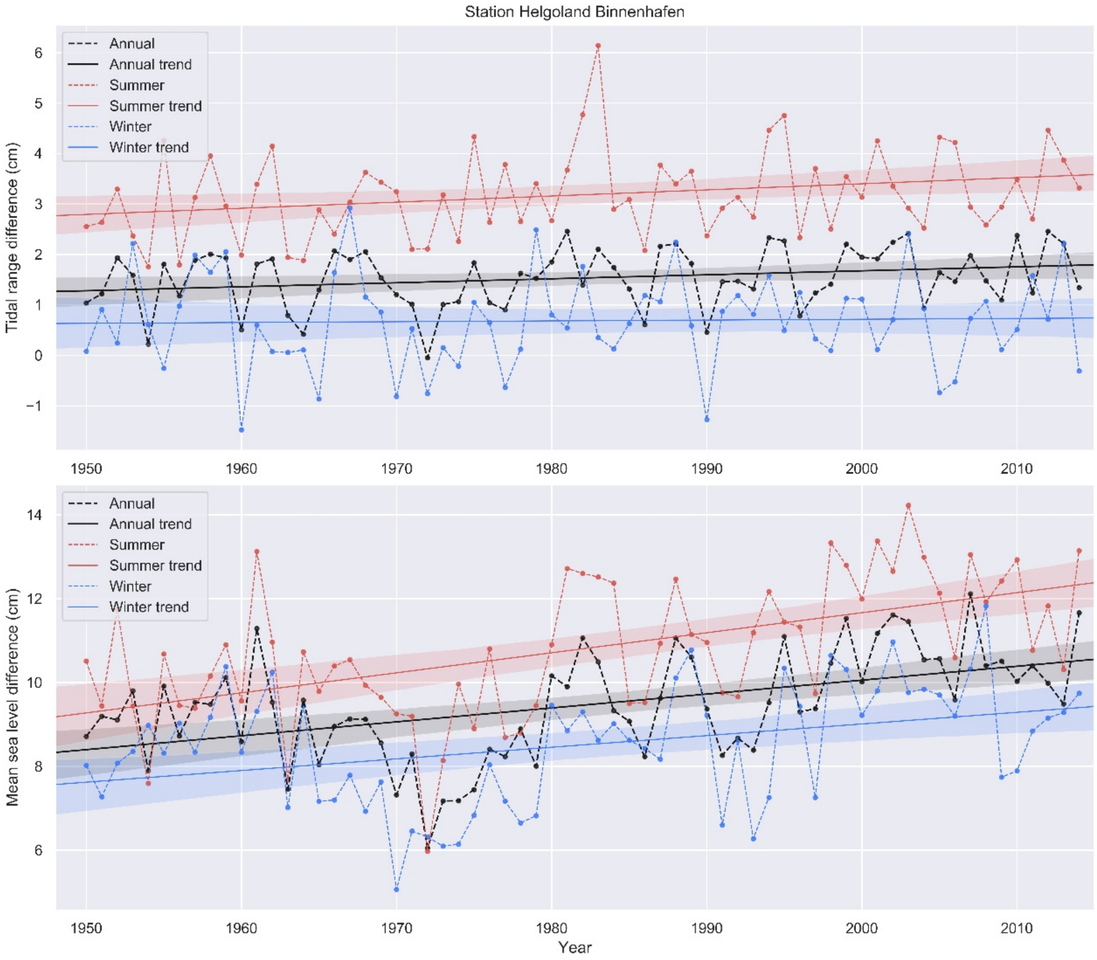

Fig. 24 Trend in annual and seasonal TRD and MSL difference (BC minus BT) at station Helgoland Binnenhafen. Dashed lines display time evolution of TRD and MSL difference. Solid lines present linear regression lines. Colored bands display 95% confidence intervals.

4.2.3 TRD

A clear measure for the effect of baroclinity on tidal ranges is the TRD defined as baroclinic tidal ranges minus barotropic ones. The northern and central North Sea is mostly stratified during summer, while most of the North Sea is vertically well mixed in winter (Sündermann and Pohlmann, 2011). Therefore, it is particularly interesting to study the effect of baroclinicity on the TRD for these two seasons. In order to present the effect of baroclinity in a more general and representative manner, a statistical analysis was carried out for those selected 22 stations mentioned in Section 4.1 for the period from 1950 to 2014.

4.2.3.1 Seasonal TRD at the tide-gauge stations

Fig. 25 Seasonal TRD in winter (December to February) and summer (June to August) at the station Helgoland Binnenhafen (a) and North Shields (b).

Figs. 25a and b present the TRD in winter and summer for the period from 1950 to 2014 at the stations Helgoland Binnenhafen and North Shields. As shown in Fig. 25a, the summer TRD is generally larger than the winter one. The average of the TRD in summer over these 65 years is about 3.2 cm, i.e., four times larger than the one in winter. The average winter TRD is quite small but not zero. The TRD induced by baroclinicity ranges from 0.06 cm (the lowest value in winter) to 6.14 cm (the highest in summer) at the station Helgoland Binnenhafen. Most stations along the Continental coast show a similar behavior. Noteworthy, all presented values are already seasonally averaged. Therefore, the actual TRD can be significantly higher particularly during spring tide in summer.

However, in particular the stations along the British coast displayed in Fig. 25b indicate that the absolute TRD in summer is also larger than the one in winter, however, showing a different behavior. For the British stations the TRD between baroclinic and barotropic simulations is generally negative for both seasons, which means that the baroclinic tidal ranges are smaller than the barotropic ones. In contrast, this negative TRD does not appear at the tide-gauge stations located in the German Bight.

Table 2 Number of years and percentage of entire period (1950-2014) with an absolute summer TRD larger than the winter TRD for 22 tide-gauge stations, as well as mean summer TRD and extreme summer TRD.

Station No.	**Station name**	**Number of years**	**Percentage of the whole period**	**Mean summer TRD (cm)**	**Extreme summer TRD (cm)**
3	Aberdeen	52	80%	-1.79	-5.26
4	Leith	32	49%	-0.69	-4.84
5	North Shields	53	82%	-2.47	-6.54
14	Dover	16	25%	-1.32	-4.50
15	Calais	27	42%	-1.32	-3.62
16	Dunkerque	39	60%	-0.65	-3.54

37	Texel Noordzee	26	40%	-1.69	-6.61
41	Terschelling Noordzee	33	51%	0.14	1.43
44	Wierumergronden	42	65%	0.75	3.35
47	Huibertgat	41	63%	1.00	3.76
49	Borkum Südstrand	62	95%	2.49	4.45
54	Norderney Riffgat und Hafen	64	98%	3.20	5.89
55	Helgoland Binnenhafen	65	100%	3.18	6.14
56	LT Alte Weser-Roter Sand	65	100%	3.67	7.37
57	Wilhelmshaven Alter Vorhafen	65	100%	5.69	10.52
59	Mellumplate	65	100%	3.93	7.82
61	Büsum	63	97%	6.48	10.54
63	Wittdün	64	98%	4.82	7.53
64	Schlüttsiel	63	97%	4.63	7.95
67	Hörnum	63	97%	3.67	5.38
68	List	53	82%	2.87	4.29
69	Esbjerg	50	77%	2.36	3.56

It is found that for most stations the absolute summer TRD is much bigger than the winter one. The result of the statistical analysis listed in Table 2 shows the percentage of entire period for each station for which the absolute summer TRD is larger than the winter one. A clearer view of this table can be obtained from the scatter and bar plot in Fig. 26. Eighteen stations (~82% of the total 22 stations) show the above mentioned behavior during more than half of the period, 13 stations (~59%) during 80% of the period, and 10 stations (~45%) during 90% of the period. Obviously, the behavior displayed in Figs. 25a and b is not only valid for one specific year neither for a specific tide-gauge station but rather for certain areas within the North Sea. In addition, the mean summer TRD shown in Fig. 26 reflects that a negative TRD mainly occurs along the British coast, and the extreme summer TRD shows that the highest value reaches 10.54 cm at the station Büsum (No. 61), corresponding to approximately 3% of local tidal range in summer. This agrees with the work by Müller et al. (2014), who concluded that seasonal variations of the M2 amplitude in the North Sea is O(1-10 cm). Interestingly, the station Büsum is located in a well-mixed area as suggested by Fig. 2 in Pingree et al. (1978). Taking this fact into account, it can be inferred that no local stratification effect is responsible for the observed TRD development. Furthermore, it is found that the larger summer TRD values generally occur in the German Bight and not at stations along the UK coast, as shown in Fig. 26. These findings suggest that the TRD signal accumulates along the propagation path of the tidal Kelvin wave.

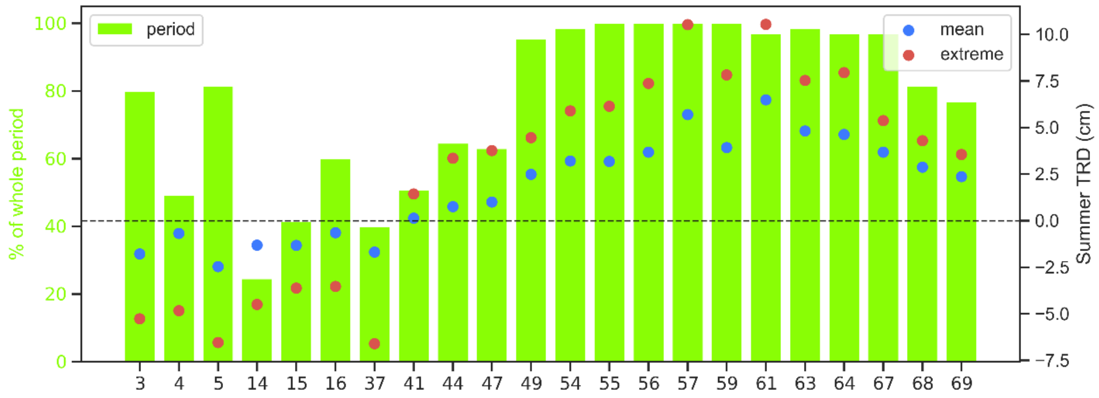

Fig. 26 Period in terms of percentage (bars) of entire period (1950-2014) with an absolute summer TRD larger than the winter TRD for 22 tide-gauge stations, as well as mean summer TRD (blue dots) and extreme summer TRD (red dots).

4.2.3.2 Horizontal distribution of seasonal TRD

The horizontal distribution of the TRD in the North Sea shown in Fig. 27 provides a better impression on the distribution of negative and positive TRD regions. The winter TRD distribution is in principal similar to the summer one, but has a significantly weaker intensity. The negative values are generally located along the British coast, while the positive ones mainly occur along the Continental coast. Moreover, higher TRD values mainly occur close to the coast, with the exception of the Southern Bight, where relatively high negative values occur in the northern part of the Southern Bight, accompanied by relatively high positive values in the central part of the Southern Bight. A similar dipole structure occurs at around 56°N, 4.5°E. Such kind of dipole structures in a difference plot suggest that the amphidromic point in the Southern Bight was shifted northward and the amphidromic point at the central North Sea moved slightly westward in the baroclinic mode, a phenomenon, which will be discussed in detail in Section 5 “Discussion”.

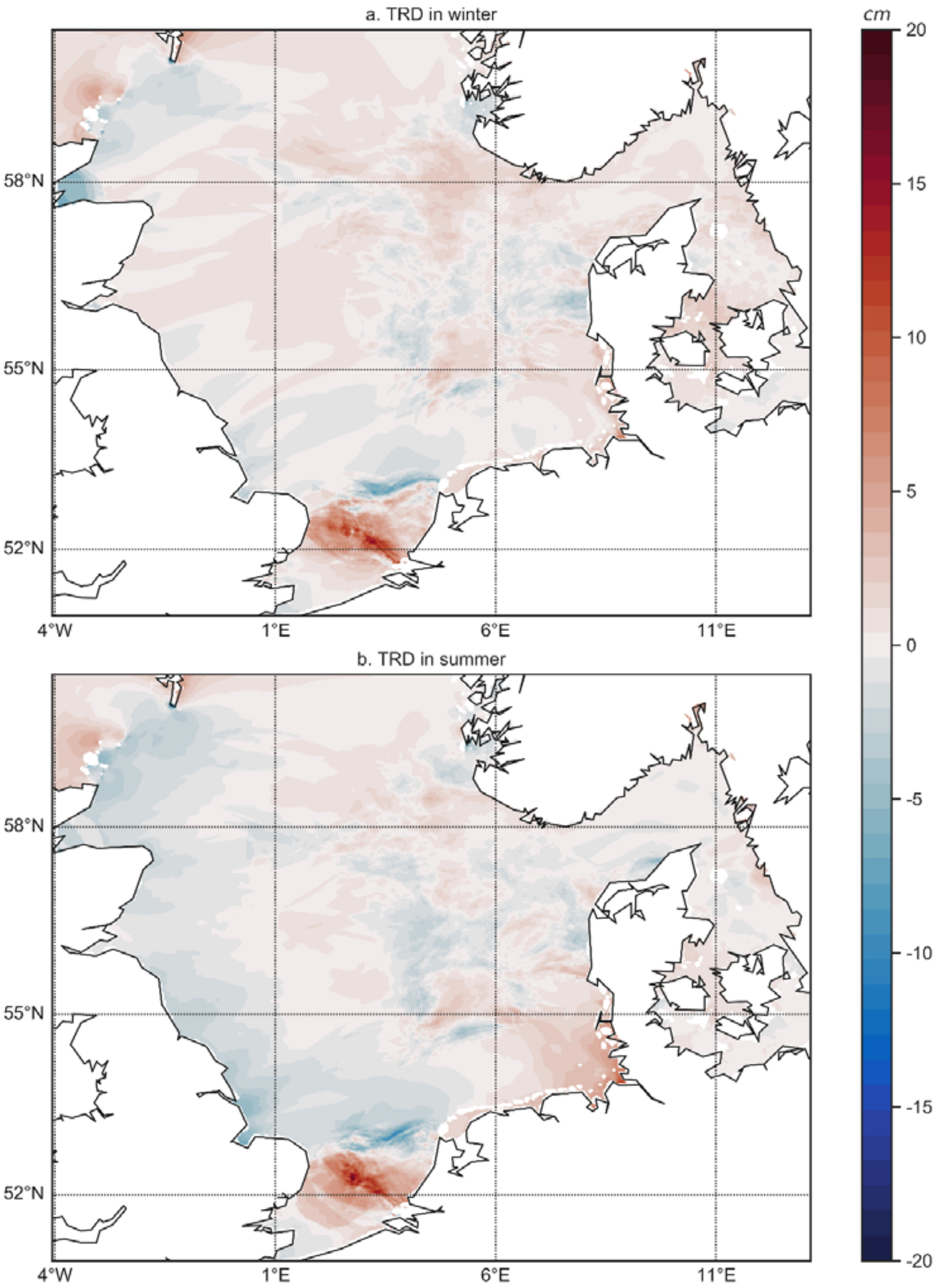

Fig. 27 Horizontal distribution of TRD during winter (December to February) and summer (June to August) in 1980 in the North Sea.

4.2.3.2 Secular scale

Regarding the effect of baroclinicity on long-term changes of coastal tidal ranges, as shown in the upper panel of Fig. 24, the annual mean TRD shows a positive trend for our investigation period at the station Helgoland Binnenhafen. This is more obvious for the summer TRD time series, while almost no trend is visible for winter. Compared to the trends of annual, winter and summer MSL differences at the station Helgoland Binnenhafen, the annual, winter and summer TRD increase relatively slower. A positive trends of TRD exist for most stations with higher trends detected at the tide-gauge stations in the German Bight. A statistical analysis for the selected stations shows that the largest positive trend for the annual TRD is about 0.11 mm yr^{-1} and 0.17 mm yr^{-1} for the summer TRD at the station LT Alte Weser-Roter Sand (No. 56) while annual and summer MSL difference at this station amount to 0.33 mm yr^{-1} and 0.48 mm yr^{-1}, respectively.

5. Discussion

5.1 MSL trends

Tidal properties are strongly influenced by the water depth (Talke & Jay, 2020). In our simulations, bathymetry is kept constant for both the outer and inner model domains, so the changes of water depth only may arise from the changes of the sea level. Consequently, we first discuss the MSL changes at the 22 tide-gauge stations in order to understand the detected changes of the tidal ranges.

Coastal MSL could be altered not only directly by the open boundary SSH signal but also by the local heat flux, wind stress and river input. The contributions of changes in trends of MSL by boundary SSH, heat flux, wind stress, and river input are reflected by the differences between CR and the corresponding scenario (CR minus BS/HF/WS/RI), as shown in Fig. 28.

The dominant contributor to the annual coastal MSL rise is the increase of the open boundary SSH. Noteworthy, the respective contribution is spatially similar for all investigated coastal stations (Fig. 28a). This indicates that the sea level rise signal from the open boundary SSH propagates uniformly to all coastal areas, with an average contribution of 1.59 mm yr^{-1} on the coastal MSL, reflecting that most of the sea level rise signal (1.73 mm yr^{-1}) from the open boundary SSH directly intrudes into coastal zone.

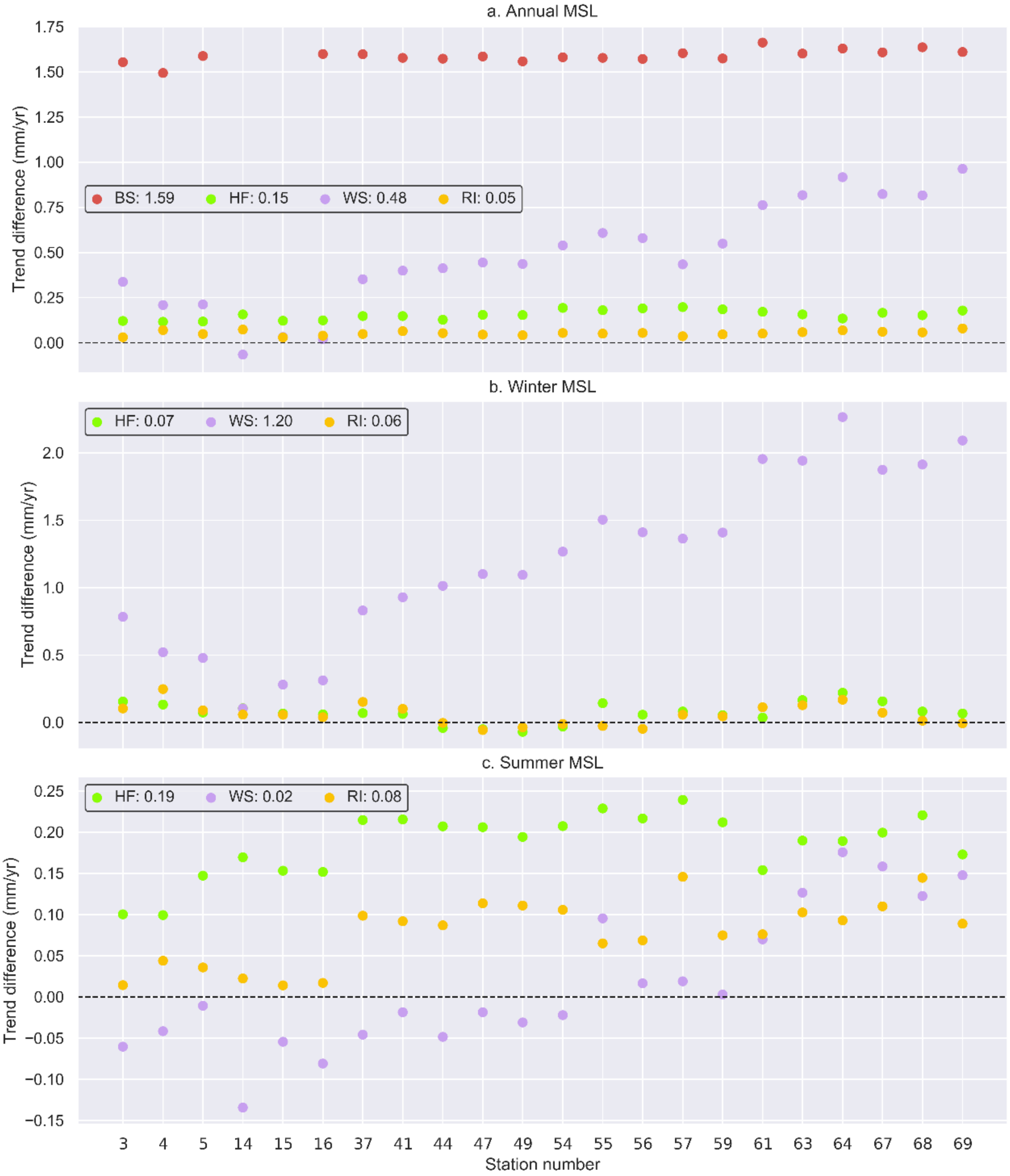

Fig. 28 Trend difference of annual (a), winter (b), summer (c) MSL at 22 stations (CR minus BS/HF/WS/RI).

Small trends can still be detected for the annual MSL for the BS experiment, with an average value of 0.67 mm yr^{-1} (Fig. 14a). This could originate from variations of the remaining forcing functions, i.e., of the heat flux, wind stress and river input. The increasing surface heat flux and river input both have small positive influences on annual MSL with a similar spatial distribution as seen for the open boundary SSH (Fig.

28a). In contrast, the increasing wind stress exerts a much stronger impact on annual MSL, showing spatially different contributions (Fig. 28a). These spatial differences of the contributions match the distribution of the annual MSL trends for the BS experiment, with an average contribution of 0.48 mm yr^{-1} induced by the increasing wind stress. This indicates that rising wind stress is the second largest contributor to the local MSL rise. In fact, it is the major source of spatial inhomogeneity of the MSL rise.

In order to explain this spatial inhomogeneity of the wind impact, the specific locations of the tidal stations should be considered together with the wind-driven Ekman transport. Obviously, the more frequent SW wind (Fig. 21a) transports a larger water volume into the German Bight, leading to a coastal MSL rise. Along the British coast, however, a SW wind causes an offshore transport resulting in a negative effect on local MSL. Nevertheless, this negative contribution is opposite to our findings. Therefore it must be suspected that the positive wind contribution along the British coast results from an increasing W wind (Fig. 21b), which counteracts the negative effect of increasing SW wind. It is known that increasing W winds leads to an increased transport of water masses into the North Sea through the northern entrance (Schrum et al., 2003), which dominates the MSL rise along the British coast. Additionally, this also explains why the wind contribution is smaller along the British coast than in the German Bight, where both SW and W wind contribute to the MSL rise.

Regarding the trends of the seasonal MSL, the contribution of heat flux in summer (accounting for 0.19 mm yr^{-1} on the average) is larger than the one in winter (0.07 mm yr^{-1}), as shown in Fig. 28b and c, which overrules the influence of the larger difference in heat flux trends between CR and HF (Fig. 19) in winter. The contribution of river input in summer (0.08 mm yr^{-1}) is also slightly larger than in winter (0.06 mm yr^{-1}), as shown in Fig. 28b and c, in spite of the much larger trend of river input in winter. These phenomena are induced by the stronger steric effect in summer. Since a less dense water column requires higher local sea level to balance the bottom pressure, which is called the steric effect, warmer water temperature in summer in turn contributes to a higher local sea level. Regarding the river input, local MSL is not only directly raised by water mass input but also caused by the salinity dilution and the subsequently induced steric sea level increase. However, warmer water temperature in summer reduces the difference of contributions of the river-runoff between winter and summer.

In contrast, wind stress has a more important influence on the MSL in winter (1.20 mm yr^{-1}) than in summer (0.02 mm yr^{-1}), as shown in Fig. 21b and c, which can be explained by the much stronger winds in winter. In addition, the contribution of wind stress is positive for all stations in winter (similar to the annual mean distribution), whereas it exhibits a more complex structure for summer, with negative contributions for most stations along the British and Dutch coast and positive ones for stations located along the coasts of Germany and Denmark. In summer, the decreasing W wind (Fig. 21a and b) cause a reduced water transport into the German Bight and the North Sea, respectively. Thus, negative contributions are expected in the German Bight and along the British coast. However, an increasing NW wind (Fig. 21c) leads to a strong piling up of the water masses in the German Bight and along the Danish coast, resulting in an overall positive wind contribution to the MSL in this area.

5.2 MTR trends

In accordance with the procedure presented for the MSL, the contributions of different forcing mechanisms on local MTR trend can be derived from the differences of the MTR trends between CR and the respective forcing scenario. Looking at the contributions on the annual trends (Fig. 29a), the SSH rise at the open boundary dominates the trends of annual MTR among those mechanisms, with an averaged contribution of 0.28 mm yr^{-1} over 22 tide-gauge stations. In contrast, the increasing wind stress has a negative average contribution of -0.04 mm yr^{-1}. Besides, the increasing surface heat flux and river input have the same but positive average contributions of 0.03 mm yr^{-1}, whereas the contribution of the former one shows a slightly higher spatial variability between the individual stations, reflecting that the heat flux contributes slightly more to the MRT trend than the freshwater discharge.

Considering the contributions on the trends of the seasonal (winter and summer) MTR, in winter (Fig. 29b) the increasing wind stress has a very important contribution on the trends of the MTR, with an average value of -0.10 mm yr^{-1}. In contrast, the growing heat flux and river input in winter hardly contributes to the trends of winter MTR, despite the fact that (a) the trends for the winter heat flux show large differences between the CR and HF scenario, and (b) in CR a significant increase of river input occurs in winter compared to the RI scenario.

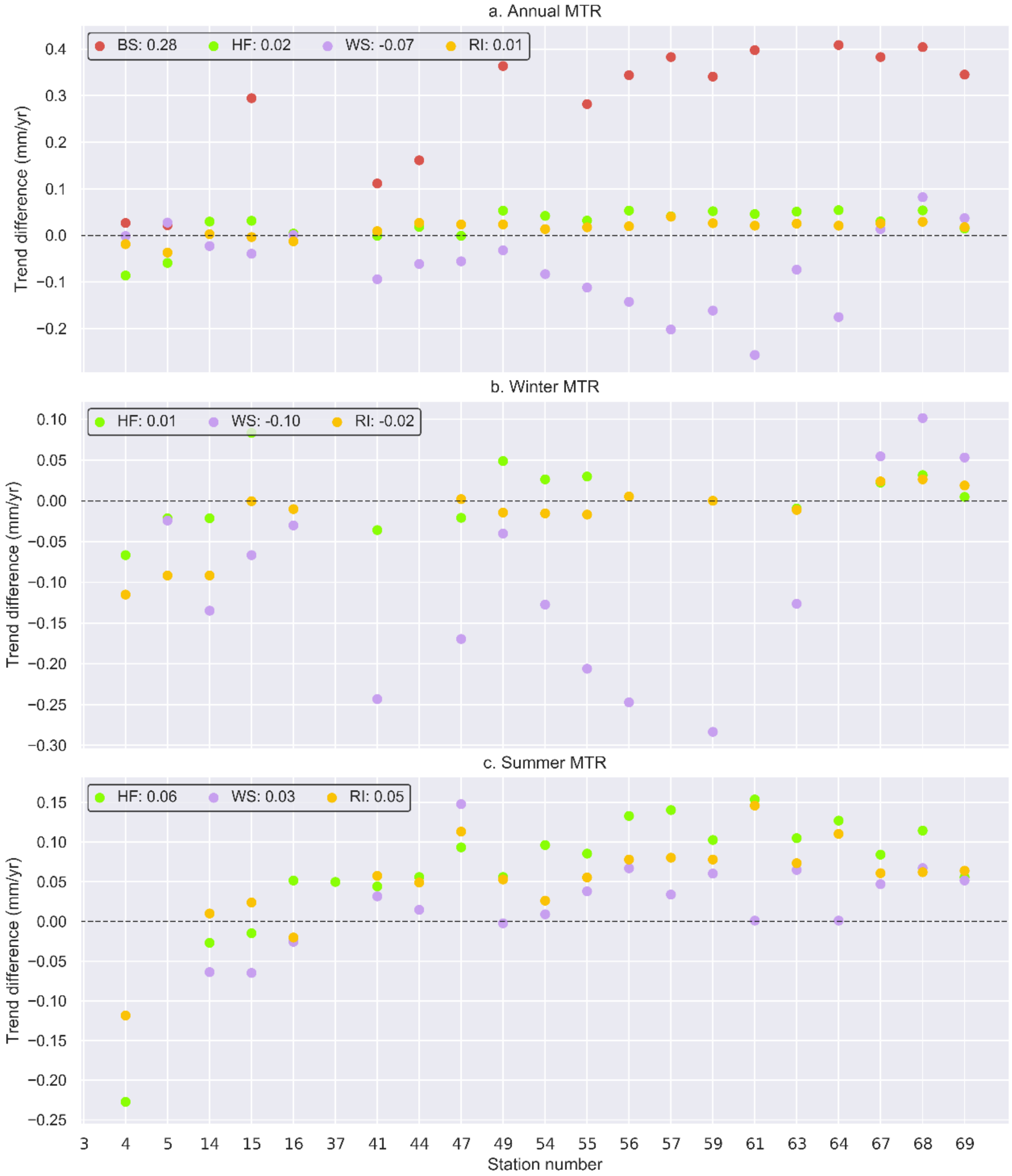

Fig. 29 Trend difference of annual (a), winter (b), summer (c) MTR at 22 stations (CR minus BS/HF/WS/RI).

In summer (Fig. 29c), however, the heat flux (the average accounting for 0.06 mm yr^{-1}) and river input (0.05 mm yr^{-1}) have a relatively larger influence on tidal ranges compared with the influence of the wind stress (0.03 mm yr^{-1}). Moreover, the heat flux also shows slightly larger contributions than the river input for most stations, which is similar to the contributions for the annual MTR. The average contribution of wind stress in summer is positive, which is consistent with the situation for winter, since the average wind in summer exhibits a negative trend.

The fractional contributions of the different forcing mechanisms on annual MTR trends are also calculated to provide a more general overview over detected changes and their causes. In order to determine the unbiased fractional contributions of each forcing function, the nodal cycle has been removed from the MTR. Considering these changes on a centennial scale, the annual mean boundary MSL rise of 0.17 m century^{-1} leads to an annual MTR increase of 1.14 % century^{-1}. This is much higher than findings from former researchers, who determined that a 1 m change in sea level results in changes in tidal amplitudes of approximately 1% (Haigh et al., 2020; Müller et al., 2011). However, in these former studies a coupled oscillator model of shelf and ocean tides was applied (Arbic & Garrett, 2010), which only provided a relatively rough estimate. In contrast, our study is based on a more realistic three-dimensional baroclinic primitive equation model, which obviously shows a much higher sensitivity to changes of MSL. Changes in annual mean heat flux of 3.5 W m^{-2} century^{-1} lead to an annual MTR increase of 0.10 % century^{-1}. Changes in annual mean river input of 10.1 m^3 s^{-1} century^{-1} lead to an annual MTR increase of 0.06 % century^{-1}. In contrast, changes in annual mean wind stress of 1.1 m s^{-1} cy^{-1} lead to an annual MTR decrease of 0.23 % century^{-1}.

It has to be noted that the simulated annual MTR trends for the realistic run (CR) in our study are generally one order smaller than the values estimated from observational data by Jänicke et al. (2021), and the simulated trends along the British coast show even different signs from their assessments. Although their analysed period is not exactly the same as ours, nevertheless, it must be concluded that our model obviously underestimates trends of the annual MTR in the North Sea.

Our hypothesis is that this difference results from the tidal signal, which is prescribed along the open boundary of the outer model. These tidal boundary values were extracted from a global tide model, which does not account for changing tidal characteristics due to climate change. However, recent studies strongly suggest, that climate change definitely has an impact on the global tidal system (Greenberg et al., 2012; Pickering et al., 2017). In our study, this change of tidal characteristics in the entire North Atlantic basin could not be considered realistically due to the limited area of our model study. Due to this limitation, we were not able to determine the full effect of climate-related changes in the MSL and stratification in the Atlantic Ocean on the MTR trends in the North Sea. Nevertheless, we were able to quantify the MTR trends induced by changes of governing forcing mechanisms occurring on the Northwestern European shelf. This quantification can be seen as the main purpose of our study.

5.3 Underlying dynamics

5.3.1 MSL

As shown before, open boundary SSH rise dominates the coastal MSL rise. The question now is, how this relates to the trend, which we found for the MTR. Obviously, the increasing MSL leads to an increase of the water depth at tidal stations and along the path of the tidal wave, which enters the North Sea via the northern open boundary. Increasing water depth will accelerate the propagation speed of tidal waves and reduce the depth averaged energy dissipation via a modification of bottom friction (Devlin et al., 2017; Arbic & Garrett, 2010; Pugh, 1987). The thicker the water column is, the less the surface flow and the depth averaged flow “feels” the decelerating effect by bottom friction (Talke et al, 2020; Talke et al, 2013). This eventually explains why trends of MTR for CR are larger than for the BS scenario, sine for CR the tidal wave is less disturbed by bottom friction. Idier et al. (2017) and Pickering et al. (2012) observed a reorganization of the amphidromic points when assuming a spatially uniform sea level rise. This is not observed in the present paper, since the rise of open boundary SSH is not spatially uniform and its magnitude is much smaller than the setting in their study.

5.3.2 Wind stress

When looking at the impact of the wind stress on the tidal ranges, there is an indirect effect via the MSL as described above. We see also that wind is generally positively correlated with MSL at most tidal stations. On the other hand, it turned out that an increasing wind stress does not lead to an increase of the tidal ranges at most coastal stations, which suggests that water depth change is not the only factor responsible for the tidal range changes. Considering the Ekman theory, the wind effects the water column down to the Ekman depth - or the bottom in shallower regions, where most tidal stations are located. In those areas, there still occurs a significant momentum input to the bottom flow by the surface wind. This additional momentum input is more significant in winter due to stronger winds and negligible stratification during this season. Figs. 30a and b display the SSH and energy dissipation at station Helgoland Binnenhafen. The energy dissipation is calculated from bottom stress multiplied with bottom current velocity, which is proportional to cube of velocity over depth. As expected, the SSH is higher in the CR than in the WS scenario. Interestingly, the same is true for the integral of energy dissipation. This means that the bottom current velocity, which is the dominant factor determining the energy dissipation term, is stronger in the CR than in the WS scenario. Consequently, this increased energy dissipation due to increasing wind speed leads to a decrease of tidal ranges. Obviously, this wind induced dissipation process overrules the effect caused by an increasing water depth.

For several other stations along the British coast like station North Shields, the situation in winter is different than for station Helgoland Binnenhafen. For station North Shields, an increasing wind stress has a positive contribution to the trend of winter MTR (Fig. 29b). Here, the positive MSL trend produced by the changing winds is larger (Fig. 28b), and obviously has a more dominant influence on the energy dissipation than the increased bottom flow by the increased wind as seen from smaller energy dissipation for CR than for WS (Fig. 30d).

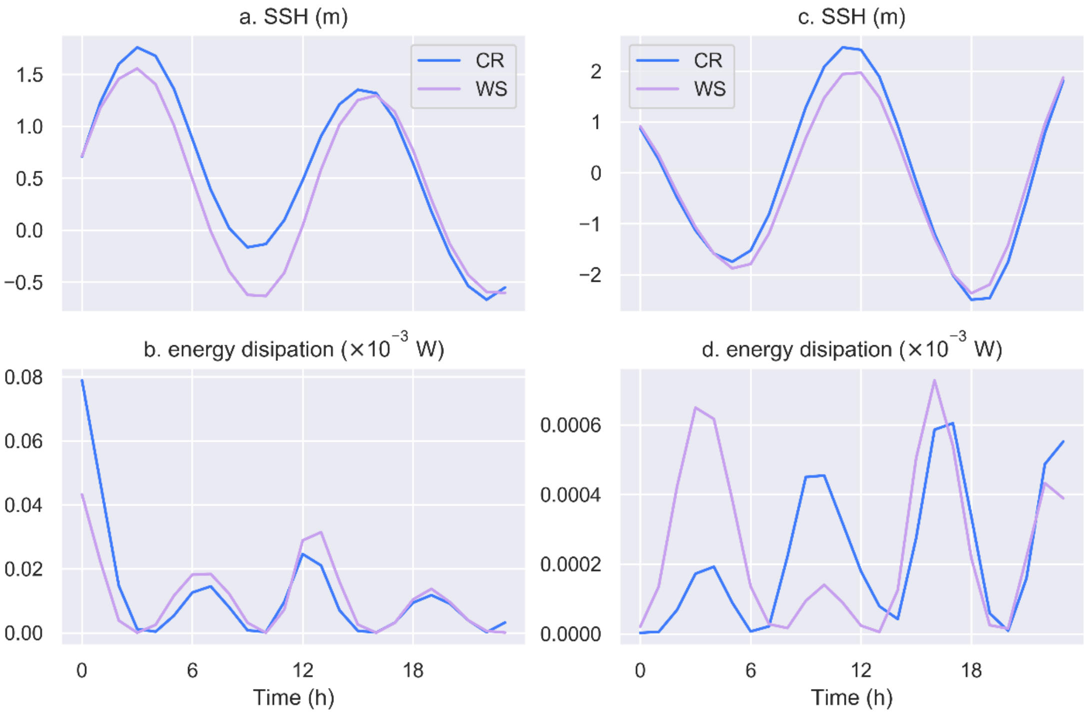

Fig. 30 SSH and energy dissipation at Helgoland Binnenhafen on 3rd Jan (a, b) and North Shields on 5th Feb in 2001 (c, d).

5.3.3 Baroclinicity

Growing surface heat flux and river input have similar contributions to the trends of the annual MTR, which also holds true for winter and summer seasons. Despite the fact that (a) the difference of trends in heat flux between CR and HF is larger for winter than for summer, and (b) also the river input increases faster in winter than in summer, their contributions to the trends of the tidal ranges are smaller in winter than in summer. Moreover, these contributions show common spatial characteristics with a negative influence along the British coast and a positive one in the German Bight. This behaviour is consistence with the results of comparison between BT and BC simulations in Section 4.2: (a) a negative TRD along the British coast but positive one in the German Bight; (b) a stronger TRD trends in summer than in winter. Consequently, the contributions of growing heat flux and river input on the coastal MTR are supposed to be related to the change of baroclinicity in the North Sea. In consequence, in the following we discuss the baroclinicity effect on the basis of a comparison between BC and BT simulations presented in Section 4.2.

5.3.3.1 Indirect effect

Considering the impact of baroclinicity on the tidal ranges, it has to be noted that also an indirect effect via the MSL change already described above may occur. The influence of baroclinity on local MSL is indicated by the contributions of heat flux and river input on seasonal MSL trends discussed above. It is more obvious when looking at the seasonal MSL difference between BC and BT simulations.

The MSL difference at the coastal stations is strongly influenced by the local salinity dilution and water temperature due to the steric effect, as the direct SSH increase by the river input is the same for both baroclinic and barotropic conditions. Temperature changes mainly dominate the seasonal differences of the local sea level. In winter, cold temperatures in coastal areas weaken the local sea level increase induced by fresh water input, while warm temperatures in summer enhance the sea level increase at the coast. Seasonal variations of fresh water input also have a significant influence on the seasonal differences of the local sea level. It is even a dominant factor at the station North Shields, where the winter MSL difference is slightly larger than the summer one (Fig. 23b). The latter is due to a higher rate of fresh water input in winter than in summer (Fig. 22). Due to the increase of the thickness of the water column, an increase of the local MSL potentially reduces the damping effect caused by the bottom friction, and in turn will lead to an increase of the coastal tidal ranges. However, this effect may not be the dominant factor for the observed summer TRD as indicated by Idier et al. (2017), who showed that the maximum ratio of M2 amplitude changes to sea level rise is 10% and only occurs in the German Bight close to the coast. For our specific study, this would mean, that a change of the M2 tidal range of approximately only 2 cm may result from the local MSL rise, which is a relatively small part of observed summer TRD (listed in Tab. 2). However, this effect may dominate the winter TRD, as in this season stratification is very weak in the North Sea.

5.3.3.2 Amphidromic system

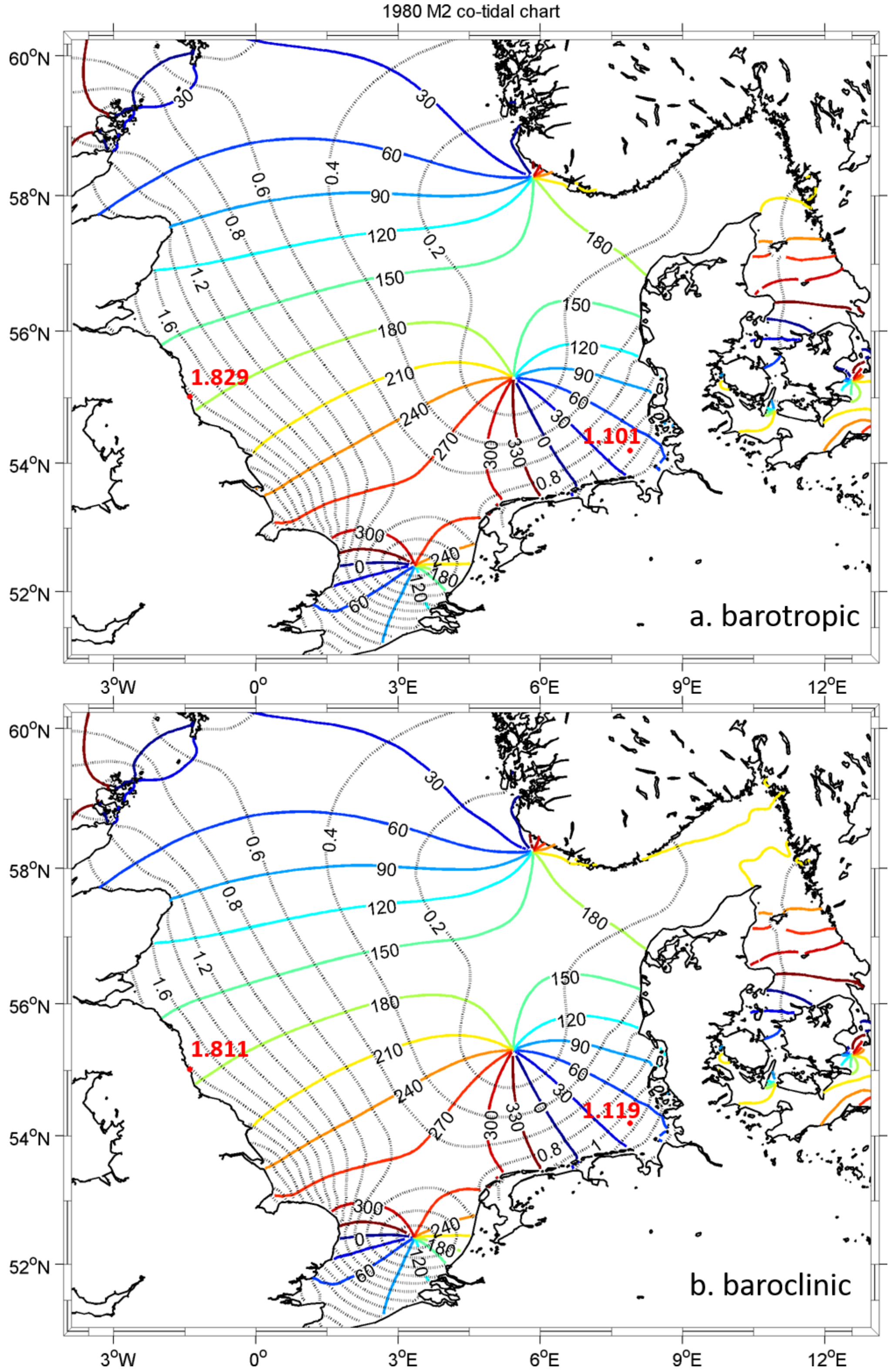

Fig. 31 M2 co-tidal charts calculated from simulated sea surface elevations in July 1980 for the barotropic (a upper panel) and the baroclinic (b lower panel) simulations.

The occurrence of positive and negative values in the horizontal distribution of TRD (Fig. 27) indicates that the amphidromic points were shifted. The dipole structures also reflect the shift of amphidromic points in the Southern Bight and central North Sea. In order to more clearly investigate such a shift, a tidal harmonic analysis was carried out for July 1980 for the whole North Sea for the dominating partial tide M2. Fig. 31 presents the co-tidal charts of the M2 tide for the barotropic and the baroclinic modes. In the baroclinic mode, the amphidromic points around the English Channel and in the German Bight move slightly westward compared to the barotropic one. It is hardly visible directly from the co-tidal charts, but the M2 amplitudes decline along the UK coast, while they increase in the German Bight, as seen from a M2 amplitude decrease of 1.8 cm at North Shields and an increase of the same amount at Helgoland Binnenhafen. This indicates that the contour lines of tidal amplitudes move from the German Bight towards the British coast, due to baroclinic processes. As the amplitudes of the major partial tide M2 are altered by the slightly westward shift in the amphidromic system, it can be explained that also changes in tidal ranges occur, with negative TRD values along the British coast and positive ones in the German Bight. Noteworthy, the westward shift of the amphidromic point is much smaller in winter due to a strongly reduced stratification, in turn leading to significantly smaller TRD values.

5.3.3.3 Stratification effect on tidal velocity profiles

To explain the changes of the amphidromic system by baroclinicity, we first look at the effect of stratification on tidal current velocities. Stratification can decouple the bottom water and surface layer, which is reflected in the vertical eddy viscosity profiles

(Müller, 2012). Vertical eddy viscosity is an indicator of vertical mixing processes. In areas under stratified conditions, the eddy viscosity is very low, thus only little mixing occurs, which leads to the above mentioned decoupling. This decoupling induced by stratification can alter the tidal current velocity profile, which was already demonstrated with the General Ocean Turbulence Model applied by Müller (2012) (see Fig. 7 in his paper). Also in our realistic simulations, a similar behavior of current velocity profiles can be observed (Fig. 32). Under baroclinic conditions, the tidal current in the upper layer will be enhanced due to the low vertical eddy viscosity, reaching a peak value at the depth of largest stratification, whereas a stronger velocity shear and higher turbulence occur below the pycnocline. Hence, the velocity in the lower layer may decline faster than in the barotropic case. The alteration of vertical average of tidal current velocity due to the stratification is determined by the competition between upper and lower layer transports, which depends on mixed-layer depth and local water depth (Müller, 2012). Therefore, the vertical average of the tidal current velocity, which eventually determines the characteristic of the tidal Kelvin wave, can be altered in both ways; it can be enhanced or decreased by the baroclinicity.

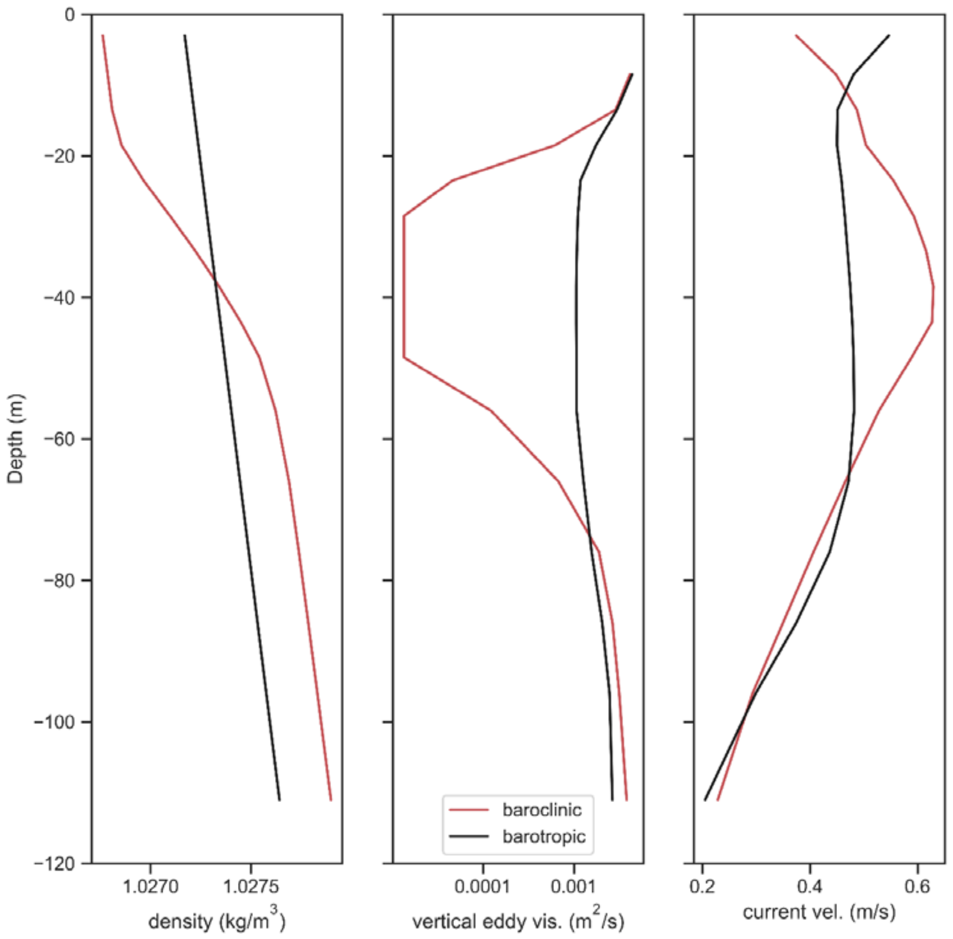

Fig. 32 Vertical profiles of density, vertical eddy viscosity and tidal current at the west of Fair-Isle-Passage.

5.3.3.4 Tidal Kevin wave

Two tidal waves enter the North Sea. One intrudes through the Fair-Isle-Passage in the northwest and another one through the English Channel in the southeast. Both waves are Kelvin waves bordered by the coastal boundaries at the right hand side of the wave. Both Kelvin waves propagate anticlockwise in the North Sea generating an amphidromic system, which is determined by the basin shape. Noteworthy, the coastline and topography of the North Sea are not changed over time in both barotropic and baroclinic simulations. Hence, these two factors cannot be responsible for changes in the amphidromic system.

The dynamics of Kelvin waves in theory follows the balance between the Coriolis force and the barotropic pressure gradient induced by the sea surface excursion perpendicular to the coastline (Taylor, 1922). Under barotropic and baroclinic conditions, this balance holds, and the Coriolis term is derived from the vertically averaged current velocity, i.e., the barotropic velocity, which in the North Sea is dominated by the tidal current. Under baroclinic conditions, the vertically averaged tidal currents can be altered by local stratification, as shown in Fig. 32. Therefore, they may differ significantly from the ones in the barotropic mode, if stratification is present, as it is the case at the northwestern entrance of the North Sea. Consequently, also the sea surface gradient will be adjusted due to baroclinicity. This alteration of the external Kelvin wave, which already starts at the entrance of the North Sea, modifies the amphidromic system causing a change of tidal ranges even in well-mixed coastal areas, e.g., at station Büsum as exemplified in this study.

5.3.3.5 Summary

In summary, a sound hypothesis is proposed in this thesis that the TRD in coastal well-mixed areas is highly related to the alteration of vertically averaged tidal current velocity in stratified regions, which in turn also affects well-mixed regions. Stratification can decouple surface and bottom waters, resulting in altered tidal current profiles and a modified barotropic transport. Consequently, change of the vertically averaged tidal current velocity forms a new equilibrium between Coriolis force and sea surface gradient. By this means, the characteristics of the external Kelvin wave can be altered, which in turn may modulate the amphidromic system, finally causing changes in coastal tidal ranges. This argumentation could be confirmed by the evidence of the dipole structures in the spatial distribution of the TRD and the alteration of the M2 amphidromic system. Moreover, as studied by Müller (2012), the variation of the barotropic tidal transport by stratification is O(1-5%), i.e. the changes in vertically averaged tidal current is O(1-5%). Considering an average M2 amplitude of 1-2 m at coastal stations, a rough change in M2 amplitude by stratification is within 1-10 cm, determined by the equilibrium equation between Coriolis force (proportional to tidal current velocity) and sea surface gradient. Hence, the alteration of the M2 tidal range is within 2-20 cm, which is consistent with the TRD magnitude observed in our study. As stated earlier, local MSL rise only has a relatively small contribution on tidal ranges. Therefore, it can be inferred that the effect of stratification is the major factor for changes in coastal tidal ranges, at least in summer.

Consequently, it can be concluded that changes in heat flux and river input alter coastal tidal ranges by modifying the baroclinicity (majorly stratification) in the North Sea. In winter, most parts of the North Sea are well mixed by surface cooling and strong winds. Thus, the changes in stratification are very small despite of the larger changes in heat flux and river input forcing during the winter season. In contrast, in summer, the northern and central North Sea is fully stratified, and hence, the stratification is much more sensitive to variations of surface heat flux. Therefore, it becomes clear why more significant contributions of heat flux and river input are found for summer than for winter. In addition, we noticed that the heat flux has slightly larger contributions than river input for most stations, which can be explained by the stronger influence of baroclinicity in the central and northern North Sea on the propagation characteristic of the Kelvin wave.

Noteworthy, the contribution of increasing river input on MTR is different from results presented by Moftakahri et al. (2013) and Rodríguez-Padilla & Ortiz (2017), who showed that a decrease of the river input contributes to the growth of M2 tide. In their studies, they did not consider the effect of density gradients induced by the fresh water input from the rivers. However, in our study, it could be demonstrated that the baroclinity effect from river input is of large significance, and hence, should not be neglected.

The observed positive trends in annual and summer TRD and MSL differences (Fig. 24) are clearly related to the variation of local heat flux as well as freshwater input. The atmospheric forcing data in our model contain the global warming signal, thus in the baroclinic mode the local heat flux between ocean and atmosphere is also affected by the global warming signal (shown in Fig. 19), resulting in a warming of the ocean. In contrast, in the barotropic mode no heat flux forcing is considered, and hence, the ocean always has a constant density in space and time. Consequently, only in the baroclinic mode, stratification can be altered due to ocean warming, which in turn may affect the shift of amphidromic points and finally causes a positive trend in the summer and annual TRD. In addition, the warming of the upper ocean affects the steric equilibrium, and results in a positive trend in the MSL difference. This increasing MSL difference principally could further contribute to the positive trend in the TRD. However, this contribution is only of the order of O(0.01 mm yr^{-1}) if applying the ratio between tidal amplitude changes and the sea level rise stated in Idier et al. (2017), Consequently, the contribution of MSL differences to the overall observed summer TRD trend is comparably small.

6. Summary and conclusions

In the present study, we applied the 3D baroclinic circulation model HAMSOM to investigate how the trends of MTR at coastal tide-gauge stations in the North Sea coast are influenced by long-term changes in open boundary SSH, heat flux, wind stress, and river input.

The realistic run (CR) and scenario runs (BS/HF/WS/RI) were performed from 1948 to 2014, with repeated corresponding forcing (boundary SSH, heat flux, wind stress, and river input) applied for each scenario run. The simulated SSH is compared with observations at 70 tide-gauge stations widely distributed over the North Sea, showing good agreement (small bias and RMSE) in phase and amplitude at 22 stations.

Based on the convincingly reproduced sea surface elevation at those 22 tide-gauge stations, annual and seasonal MSL and MTR are calculated over the period from 1950 to 2014 in order to analyze their trends. Winter and summer seasons are specifically focused as heat flux, wind stress, and river input exhibit strong seasonal variations in the North Sea.

The comparison of the reference run and the scenario runs reflects, that open boundary MSL rise dominates changes in MSL at costal tidal stations, with an average contribution of 1.59 mm yr^{-1} to the trends of the annual MSL. The increasing annual mean wind stress exhibits a positive influence on annual MSL, giving an average contribution of 0.48 mm yr^{-1}. Growing surface heat flux and riverine freshwater input also influence the coastal MSL, contributing approximately 0.15 mm yr^{-1} and 0.05 mm yr^{-1} to the averaged trend, respectively. Seasonally, the wind stress shows a much stronger impact in winter (1.20 mm yr^{-1}) than in summer (0.02 mm yr^{-1}) due to the enhanced winds in winter. In summer, wind shows a minor contribution as a response to no significant trends of winds. River discharge also exhibit a stronger influence in summer (0.08 mm yr^{-1}) than in winter (0.06 mm yr^{-1}) mainly caused by a stronger steric effect in summer than in winter. In addition, heat flux exhibit a stronger influence in summer (0.19 mm yr^{-1}) than in winter (0.07 mm yr^{-1}) due to the strong steric effect induced by warmer water in summer.

Regarding the trends in MTR, obviously, the open boundary MSL rise dominates changes in tidal ranges at costal tidal stations, with an average contribution of 0.28 mm yr^{-1} to the trend of the annual MTR. Growing surface heat flux and riverine freshwater input also influence coastal tidal ranges, only contributing approximately 0.02 mm yr^{-1} to the averaged trend. In contrast, the increasing annual mean wind stress has a negative influence, giving an average contribution of -0.07 mm yr^{-1}. Seasonally, the wind stress shows a much stronger impact in winter (-0.10 mm yr^{-1}) due to the enhanced winds in this season. Contrarily, in summer, the wind has a minor average contribution of 0.03 mm yr^{-1} in response to no significant trends of winds. Heat flux and river discharge also exhibit a stronger influence in summer (about 0.06 mm yr^{-1}) than in winter despite the fact that (a) the difference of trends in heat flux forcing between the CR and HF scenario is larger for winter than for summer, and (b) the river input increases faster in winter than in summer. Noteworthy, the trends of summer heat flux and river discharge forcing account for negative contributions along the British coast but for positive contributions in the German Bight.

When investigating the underlying dynamics for each individual forcing mechanism, it turned out that boundary SSH rise alters coastal tidal ranges through increasing coastal water depth. In contrast, increasing wind stress not only modifies the coastal water depth but also enhances bottom stress by input of additional momentum, which at the end is the major factor for the detected reduction of tidal ranges.

When considering the influence of heat flux and river input on tidal ranges, stratification is supposed to be the major influencing factor. To prove this, additional baroclinic and barotropic simulations are conducted in order to understand the effect of baroclinicity on MTR. Analogously, to the investigation of the scenario simulations, the MSL difference and the TRD between the baroclinic and barotropic simulations are analyzed at those previously chosen 22 tide-gauge stations for the same investigation period.

As stated above, the local MSL can be altered by baroclinicity, which in turn affects local tidal ranges. Due to the steric effect, the MSL of the baroclinic simulation is higher than of the barotropic one, in particular at coastal stations. However, it could be shown that the baroclinically driven increase of the local MSL only causes a relatively small increase of the coastal tidal ranges.

A statistical analysis at the previously selected 22 stations for 65 years suggests that the TRD between the baroclinic and the barotropic simulations is more significant in summer than in winter, reaching up to about 11 cm at the station Büsum, corresponding to approximately 3% of the local tidal range. In addition, the spatial distribution of the TRD is presented, showing negative values along the British coast and positive ones in the German Bight. This is consistent with findings mentioned above that heat flux and river discharge forcing provide negative contributions along the British coast and positive ones in the German Bight.

Investigating the trend in the annual and seasonal TRD and the MSL difference during the period from 1950 to 2014, positive trends can be identified in the German Bight, being significantly larger for the summer than for the winter season. The observed maximum trends for the summer TRD and MSL difference amount to 0.17 mm yr^{-1} and 0.48 mm yr^{-1}, respectively, which must be attributed to an altered ocean stratification by global warming. The larger TRD trends in summer than in winter again coincided with findings stated above that larger contributions to MTR trends induced by heat flux and river input are detected for summer than for winter.

Both, the spatial distribution of the TRD and the stronger TRD trend in summer are induced by stratification, which only is considered in the baroclinic run. Hence, it can be inferred that heat flux and river input alter coastal tidal ranges through modifying ocean stratification in the North Sea. Stratification decouples surface water and bottom layer, resulting in altered tidal current profiles, which modifies the depth-averaged barotropic transport. Consequently, the characteristics of the external Kelvin wave can be altered, which in turn may modulate the amphidromic system, finally causing changes in coastal tidal ranges. Noteworthy, the influence of stratification on tidal ranges is a far-field effect, since most stations are located in well-mixed areas, while the influence by the MSL increase is combined far-field and local effect.

The present study focuses on the influence of a limited number of climate-related forcing factors, i.e., open boundary SSH, heat flux, wind stress and river input, on coastal tidal ranges in the North Sea. The bathymetry within the model domain was constant over the entire investigation period. Hence, local changes of the water depth, caused by sedimentation, channel deepening for shipping or installation of offshore wind farms are not considered at the moment. In addition, the friction parameter (bottom roughness) presently employed in the model is spatially uniform and temporal constant. It is known that this parameter as well as the bathymetry have a decisive impact on tidal characteristics. Therefore, both of these aspects should be taken into account in further studies in order to achieve a better representation of coastal tidal ranges and to improve the understanding of their long-term changes.

The findings in the present study emphasize that the global warming does not only cause a rise of the coastal mean sea level but also an increase of the local tidal ranges, which could result in larger coastal inundations and a related threatening to the coastal environment and marine activities.

Reference

Arakawa, A. and Lamb, V. R. (1977). Computational design of the basic dynamical processes of the ucla general circulation model. General circulation models of the atmosphere, 17:173–265.

Arbic, B. K., Garner, S. T., Hallberg, R. W., & Simmons, H. L. (2004). The accuracy of surface elevations in forward global barotropic and baroclinic tide models. Deep Sea Research Part II: Topical Studies in Oceanography, 51(25-26), 3069-3101.

Arbic, B. K., & Garrett, C. (2010). A coupled oscillator model of shelf and ocean tides. Continental Shelf Research, 30(6), 564-574.

Backhaus, J. O. (1985). A three-dimensional model for the simulation of shelf sea dynamics. Deutsche Hydrografische Zeitschrift, 38(4), 165-187.

Becker, J. J., Sandwell, D. T., Smith, W. H. F., Braud, J., Binder, B., Depner, J. L., ... & Ladner, R. (2009). Global bathymetry and elevation data at 30 arc seconds resolution: SRTM30_PLUS. Marine Geodesy, 32(4), 355-371.

British Admiralty (2010) Admiralty tide tables, volume 1&2. Published by the United Kingdom hydrographic office.

Church, J. A., & White, N. J. (2006). A 20th century acceleration in global sea-level rise. Geophysical research letters, 33(1).

Church, J. A., & White, N. J. (2011). Sea-level rise from the late 19th to the early 21st century. Surveys in geophysics, 32(4), 585-602.

Colosi, J. A., & Munk, W. (2006). Tales of the venerable Honolulu tide gauge. Journal of physical oceanography, 36(6), 967-996.

Dangendorf, S., Hay, C., Calafat, F. M., Marcos, M., Piecuch, C. G., Berk, K., & Jensen, J. (2019). Persistent acceleration in global sea-level rise since the 1960s. Nature Climate Change, 9(9), 705-710.

Devlin, A. T., Jay, D. A., Zaron, E. D., Talke, S. A., Pan, J., & Lin, H. (2017). Tidal variability related to sea level variability in the Pacific Ocean. Journal of Geophysical Research: Oceans, 122(11), 8445-8463.

Egbert, G. D., & Erofeeva, S. Y. (2002). Efficient inverse modeling of barotropic ocean tides. Journal of Atmospheric and Oceanic Technology, 19(2), 183-204.

Flick, R. E., Murray, J. F., & Ewing, L. C. (2003). Trends in United States tidal datum statistics and tide range. Journal of Waterway, Port, Coastal, and Ocean Engineering, 129(4), 155-164.

Gilbert, R.O. (1987). Statistical Methods for Environmental Pollution Monitoring, Wiley, NY.

Greenberg, D. A., Blanchard, W., Smith, B., & Barrow, E. (2012). Climate change, mean sea level and high tides in the Bay of Fundy. Atmosphere-ocean, 50(3), 261-276.

Griffies, S. M. and Hallberg, R. W. (2000). Biharmonic Friction with a Smagorinsky-Like Viscosity for Use in Large-Scale Eddy-Permitting Ocean Models. Monthly Weather Review, 128(8):2935–2946.

Griffiths, S. D., & Peltier, W. R. (2009). Modeling of polar ocean tides at the Last Glacial Maximum: Amplification, sensitivity, and climatological implications. Journal of Climate, 22(11), 2905-2924.

Haigh, I. D., Wijeratne, E. M. S., MacPherson, L. R., Pattiaratchi, C. B., Mason, M. S., Crompton, R. P., & George, S. (2014). Estimating present day extreme water level exceedance probabilities around the coastline of Australia: tides, extra-tropical storm surges and mean sea level. Climate Dynamics, 42(1-2), 121-138.

Haigh, I. D., Pickering, M. D., Green, J. M., Arbic, B. K., Arns, A., Dangendorf, S., ... & Woodworth, P. L. (2020). The tides they are a‐Changin': A comprehensive review of past and future nonastronomical changes in tides, their driving mechanisms, and future implications. Reviews of Geophysics, 58(1), e2018RG000636.

Hall, G. F., Hill, D. F., Horton, B. P., Engelhart, S. E., & Peltier, W. R. (2013). A high-resolution study of tides in the Delaware Bay: Past conditions and future scenarios. Geophysical Research Letters, 40(2), 338-342.

Hay, C. C., Morrow, E., Kopp, R. E., & Mitrovica, J. X. (2015). Probabilistic reanalysis of twentieth-century sea-level rise. Nature, 517(7535), 481-484.

Hense, A., Glowienka-Hense, R. (2008) Auswirkungen der Nordatlantischen Zirkulation [Effects of the North Atlantic Circulation]. Promet 34:89–94

Hill, D. F. (2016). Spatial and temporal variability in tidal range: evidence, causes, and effects. Current Climate Change Reports, 2(4), 232-241.

Hill, D. F., Griffiths, S. D., Peltier, W. R., Horton, B. P., & Törnqvist, T. E. (2011). High-resolution numerical modeling of tides in the western Atlantic, Gulf of Mexico, and Caribbean Sea during the Holocene. Journal of Geophysical Research: Oceans, 116(C10).

Holleman, R. C., & Stacey, M. T. (2014). Coupling of sea level rise, tidal amplification, and inundation. Journal of Physical Oceanography, 44(5), 1439-1455.

Holleman, R. C., & Stacey, M. T. (2014). Coupling of sea level rise, tidal amplification, and inundation. Journal of Physical Oceanography, 44(5), 1439-1455.

Howarth, M. J. (1998). The effect of stratification on tidal current profiles. Continental shelf research, 18(11), 1235-1254.

Hurrell, J. W. (1995). Decadal trends in the North Atlantic Oscillation: Regional temperatures and precipitation. Science, 269(5224), 676-679.

Hurrell, J. W., & Van Loon, H. (1997). Decadal variations in climate associated with the North Atlantic Oscillation. In Climatic change at high elevation sites (pp. 69-94). Springer, Dordrecht.

Idier, D., Paris, F., Le Cozannet, G., Boulahya, F., & Dumas, F. (2017). Sea-level rise impacts on the tides of the European Shelf. Continental Shelf Research, 137, 56-71.

Jänicke, L., Ebener, A., Dangendorf, S., Arns, A., Schindelegger, M., Niehüser, S., ... & Jensen, J. (2020). Assessment of tidal range changes in the North Sea from 1958 to 2014. Journal of Geophysical Research: Oceans, e2020JC016456.

Kalnay, E., Kanamitsu, M., Kistler, R., Collins, W., Deaven, D., Gandin, L., ... & Zhu, Y. (1996). The NCEP/NCAR reanalysis 40-year project. Bull. Am. Meteorol. Soc, 77(3), 437-471.

Kendall, M.G. (1975). Rank Correlation Methods, 4th edition, Charles Griffin, London.

Li, W., Mayer, B., Pohlmann, T. (2018). Resource Assessment of Tidal Current Energy and Hydrodynamic Impacts of the Energy Extraction in the North Sea. Master thesis.

Locarnini, R. A., Mishonov, A. V., Antonov, J. I., Boyer, T. P., Garcia, H. E., Baranova, O. K., Zweng, M. M., Paver, C. R., Reagan, J. R., Johnson, D. R., Hamilton, M. & Seidov, D. (2013). World Ocean Atlas 2013, Volume 1: Temperature. S. Levitus, Ed., A. Mishonov Technical Ed.; NOAA Atlas NESDIS 73, 40 pp.

Mann, H.B. (1945). Non-parametric tests against trend, Econometrica 13:163-171.

Mathis, M., Pohlmann, T., Backhaus, J. (2013). Projected Forecast of Hydrodynamic Conditions in the North Sea for the 21st Century. PhD thesis.

Mawdsley, R. J., Haigh, I. D., & Wells, N. C. (2015). Global secular changes in different tidal high water, low water and range levels. Earth's Future, 3(2), 66-81.

Mellor, G. L., & Yamada, T. (1974). A hierarchy of turbulence closure models for planetary boundary layers. Journal of Atmospheric Sciences, 31(7), 1791-1806.

Moftakhari, H. R., Jay, D. A., Talke, S. A., Kukulka, T., & Bromirski, P. D. (2013). A novel approach to flow estimation in tidal rivers. Water Resources Research, 49(8), 4817-4832.

Müller, M., Arbic, B. K., & Mitrovica, J. X. (2011). Secular trends in ocean tides: Observations and model results. Journal of Geophysical Research: Oceans, 116(C5).

Müller, M. (2012). The influence of changing stratification conditions on barotropic tidal transport and its implications for seasonal and secular changes of tides. Continental Shelf Research, 47, 107-118.

Müller, M., Cherniawsky, J. Y., Foreman, M. G., & von Storch, J. S. (2014). Seasonal variation of the M2 tide. Ocean Dynamics, 64(2), 159-177.

Müller Schmied, H., Eisner, S., Franz, D., Wattenbach, M., Portmann, F. T., Flörke, M., & Döll, P. (2014). Sensitivity of simulated global-scale freshwater fluxes and storages to input data, hydrological model structure, human water use and calibration. Hydrology and Earth System Sciences, 18(9), 3511-3538.

Pan, H., Lv, X., Wang, Y., Matte, P., Chen, H., & Jin, G. (2018). Exploration of Tidal‐Fluvial Interaction in the Columbia River Estuary Using S_TIDE. Journal of Geophysical Research: Oceans, 123(9), 6598-6619.

Passeri, D. L., Hagen, S. C., Plant, N. G., Bilskie, M. V., Medeiros, S. C., & Alizad, K. (2016). Tidal hydrodynamics under future sea level rise and coastal morphology in the Northern Gulf of Mexico. Earth's Future, 4(5), 159-176.

Pelling, H. E., Uehara, K., & Green, J. M. (2013). The impact of rapid coastline changes and sea level rise on the tides in the Bohai Sea, China. Journal of Geophysical Research: Oceans, 118(7), 3462-3472.

Pickering, M. D., Wells, N. S., Horsburgh, K., & Green, J. A. M. (2012). The impact on the European Shelf tides by future sea-level rise. Continental Shelf Research, 35, 1-15.

Pickering, M. D., Horsburgh, K. J., Blundell, J. R., Hirschi, J. M., Nicholls, R. J., Verlaan, M., & Wells, N. C. (2017). The impact of future sea-level rise on the global tides. Continental Shelf Research, 142, 50-68.

Pingree, R. D., Holligan, P. M., & Mardell, G. T. (1978). The effects of vertical stability on phytoplankton distributions in the summer on the northwest European Shelf. Deep Sea Research, 25(11), 1011-1028.

Pohlmann, T. (1996). Predicting the thermocline in a circulation model of the North Sea—Part I: model description, calibration and verification. Continental Shelf Research, 16(2), 131-146.

Pohlmann, T. (2006). A meso-scale model of the central and southern North Sea: consequences of an improved resolution. Continental Shelf Research, 26(19), 2367-2385.

Pugh, D. T. (1987). Tides, surges and mean sea level: A handbook for engineers and scientists (472 pp.). Chichester, UK: Wiley.

Pätsch, J., Burchard, H., Dieterich, C., Gräwe, U., Gröger, M., Mathis, M., ... & Su, J. (2017). An evaluation of the North Sea circulation in global and regional models relevant for ecosystem simulations. Ocean Modelling, 116, 70-95.

Quante, M., & Colijn, F. (2016). North Sea region climate change assessment (p. 528). Springer Nature.

Rahmstorf, S. (2007). A semi-empirical approach to projecting future sea-level rise. Science, 315(5810), 368-370.

Ray, R. D. (2006). Secular changes of the M2 tide in the Gulf of Maine. Continental Shelf Research, 26(3), 422-427.

Ray, G. C. and McCormick-Ray, J. (2009). Coastal-marine conservation: science and policy. John Wiley & Sons.

Ray, R. D. (2009). Secular changes in the solar semidiurnal tide of the western North

Atlantic Ocean. Geophysical Research Letters, 36(19).

Rodríguez-Padilla, I., & Ortiz, M. (2017). On the secular changes in the tidal constituents in San Francisco B ay. Journal of Geophysical Research: Oceans, 122(9), 7395-7406.

Schrum, C., Siegismund, F., & St John, M. (2003). Decadal variations in the stratification and circulation patterns of the North Sea. Are the 1990s unusual. In ICES J Mar Sci, Symp Ser (Vol. 219, pp. 121-131).

Smagorinsky, J. (1993). Some historical remarks on the use of nonlinear viscosities. Large eddy simulation of complex engineering and geophysical flows, 1:69–106.

Steele, J. H., Thorpe, S. A., and Turekian, K. K. (2009). Ocean Currents: A derivative of the encyclopedia of Ocean Sciences. Academic Press.

Sündermann, J., & Pohlmann, T. (2011). A brief analysis of North Sea physics. Oceanologia, 53(3), 663-689.

Talke, S. A., & Jay, D. A. (2020). Changing tides: The role of natural and anthropogenic factors. Annual review of marine science, 12, 121-151.

Talke, S. A., Horner-Devine, A. R., Chickadel, C. C., & Jessup, A. T. (2013). Turbulent kinetic energy and coherent structures in a tidal river. Journal of Geophysical Research: Oceans, 118(12), 6965-6981.

Taylor, G. I. (1922). Tidal oscillations in gulfs and rectangular basins. Proceedings of the London Mathematical society, 2(1), 148-181.

Thomas, M., & Sündermann, J. (1999). Tides and tidal torques of the world ocean since the last glacial maximum. Journal of Geophysical Research: Oceans, 104(C2), 3159-3183.

Trigo, R. M., Osborn, T. J., & Corte-Real, J. M. (2002). The North Atlantic Oscillation influence on Europe: climate impacts and associated physical mechanisms. Climate research, 20(1), 9-17.

Uehara, K., Scourse, J. D., Horsburgh, K. J., Lambeck, K., & Purcell, A. P. (2006). Tidal evolution of the northwest European shelf seas from the Last Glacial Maximum to the present. Journal of Geophysical Research: Oceans, 111(C9).

Van Haren, H. (2000). Properties of vertical current shear across stratification in the North Sea. Journal of Marine Research, 58(3), 465-491.

Winther, N. G. and Johannessen, J. A. (2006). North sea circulation: Atlantic inflow and its destination. Journal of Geophysical Research: Oceans, 111(C12).

Woodworth, P. L. (2010). A survey of recent changes in the main components of the ocean tide. Continental shelf research, 30(15), 1680-1691.

Woodworth, P. L., Shaw, S. M., & Blackman, D. L. (1991). Secular trends in mean tidal range around the British Isles and along the adjacent European coastline. Geophysical Journal International, 104(3), 593-609.

Yue, S., & Wang, C. (2004). The Mann-Kendall test modified by effective sample size to detect trend in serially correlated hydrological series. Water resources management, 18(3), 201-218.

Zuo, H., Balmaseda, M. A., Tietsche, S., Mogensen, K., & Mayer, M. (2019). The ECMWF operational ensemble reanalysis–analysis system for ocean and sea ice: a description of the system and assessment. Ocean science, 15(3), 779-808.

Zweng, M. M, Reagan, J. R., Antonov, J. I., Locarnini, R. A., Mishonov, A. V., Boyer, T. P., Garcia, H. E., Baranova, O. K., Johnson, D. R., Seidov, D. & Biddle, M. M. (2013). World Ocean Atlas 2013, Volume 2: Salinity. S. Levitus, Ed., A. Mishonov Technical Ed.; NOAA Atlas NESDIS 74, 39 pp.

Supplementary

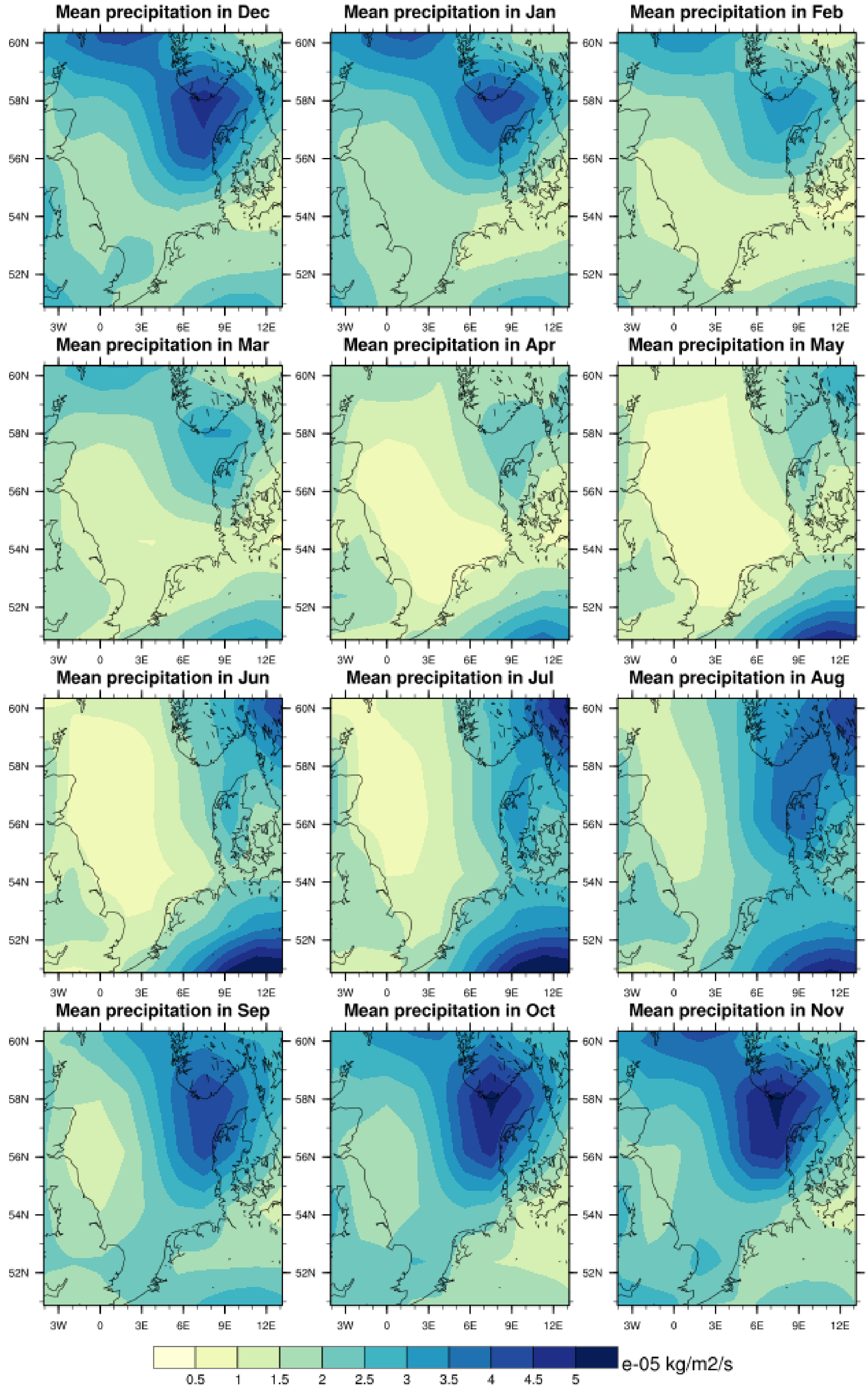

Fig. S1 Monthly mean precipitation rate at surface (1950-2014) in the North Sea. Data retrieved from NCEP R1 dataset and are interpolated into a fine resolution of 3 km.

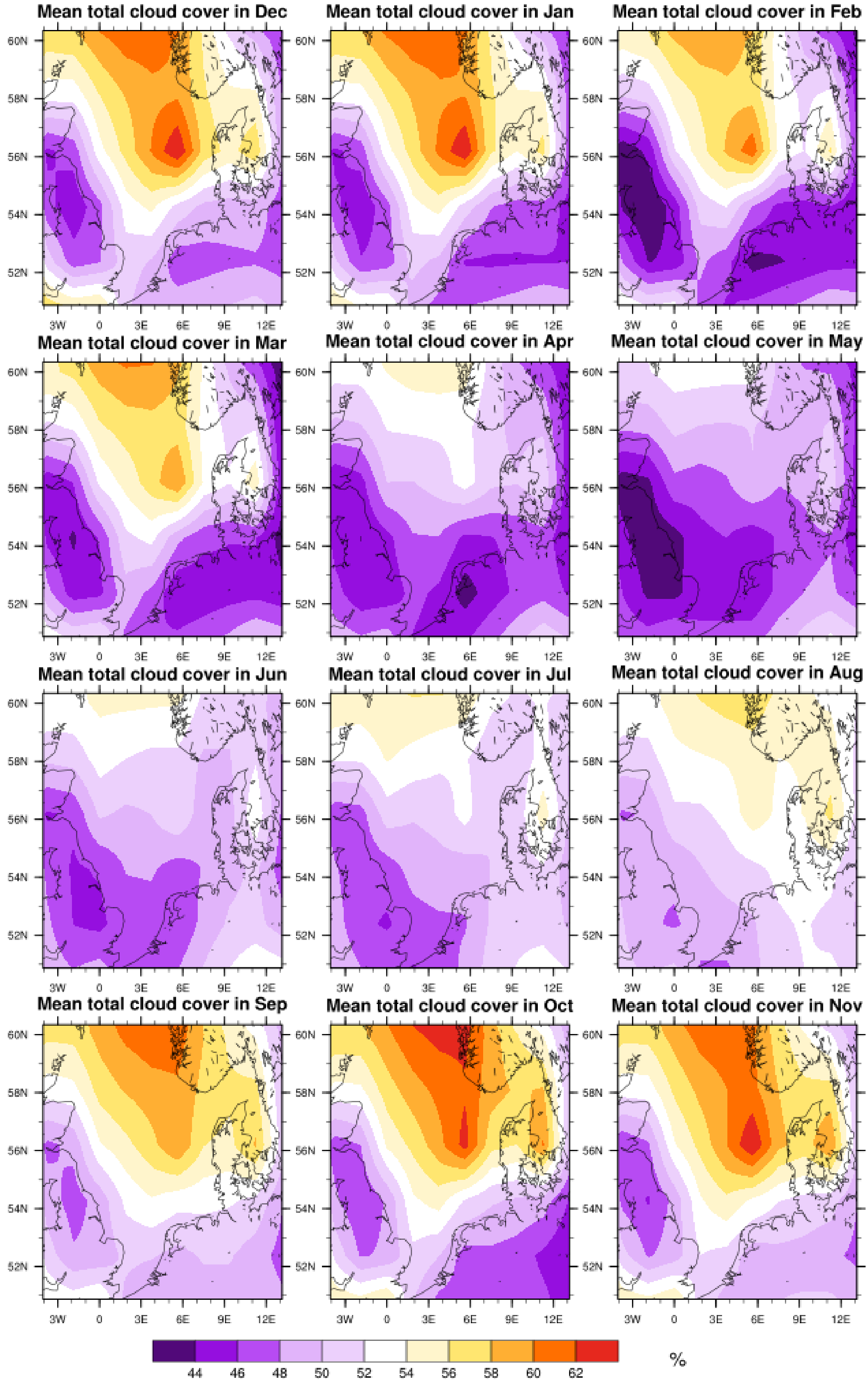

Fig. S2 Monthly mean total cloud cover (1950-2014) in the North Sea. Data retrieved from NCEP R1 dataset and are interpolated into a fine resolution of 3 km.

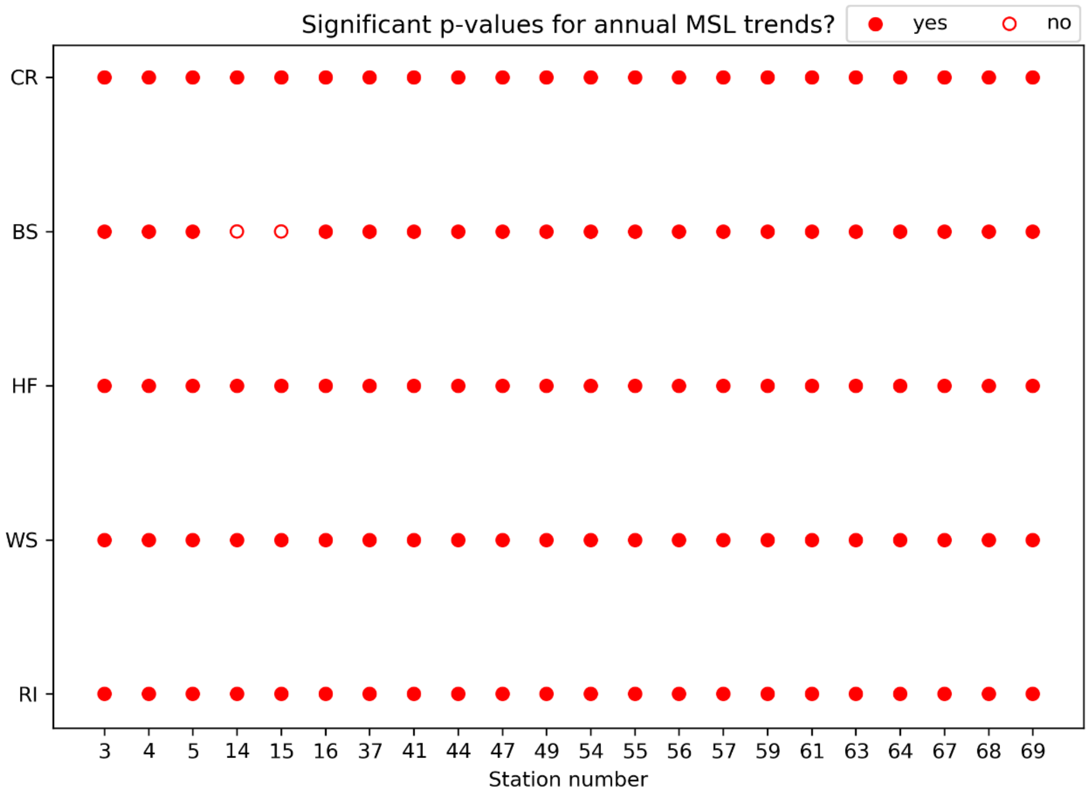

Fig. S3 p-values for annual MSL

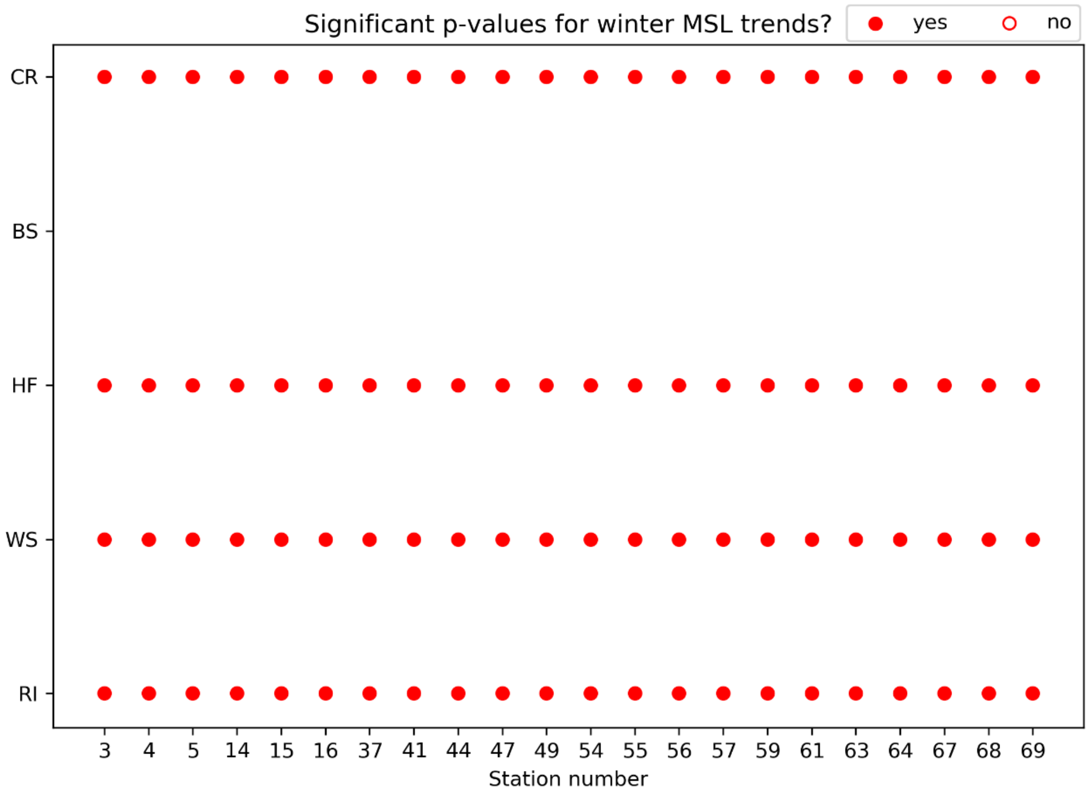

Fig. S4 p-values for winter MSL

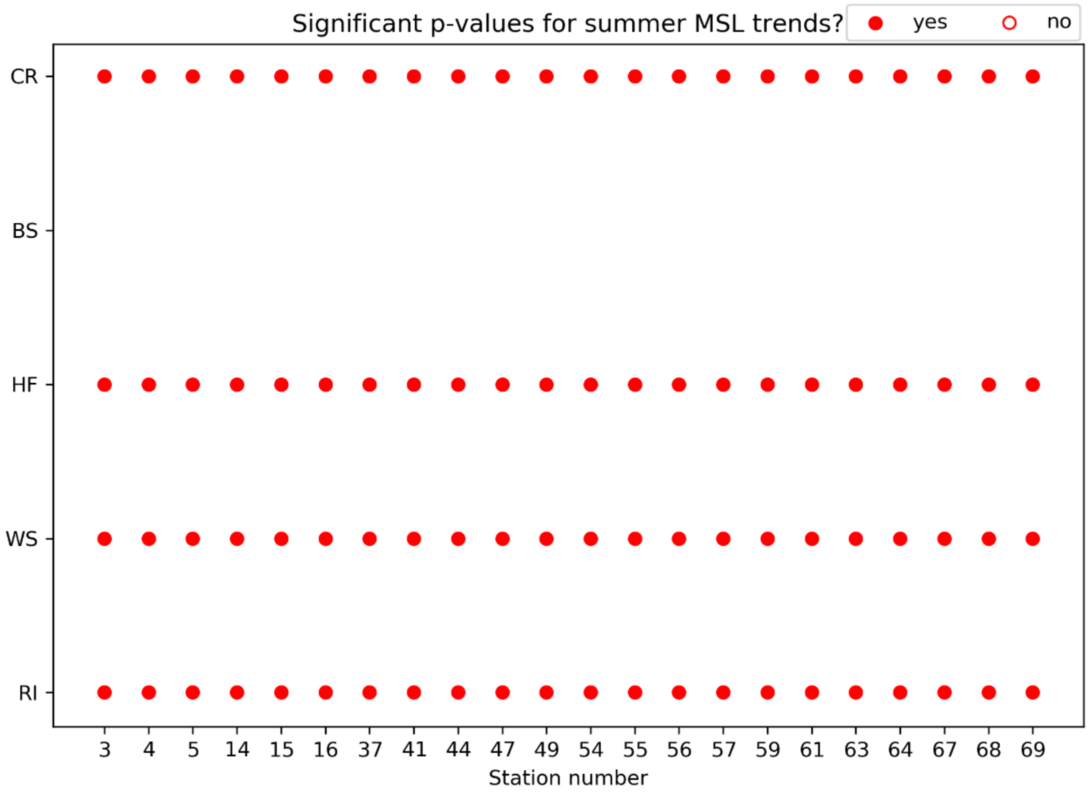

Fig. S5 p-values for summer MSL

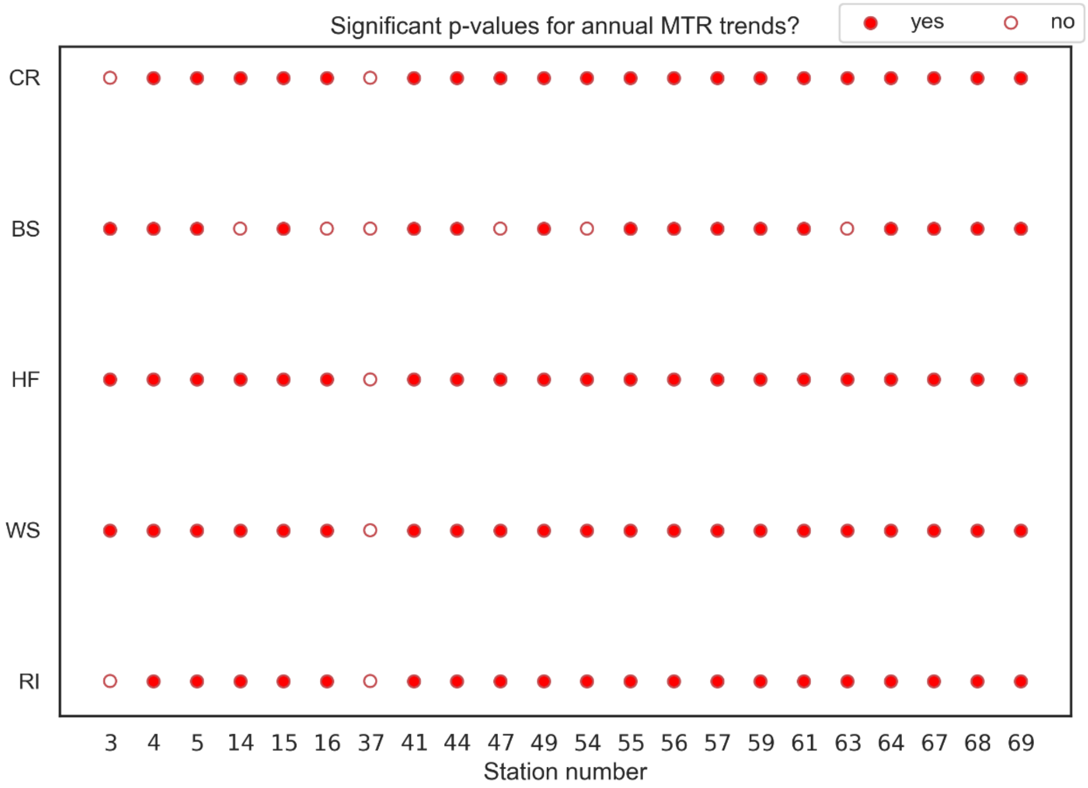

Fig. S6 p-values for Annual MTR

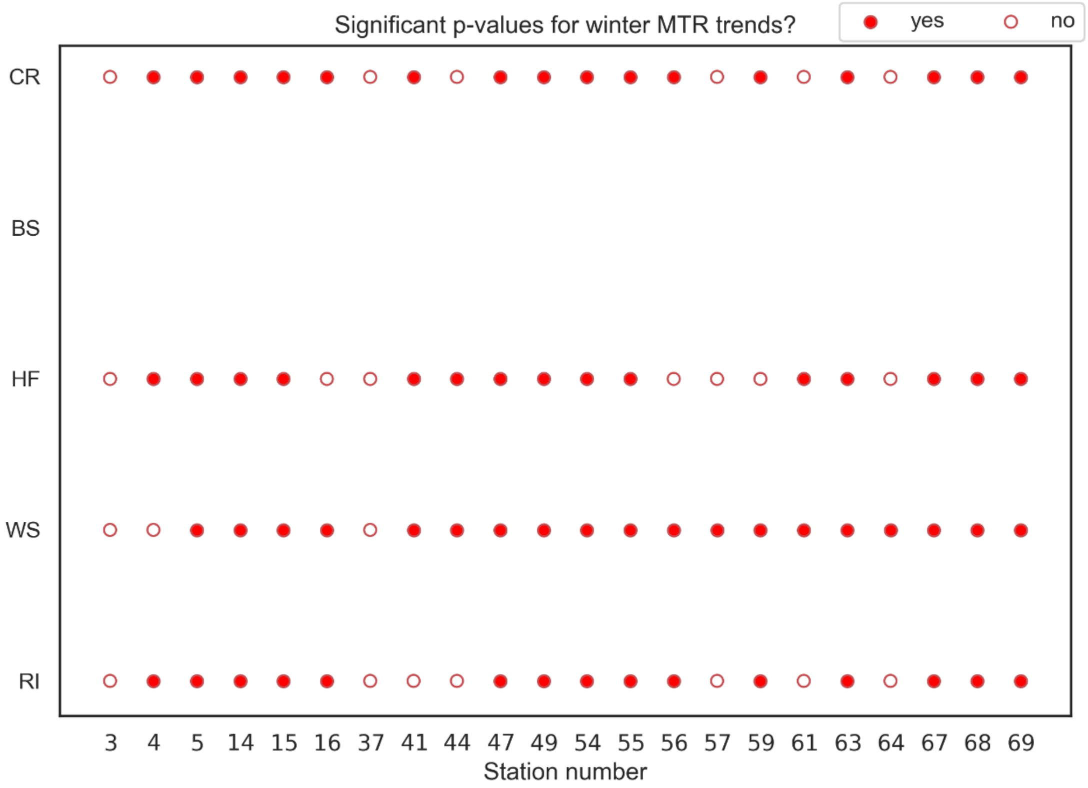

Fig. S7 p-values for winter MTR

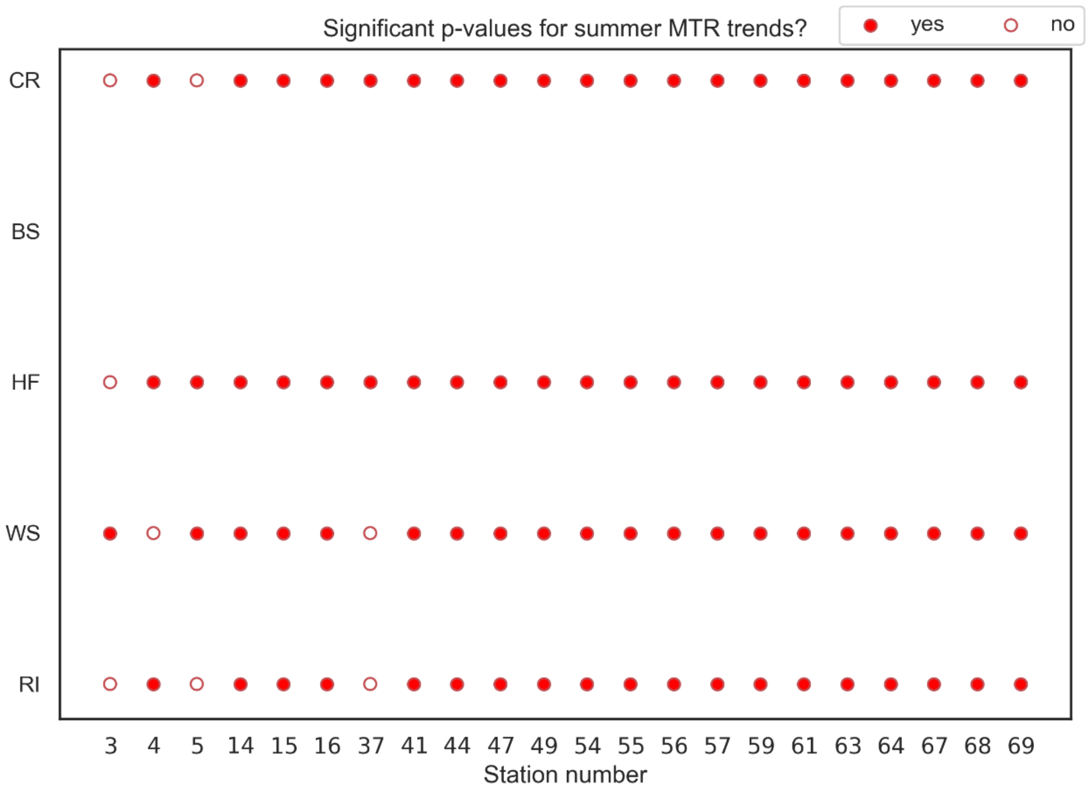

Fig. S8 p-values for summer MTR

Table S1 p-values for different forcing

P-values	**Boundary**	**Heat flux**		**wind**				**River**
	SSH	CR	HF	SW	W	NW	S	**input**
Annual	0.00	0.21	0.00	0.00	0.03	0.03	0.00	0.00
Winter	--	0.71	0.00	0.02	0.24	0.09	0.01	0.00
Summer	--	0.08	0.05	0.23	0.62	0.04	0.92	0.54

List of figures

List of tables

Acknowledgement

I would like to thank PD Dr. Thomas Pohlmann and Dr. Bernhard Mayer for their advice, encouragement, and supervision throughout my PhD thesis. They provided excellent guidance for my PhD study. I would also like to thank their comments and feedback on my work. I am also grateful to the Leon Jaenicke and Dr. Sönke Dangendorf from Research Institute for Water and Environment in University of Siegen. Leon provided me the observational data of tidal gauge stations, and Sönke provided me the dynamic height anomaly data used in this study. I would finally like to thank the support of my family and my girlfriend while I have been studying here.

Author statement

Wenguo Li: Conceptualization, Methodology, Software, Validation, Visualization, Formal analysis, Writing- Original draft preparation.

Bernhard Mayer: Conceptualization, Writing - Review & Editing, Supervision.

Thomas Pohlmann: Conceptualization, Writing - Review & Editing, Supervision.

Description of results published

Results for Section 4.2 are published in the paper below:

Li, W., Mayer, B., & Pohlmann, T. (2021). The influence of baroclinity on tidal ranges in the North Sea. Estuarine, Coastal and Shelf Science, 250, 107126.

Eidesstattliche Versicherung | Declaration on Oath

Hiermit erkläre ich an Eides statt, dass ich die vorliegende Dissertationsschrift selbst verfasst und keine anderen als die angegebenen Quellen und Hilfsmittel benutzt habe.

I hereby declare upon oath that I have written the present dissertation independently and have not used further resources and aids than those stated. I agree to my thesis being placed in the library of the department.

Ort,den | City,date

Hamburg, 24.08.2021

Unterschrift | Signature

Wenguo Li